Stockholm School of Economics
Department of Economics
5350 Master's Thesis in Economics
Spring 2026

Blowin' in the Wind: The Evolution of the Wind Merit-Order Effect Across Sweden's Bidding Zones

Patrick Sarzio (42869) and Valter Strandler (25425)

Abstract: This paper analyses the impact of wind energy production on electricity price levels and volatility across Sweden's four bidding zones from 2015 to 2025. Using hourly day-ahead prices, the paper estimates an ARMAX(3,1)-GARCH-X(1,1) model in rolling one-year windows per zone, and complements this with a quantile regression estimate. The results document a robust negative merit-order effect of wind on prices across all zones, with SE3 exhibiting the strongest price sensitivity and SE1 the weakest. The volatility effect is more heterogeneous: wind is associated with lower conditional price variance in SE1 and SE2, while the relationship is less stable in SE3 and SE4. The thesis shows that the sharp post-2024 divergence in wind-price sensitivities between SE1 and SE2 coincides with the Nordic transition from Available Transfer Capacity to Flow-Based Market Coupling. The findings suggest that transmission constraints, not generation mix alone, determine how wind energy affects prices, with direct implications for market design.

Keywords: wind power, electricity prices, volatility, merit-order effect, Sweden

JEL: Q41, Q42

Supervisor:	Rickard Sandberg
Date submitted:	31st May 2026
Date examined:	29th May 2026
Discussants:	...
Examiner:	Sampreet Singh Goraya

Acknowledgements

We want to thank our supervisor, Prof. Rickard Sandberg, for his time and input. We also want to thank Prof. Elena Paltseva for her contributions towards this paper. Lastly, we want to thank Nord Pool for granting us access to their database.

Contents

Acknowledgements **i**

List of Figures **v**

List of Tables **vi**

List of Abbreviations **vii**

1 Introduction **1**

2 Literature Review **4**

3 Electricity Markets and Nord Pool **9**
3.1 Introduction to Electricity Markets 9
3.2 Nord Pool 10

4 Data and Methodology **18**
4.1 Data 18
4.2 Methodology 22
4.2.1 Mean Equation 22
4.2.2 Variance Equation 24
4.2.3 Distributional Heterogeneity and Quantile Regression 26
4.2.4 Zone-Level Estimation Strategy 28
4.2.5 Rolling-Window Estimation 28

5 Results **29**
5.1 Model Selection 29
5.2 Baseline Estimation 30
5.3 Rolling-Window Results 33
5.3.1 Mean Equation 33
5.3.2 Variance Equation 34
5.4 SE1–SE2 Divergence and the FBMC Change 35
5.5 Quantile Regression 36

5.6 Robustness Checks . . . 38
5.6.1 Robustness to the Treatment of Negative Prices . . . 38
5.6.2 Robustness Within the ARMAX-GARCH-X Specification . . . 38
5.6.3 Robustness to Excluding the GARCH-X Variance Equation . . . 40
5.6.4 Trade-Partner Sensitivity in SE1 and SE2 . . . 42

6 Discussion and Policy Implications 44
6.1 Economic Interpretation . . . 44
6.1.1 Volatility Dynamics . . . 47
6.1.2 Distributional Heterogeneity . . . 48
6.2 Policy Implications . . . 49
6.3 Limitations . . . 51
6.4 Directions for Further Research . . . 53

7 Conclusion 55

A Appendix 57
A.1 Descriptive Statistics and Price Distributions . . . 57
A.2 Variable Treatment and Preprocessing . . . 61
A.3 Outlier Bounds by Estimation Window . . . 66
A.4 Grid Search Over ARMA Specifications . . . 68
A.5 Bilateral Net Import Coefficients . . . 70
A.6 Additional FBMC Interaction Tests . . . 72
A.6.1 SE1–SE2 FBMC Interaction Test . . . 72
A.6.2 SE2 Local Congestion Interaction Test . . . 73
A.7 Rolling-Window Coefficient, Mean Equation . . . 75
A.7.1 Mean Equation . . . 75
A.7.2 Rolling Quantile Regression Estimates . . . 76
A.8 Rolling-Window Coefficient, Variance Equation . . . 79
A.9 Robustness to the Treatment of Negative Prices . . . 80
A.10 Trade-Partner Sensitivity in SE1 and SE2 . . . 83

B Replication Code 84

C Use of Artificial Intelligence 85

Bibliography 86

List of Figures

3.1 Illustrative merit-order curve 10
3.2 Map of zones represented on Nord Pool 11
3.3 Energy net-export per bidding zone, 2015–2025 13
3.4 Electricity generation mix per bidding zone, 2015–2025 14
3.5 Wind share of annual electricity production per bidding zone 15
3.6 Absolute wind production per bidding zone 15
3.7 Price level (raw), monthly average 16
3.8 Price volatility (raw), monthly average 16

5.1 Rolling-window mean coefficient (1 year window, 1 year shift) 34
5.2 Rolling-window volatility coefficient (1 year window, 1 year shift) . . . 35

A.1.1 Price histograms per bidding zone and year 60
A.2.1 ACF of deseasonalised log prices (SE4) 61
A.2.2 ACF of AR(1) residuals under alternative deseasonalisation (SE4) . . 61
A.2.3 Seasonal patterns in wind power production forecasts (SE4) 62
A.2.4 Seasonal patterns in electricity consumption forecasts (SE4) 63
A.2.5 Seasonal patterns in hydro reservoir levels (SE4) 64
A.2.6 Amount of negative prices per zone, 2015–2025 65
A.3.1 Outlier capping bounds in SE1 and SE2 66
A.3.2 Outlier capping bounds in SE3 and SE4 67
A.7.1 Rolling-window estimates of $\hat{\beta}_{\text{wind}}(\tau = 0.10)$ 77
A.7.2 Rolling-window estimates of $\hat{\beta}_{\text{wind}}(\tau = 0.50)$ 78
A.7.3 Rolling-window estimates of $\hat{\beta}_{\text{wind}}(\tau = 0.90)$ 79
A.9.1 Rolling-window estimates of $\hat{\beta}_{\text{wind}}$ (negative-price floor) 81
A.9.2 Rolling-window estimates of $\hat{\gamma}_{\text{wind}}$ (negative-price floor) 82

List of Tables

3.1 Share of hourly price divergence between zones 17

4.1 Ljung-Box test for serial correlation in the deseasonalised log spot price 23
4.2 Engle's ARCH test for conditional heteroscedasticity in mean-only ARMAX(1,1) residuals 24

5.1 ARMAX(3,1)-GARCH-X(1,1) baseline estimates, 2025 32
5.2 Wind coefficient by specification: ARMAX(3,1)-GARCH-X(1,1), 2025 40
5.3 Wind coefficient stability across specifications: ARMAX(3,1), 2025 . . 42

A.1.1 Descriptive statistics, 2015–2025 (Panel A: SE1 and SE2) 58
A.1.2 Descriptive statistics, 2015–2025 (Panel B: SE3 and SE4) 59
A.2.1 ADF tests for transformed model variables, 2025 65
A.4.1 SE1: ARMA(p, q) grid-search results, 2025 68
A.4.2 SE2: ARMA(p, q) grid-search results, 2025 68
A.4.3 SE3: ARMA(p, q) grid-search results, 2025 69
A.4.4 SE4: ARMA(p, q) grid-search results, 2025 69
A.5.1 Bilateral net import coefficients, SE1, 2025 70
A.5.2 Bilateral net import coefficients, SE2, 2025 70
A.5.3 Bilateral net import coefficients, SE3, 2025 71
A.5.4 Bilateral net import coefficients, SE4, 2025 71
A.6.1 Pooled SE1–SE2 FBMC interaction estimates, 2024–2025 73
A.6.2 SE2 local congestion interaction estimates, 2025 74
A.7.1 Rolling-window estimates of $\hat{\beta}_{\text{wind}}$, mean equation 75
A.7.2 Rolling-window estimates of $\hat{\beta}_{\text{wind}}(\tau = 0.10)$ 76
A.7.3 Rolling-window estimates of $\hat{\beta}_{\text{wind}}(\tau = 0.50)$ 77
A.7.4 Rolling-window estimates of $\hat{\beta}_{\text{wind}}(\tau = 0.90)$ 78
A.8.1 Rolling-window estimates of $\hat{\gamma}_{\text{wind}}$, variance equation 79
A.9.1 Rolling-window estimates of $\hat{\beta}_{\text{wind}}$ (negative-price floor) 80
A.9.2 Rolling-window estimates of $\hat{\gamma}_{\text{wind}}$ (negative-price floor) 81
A.10.1 Trade-partner sensitivity of the wind coefficient in SE1 and SE2, ARMAX(3,1)-GARCH-X(1,1), 2025 83

List of Abbreviations

ACF	Autocorrelation Function
AIC	Akaike Information Criterion
AR	Autoregressive
ARCH	Autoregressive Conditional Heteroscedasticity
ARMA	Autoregressive Moving Average
ARMAX	Autoregressive Moving Average with Exogenous Inputs
ATC	Available Transfer Capacity
BIC	Bayesian Information Criterion
EEX	European Energy Exchange
FBMC	Flow-Based Market Coupling
GARCH	Generalised Autoregressive Conditional Heteroscedasticity
GWh	Gigawatt-hour
LM	Lagrange Multiplier
MA	Moving Average
MOE	Merit-order Effect
MWh	Megawatt-hour
QARX	Quantile Autoregressive Model with Exogenous Inputs
QML	Quasi-Maximum Likelihood
RSE	Robust Standard Errors
SE	Swedish Electricity Bidding Zone (SE1–SE4)
TWh	Terawatt-hour

Chapter 1

Introduction

On 28 February 2026, Israel and the United States of America launched air strikes on multiple locations within Iran (The Guardian, 2026). While long-term implications of this conflict are unclear, a significant spike in oil prices followed the attack and a subsequent blockade of the Strait of Hormuz, reminding observers of the price hike during the 2021/2022 energy crisis (Baskar, 2026; Marsh & Musafer, 2026). As negative aspects of fossil fuel dependency become apparent, sustainable and independent energy production alternatives gain public and political support. Sweden is well placed to lead this transition as the first country to establish an Environmental Protection Agency and host the first UN conference on the global environment (Swedish Institute, 2026). The country has a long-standing commitment to sustainability and positions itself as a leader in this field, aiming to achieve fossil-free energy by 2045, supported by an ambitious build-out of wind farms and hydro power (Swedish Institute, 2026). While the government points to the financial upside of green growth and the energy transition, none of these political ambitions holds without a well-functioning energy market (Swedish Institute, 2026).

However, Sweden's electricity market is fragmented. The gap between electricity prices in Sweden's different bidding zones is widening, starting in 2020 and increasingly since the 2021/2022 energy crisis. Simultaneously, wind energy production has expanded rapidly across Sweden's northern bidding zones, raising concerns about whether the market can transmit the expansion's benefits to consumers across the country. Following a change in market coupling mechanism in the Nordic day-ahead energy market on 30 October 2024, transmission constraints became binding for the SE2–SE3 corridor in a large majority of hours. This structural change alters how wind surplus in the northern zones affects prices across the market. In this environment, Sweden's Government tasked Svenska kraftnät in 2025 to reevaluate the configuration of Sweden's energy market and propose improvements, including a potential re-structuring of bidding zones

(Regeringen och Regeringskansliet, 2025; Svenska Kraftnät, 2025a). To ensure that meaningful policy suggestions can be developed, understanding the price spread and its underlying dynamics with regard to wind energy production is essential.

This requires a zone-specific analysis over time. While existing literature estimates sensitivities over shorter intervals or treats the relationship between wind and prices as stable, the evolving role of wind in a market shaped by energy crises, nuclear power plant shutdowns, and structural market changes remains insufficiently understood. A long, zone-specific analysis of how the wind merit-order effect changes over time, and why, is missing from the literature.

The research question of this thesis is twofold: How has the wind merit-order effect evolved across Sweden's bidding zones, and what could explain differences in the wind merit-order effect between zones and times?

To answer these questions, the study estimates the merit-order effect of wind from 2015 to 2025, separately per bidding zone and per year. Using an ARMAX(3,1)-GARCH-X(1,1) model with appropriate controls, the estimation captures the response of prices and price volatility to fluctuations in wind energy production. Rolling one-year windows trace the evolution of the wind coefficient over time, and quantile regressions complement the baseline model by showing how the wind effect differs across the conditional price distribution.

The results document a negative merit-order effect throughout almost the full sample, present in all four zones but heterogeneous in magnitude and time-varying. The crisis windows of 2021 to 2022 deepen the effect sharply across all zones, with SE3 emerging as the most price-sensitive zone. Post-crisis recovery is only partial. A striking finding is the sharp divergence between SE1 and SE2 after 2024, coinciding with the transition to Flow-Based Market Coupling on 30 October 2024. Volatility effects are heterogeneous across zones and time, with wind associated with a volatility decrease in the northern zones by 2025, while results for southern zones remain less clear. Quantile regression results show that the wind effect is strongest in the tails of the conditional price distribution, while the dominant tail differs by zone and time.

The main contribution of this paper is the analysis of price sensitivity to wind over a longer time frame, providing evidence relevant to Svenska kraftnät's assessment of Sweden's bidding-zone configuration. The evolution of this sensitivity is directly relevant for market design because bidding zones are meant to translate local supply conditions and transmission constraints into price signals. This paper strengthens its analysis by additionally investigating the effect of wind energy on price volatility. The analysis further distinguishes between the effect of wind across different parts of

the price distribution, showing that the merit-order effect is not uniform across price regimes. Because consumers, firms, and investors respond to both price signals and price risk, evidence on how wind affects price sensitivity and volatility is relevant for evaluating any reform of Sweden's bidding-zone configuration.

The remainder of the paper is structured as follows. Chapter 2 reviews the relevant literature and highlights previous findings. Chapter 3 describes Sweden's electricity market and Nord Pool as the respective trading platform. Chapter 4 presents the data and methodology, followed by Chapter 5 that reports the empirical results. Chapter 6 discusses the findings, derives policy implications, and highlights limitations and directions for further research before concluding the thesis.

Chapter 2

Literature Review

With wind energy becoming an ever larger share of total energy production across many countries globally, the impact of wind on spot prices has gained attention (Ketterer, 2014). Two ways of analysing the impact of wind on spot prices, known as the merit-order effect, are simulation-based counterfactual approaches and reduced-form econometric approaches. The first approach estimates the price effect of wind by comparing observed market outcomes with a simulated no-wind benchmark (Saénz de Miera et al., 2008). These studies help isolate the merit-order mechanism, but their results depend heavily on simplifying assumptions with regard to market structure, plant behaviour, and system constraints (Forrest & MacGill, 2013; Weron, 2014). This chapter focuses on the reduced-form econometric literature, which estimates the relationship directly from observed prices and wind generation. Across this literature, the central finding is consistent: higher wind power production is associated with lower day-ahead electricity prices, although the estimated magnitude differs across markets, model choices, and system conditions (Würzburg et al., 2013). The text follows the main empirical settings most relevant to this thesis, starting with Sweden and Western Denmark before turning to the broader European evidence.

Sweden and Western Denmark A starting point of this thesis is the analysis of Sandberg (2024), who investigates the effect of wind and temperature on Swedish electricity prices from 2022 to 2023. The paper demonstrates a negative (price-decreasing) effect by analysing four bidding zones and using various reference models, including a fixed effects panel data model, a piecewise linear model, and a dynamic model (Sandberg, 2024). This thesis addresses the suggestion in Sandberg (2024) to investigate the gradual impact of wind on energy prices over time in Sweden. Sandberg's recent Swedish evidence is complemented by Macedo et al. (2021). The authors research the effect of wind power production on the mean and volatility of electricity prices

in SE3, Sweden's bidding zone with the highest electricity flow, between 2016 and 2019. Their findings confirm wind power's merit-order effect in Sweden. Similar to the approach taken in this thesis, the authors in Macedo et al. (2021) use hourly data to assess each hour individually. The authors highlight that electricity prices often show autocorrelation and heteroscedasticity, emphasising the need to account for volatility-clustering, mean-reversion, outliers, and seasonality. These features are partly linked to the limited storability of electricity, since mismatches between non-dispatchable production and consumption must be absorbed through prices rather than storage (Macedo et al., 2021). Jónsson et al. (2010) focus on the effect of wind power forecasts on day-ahead electricity prices in Western Denmark between 2006 and 2007. The authors highlight that electricity spot prices are difficult to model because electricity must be balanced in real time, and short-run demand responds weakly to price. They also link price movements to the merit-order supply curve, where marginal costs rise stepwise as more expensive generation units are needed. Using a non-parametric regression model, they show that the relationship between wind power forecasts and electricity prices is nonlinear and time-dependent. In their paper, Jónsson et al. (2010) use the penetration level of wind power rather than forecasted wind production alone. They define this measure as forecasted wind generation relative to forecasted load and confirm the relevance of wind power for day-ahead prices.

Germany Due to its economic size and integration in the European energy market, research on Germany's energy market is highly relevant for understanding price formation. Ketterer (2014) is especially relevant for this thesis as the paper studies the price-level and volatility effects of wind power in a joint GARCH framework. The paper introduces wind power generation as an explanatory variable in both the mean and variance equations of German day-ahead electricity prices. This is close to the ARMAX-GARCH-X logic used in this thesis, where wind enters both the mean equation and the conditional variance equation. Using German day-ahead prices from 2006 to 2012, Ketterer (2014) estimates rolling-window models to allow the relationship between wind and prices to vary over time. A rolling-window approach re-estimates the model repeatedly on successive subsamples of fixed length, shifting the estimation window forward by one period at a time. This produces a sequence of coefficient estimates rather than a single static estimate and allows the relationship between wind and prices to change over time. The author finds that wind power decreases electricity prices but increases volatility. This thesis builds on Ketterer (2014) by applying a related ARMAX-GARCH-X framework to the Swedish electricity market and by tracing how the estimated wind-price sensitivity evolves by using a rolling-window approach. Highlighting that the volatility of electricity prices has changed after a regulatory change

in 2010, Ketterer (2014) emphasises that market design can impact and potentially smooth electricity price volatility. Ketterer (2014) uses forecasted instead of realised wind generation, arguing that only these were available to market participants when day-ahead prices are set. Ketterer's price-level findings are supported by Cludius et al. (2014), who investigate hourly energy prices between 2008 and 2012 in Germany. They model the day-ahead electricity spot price as dependent on wind electricity and solar electricity feed-in and load to indicate aggregate demand, showing that wind electricity generation lowered market prices. Furthermore, Cludius et al. (2014) develop a near-term forecast for the merit-order effect from 2013 to 2016 using different scenarios of development for load, wind power, and photovoltaic power. This thesis similarly outlines current trends in sensitivities to understand future market dynamics but differs from Cludius et al. (2014) in not explicitly modelling future scenarios. The research by Cludius et al. (2014) is complemented by Paraschiv et al. (2014), who analyse German EEX day-ahead prices between 2010 and 2013. The authors find that renewable generation reduced spot prices and increased the occurrence of extreme price movements, especially negative prices during hours with high wind and low demand. They employ a dynamic fundamental model to indicate a continuous adaptation of electricity prices to market fundamentals, including fossil fuel prices, expected demand, and prices for emission certificates (Paraschiv et al., 2014). Similarly to the approach of this thesis, the authors outline the change of sensitivities over time (Paraschiv et al., 2014). Where Paraschiv et al. (2014) track these time-varying sensitivities using a Kalman filter, this thesis re-estimates the wind coefficient on successive one-year rolling-windows. Hence, the wind coefficient can change from one window to the next, but we do not specify an equation for how the coefficient itself evolves.

Global The broader international literature provides further evidence that the wind merit-order effect is not specific to Northern Europe. Clò et al. (2015) analyse the merit-order effect of solar and wind energy in Italy from 2005 to 2013, using a rolling-window approach. The authors find that wind generation lowers wholesale electricity prices but amplifies price volatility, which links the merit-order effect to both the mean and variance of electricity prices (Clò et al., 2015). For Australia, Mwampashi et al. (2021) study the relationship between electricity prices and wind electricity generation in the National Electricity Market using an eGARCH model. The authors find that higher wind generation reduces daily electricity prices but tends to increase price volatility. Their results show that the merit-order effect can coincide with greater price uncertainty in markets with high shares of weather-dependent generation. Their findings are in line with Csereklyei et al. (2019), who also document a negative effect of wind generation on wholesale electricity prices in Australia. Together, these studies

motivate the methodology employed in this thesis by showing that wind power can affect both the price level and volatility of electricity prices. Maniatis and Milonas (2022) investigate the impact of wind and solar power on price and volatility in Greece between 2012 and 2018. They employ a GARCH-in-Mean model using daily series constructed from hourly market data, confirming the merit-order effect and showing that the volatility effect differs across renewable technologies. Wind power tends to increase price volatility, while solar power tends to reduce it, after controlling for regulatory mechanisms (Maniatis & Milonas, 2022). They follow previous literature in using forecasted wind output and system load for their analysis (Ketterer, 2014; Maniatis & Milonas, 2022). Their findings are supported by Macedo et al. (2020), who analyse the integration of renewable energy into electricity price formation in Portugal from 2011 to 2019. The authors use a SARMAX/eGARCH approach, concluding that wind power reduces the price level of electricity but increases its volatility (Macedo et al., 2020). In Spain, Macedo et al. (2022) analyse the effect of wind and solar generation on the mean and volatility of day-ahead electricity prices from 2015 to 2020. The authors conclude that a merit-order effect exists during most hours of the day but varies in magnitude. They also find that wind power increases price volatility at all hours (Macedo et al., 2022).

Quantile regression The papers reviewed above mainly estimate average price and volatility effects. A smaller but relevant part of the literature uses quantile regression to study whether renewable generation affects different parts of the price distribution. The method follows the regression-quantile framework of Koenker and Bassett (1978), which estimates conditional quantiles rather than only the conditional mean. This difference is useful in electricity markets because wind power may affect low-price and high-price hours differently. Hagfors et al. (2016) use quantile regression to analyse how wind and solar generation affect day-ahead electricity prices in Germany. Their approach estimates the price effects of wind and solar separately across delivery hours and price quantiles. This allows the merit-order effect to vary with the position of prices in the distribution. The authors find that wind and solar generation lower prices overall. For wind, the strongest effects occur in the lower quantiles, especially during night hours when demand is low. This links quantile regression directly to the study of negative and very low prices, which can be hidden in models focused only on average effects. Maciejowska (2020) applies a related quantile-regression approach to German spot prices and focuses on both price levels and price variability. The author finds that wind and solar generation reduce the median electricity price. The paper uses the inter-quantile range to measure how renewables affect the spread between lower and higher price outcomes. The results show that wind increases this spread when

demand is low and reduces it when demand is high. Huisman and Stet (2022) further emphasise that the effect of variable renewable supply is not concentrated at the centre of the price distribution. Using panel quantile regressions, they find that lower and higher price quantiles respond more strongly to renewable supply than median price outcomes. Their approach accounts for the fact that all hourly day-ahead prices are set in the same auction. This makes the paper relevant for analysing whether wind affects the tails of the electricity-price distribution differently from the median.

This thesis extends the existing literature by combining three elements that are usually studied separately. First, it applies an ARMAX-GARCH-X framework to estimate the association between wind power production and both the level and volatility of the day-ahead spot price. Second, it uses a rolling-window design to examine whether the wind coefficient changes over time rather than treating the relationship as fixed. Third, it complements the mean analysis with quantile regression to assess whether the wind effect differs across the conditional price distribution. This combination allows the thesis to study how wind-price sensitivities vary across SE1–SE4, across market periods, and across different parts of the price distribution.

Chapter 3

Electricity Markets and Nord Pool

This chapter provides background on electricity markets, including the merit-order effect, describes the structure of Nord Pool, and highlights Sweden's bidding zones and their differences.

3.1 Introduction to Electricity Markets

In many electricity markets, energy is traded on a central platform that connects buyers and suppliers. Buyers and suppliers submit bids for the quantities they are willing to buy or sell at respective prices. These bids form the demand and supply curves, and the intersection of these determines the market-clearing price. To create the supply curves, a ranking of suppliers is necessary. This ordering is called a merit-order, defined as the ranking of a market's energy suppliers based on their production price, starting with the lowest-cost energy provider. In the merit-order, renewable energy sources are among the lowest-cost producers, whereas gas turbines tend to enter the supply curve later due to their higher production costs (Zeier, 2026). As demand in the market increases, more electricity is needed. Additional producers then contribute to the total supply of electricity, despite their comparatively higher production costs (Cludius et al., 2014). To incentivise suppliers to enter the market, the market-clearing price is equal to the marginal production cost of the most expensive supplier that is needed to serve a respective energy demand. By relying on the merit-order, producers enter the markets sequentially according to their increasing production price, thereby using market resources efficiently (Zeier, 2026). Since renewable energy sources such as solar and wind power are located at the lower end of the price curve, their expansion changes the supply curve for electricity. This shifts the merit-order curve outward and reduces the market-clearing price (Zeier, 2026). Figure 3.1 provides an illustrative

merit-order curve for Sweden, highlighting the price-decreasing effect that an increase in wind power supply has under unchanged demand. This shift in price, dependent on the supply of certain energy sources, is called the merit-order effect.

Changes in temperature, economic activity, and broader European market coupling (among others) affect electricity demand and shift the demand curve (Sandberg, 2024). On the supply side, the available quantity of electricity depends on transmission constraints, cross-border market conditions, and changes in wind power production (Sandberg, 2024). These demand- and supply-side shifts change the market-clearing price, which is the price paid per unit of electricity.

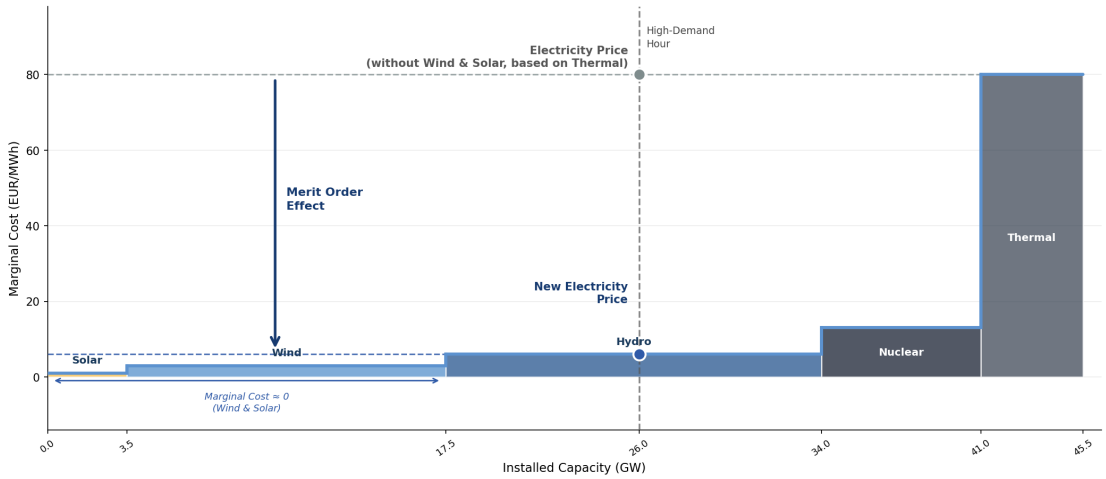


Figure 3.1: Illustrative merit-order curve

Source: Authors' own representation.

3.2 Nord Pool

Nord Pool is a power exchange platform that follows the outlined energy market principles, enabling market participants to submit their bids and offers (Zeier, 2026). Sweden is part of the Nordic-Baltic segment of the Nord Pool electricity market, which includes Sweden, Norway, Finland, Denmark, Estonia, Latvia, and Lithuania (Macedo et al., 2021; Nord Pool, 2026c). Since 2011, Sweden has been divided into four different bidding zones, SE1, SE2, SE3, and SE4. Figure 3.2 outlines the entire area covered by the Nord Pool market and highlights the geographic scope of the individual zones. Sweden's electricity market is connected to Denmark (DK1 and DK2), Norway (NO1, NO3, and NO4), Germany, Lithuania, Poland, and Finland.



Figure 3.2: Map of zones represented on Nord Pool

Source: Nord Pool, authors' own representation.

The Nord Pool market consists of a day-ahead market and an intra-day market for electricity (Nord Pool, 2026c; Sorknæs et al., 2019). This paper focuses on energy traded on the day-ahead market, which constitutes 99.8% of all energy traded in Sweden in 2025 (Nord Pool, 2026c). On the day-ahead market, electricity is traded at 12:00 central European time (midday) for all 24 hours of the following day separately, using the marginal price principle (Sorknæs et al., 2019). Hence, the market price is dependent on forecasted consumption, forecasted production, and transmission capacity for every hour on the day, determined one day in advance on the day-ahead market. In October 2025, Nord Pool switched to 15-minute intervals instead of hourly intervals for electricity trading, allowing more flexibility in the market and a better match of supply and demand. For this paper, the 15-minute prices from October 2025 onward are aggregated to hourly averages to preserve consistency with the hourly frequency used throughout the analysed period. The aggregation introduces a mild smoothing of within-hour price variation in the final months of the 2025 estimation window, but does not affect the daily or seasonal patterns that drive the wind-price relationship. The final price is set by compiling all orders at which participants are willing to sell, starting at −500 EUR to +4000 EUR per MWh. An identical process compiles buy orders for electricity in

the market. To eliminate price differences between zones, interconnections allow for cross-border energy flows. In the Nord Pool day-ahead market, planned cross-border exchanges are used to reduce price differences between areas where possible (Unger et al., 2018). After bids and offers have been submitted, Nord Pool derives a common unconstrained system price. Actual equilibrium prices, however, are determined by bidding zone once transmission constraints are imposed. Therefore, limited or congested interconnections can prevent full price convergence across areas (Unger et al., 2017, 2018). Svenska kraftnät is the public authority responsible for operating and developing Sweden's national electricity transmission grid and for managing transmission capacity (Svenska kraftnät, 2025; Sveriges Riksdag, 2025). The boundaries of Sweden's bidding zones are set where the main transmission grid bottlenecks are located. When the transmission capacity between zones is constrained, prices cannot fully converge across zones, so bidding-zone price differences reflect local supply and demand and transmission constraints rather than a failure of market participants to arbitrage observable price differences.

SE1 and SE2, the bidding zones in northern Sweden, tend to have a deficit in electricity consumption, while SE3 and SE4 in southern Sweden have a deficit in electricity production (Macedo et al., 2021). This North-South imbalance is reflected in Figure 3.3, which shows persistent net exports in SE1 and SE2 and persistent net imports in SE3 and SE4 over 2015–2025, hence a flow from North to South. The SE2–SE3 corridor carries by far the largest volume, reflecting SE2's role as the main transmission channel through which surplus from SE1 reaches SE3 and SE4. The SE1–SE2 and SE3–SE4 corridors carry substantially lower volumes, consistent with SE1 exporting a smaller surplus into SE2, and SE3 transmitting a share of its imports into SE4. During 2025, Sweden as a whole was a net exporter of energy.

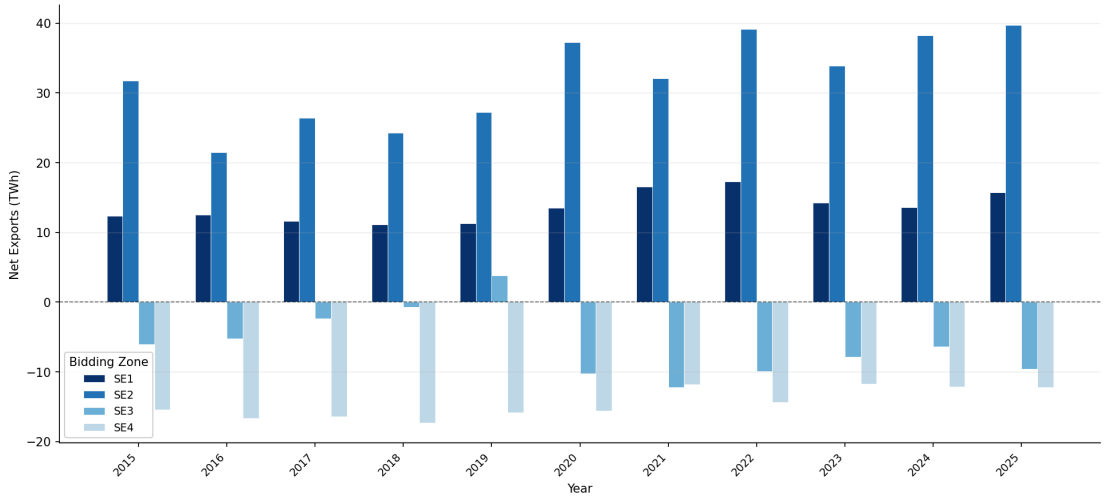
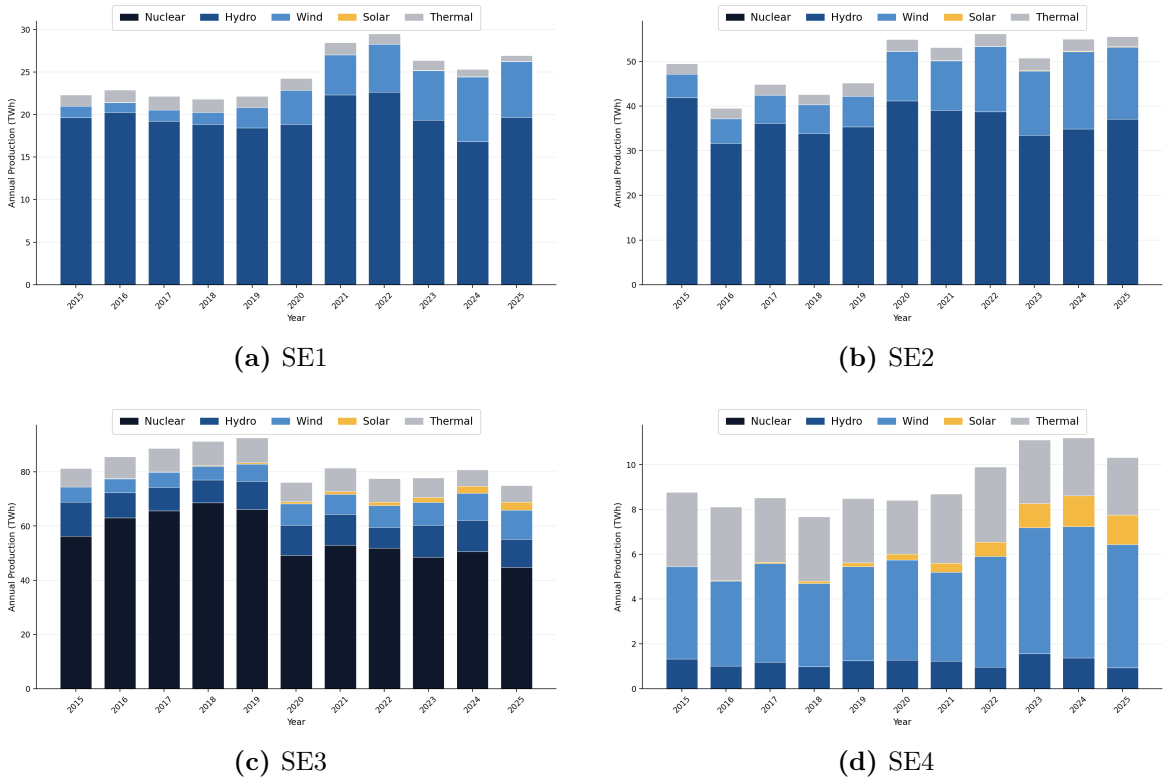


Figure 3.3: Energy net-export per bidding zone, 2015–2025

Source: Nord Pool, own calculations.

Sweden's bidding zones also differ in their means of electricity generation. As shown in Figure 3.4, SE1 and SE2 are strongly dependent on hydropower, while SE3 incorporates a significant share of nuclear energy in its energy composition. These differences in generation mix imply different marginal cost curves across zones. In particular, the large share of nuclear power in SE3 with low marginal costs contributes to a cost structure that differs from the other bidding zones (Macedo et al., 2021). When transmission between zones is constrained, such differences in marginal cost structure can translate into different equilibrium prices between bidding zones.



(a) SE1 **(b)** SE2

(c) SE3 **(d)** SE4

Figure 3.4: Electricity generation mix per bidding zone, 2015–2025

Source: Statistics Sweden (SCB) (2025), Nord Pool, own calculations.

Within this broader generation structure, wind power is the focus of this thesis. To assess the development of Sweden's wind power penetration over time, Figure 3.5 displays the wind share of total production per zone. It is observed that SE4 is the zone with the strongest relative share of wind power production in its production mix, aligning with Figure 3.4d. However, when looking at the absolute amount of energy produced from wind, this picture changes (Figure 3.6). SE2 is clearly the largest producer of wind energy overall, followed by SE3 and SE1, which surpassed the wind energy production of SE4 in 2020. Furthermore, the data shows that SE1 and SE2 strongly expanded their relative and absolute production of wind energy during the sample period.

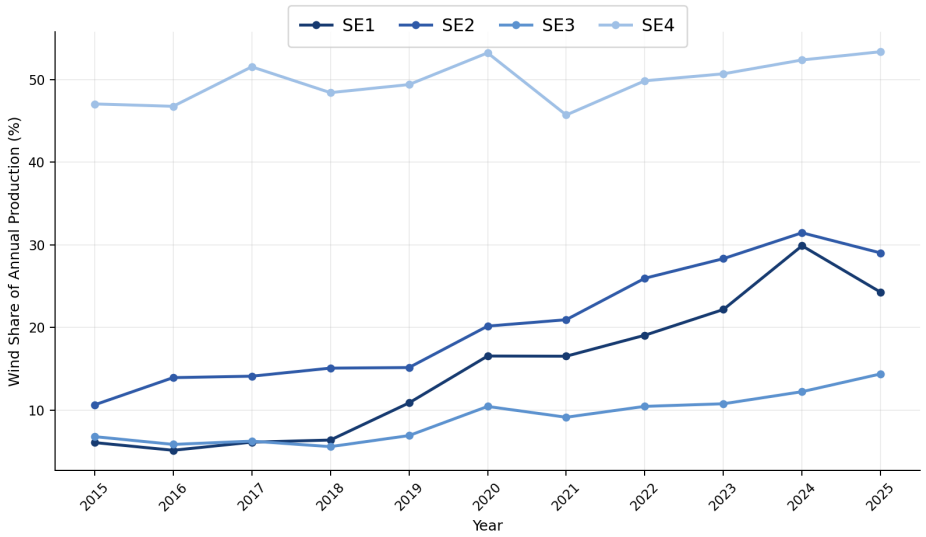


Figure 3.5: Wind share of annual electricity production per bidding zone

Source: Nord Pool, own calculations.

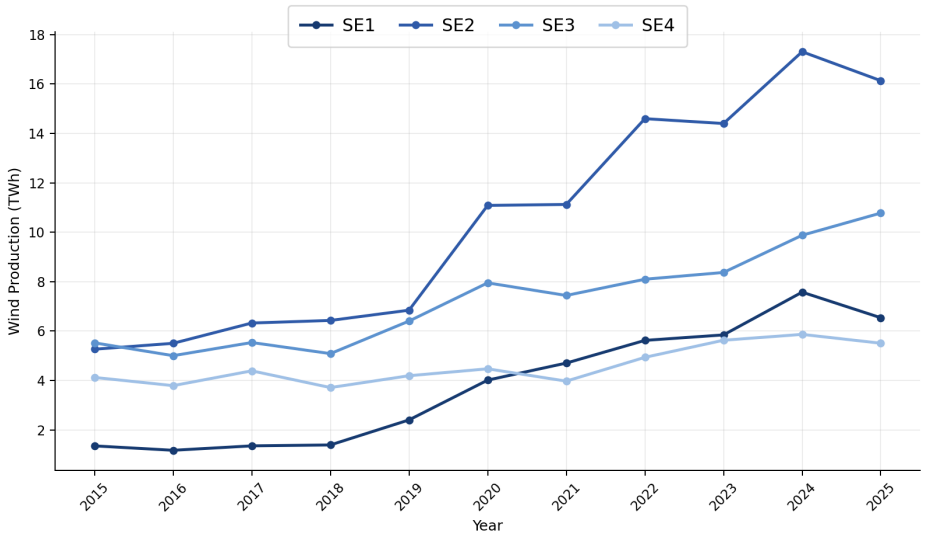


Figure 3.6: Absolute wind production per bidding zone

Source: Nord Pool, own calculations.

Structural differences between zones are reflected in the evolution of price levels and volatility over the analysed period. Until 2020, day-ahead prices moved closely together across all bidding zones. This suggests that transmission constraints did not create persistent price differences between Swedish zones during this period. From 2020 onwards, and particularly during the 2021/2022 energy crisis, day-ahead prices began to diverge across bidding zones (Figure 3.7). Price volatility followed a similar pattern, rising sharply during the crisis period and remaining elevated relative to pre-2020 levels (Figure 3.8). The divergence makes transmission constraints central to the analysis.

When prices separate across bidding zones, the relationship between wind production, prices, and volatility can differ depending on where wind enters the system. The following paragraph describes how transmission capacity on intra-Swedish corridors is determined.

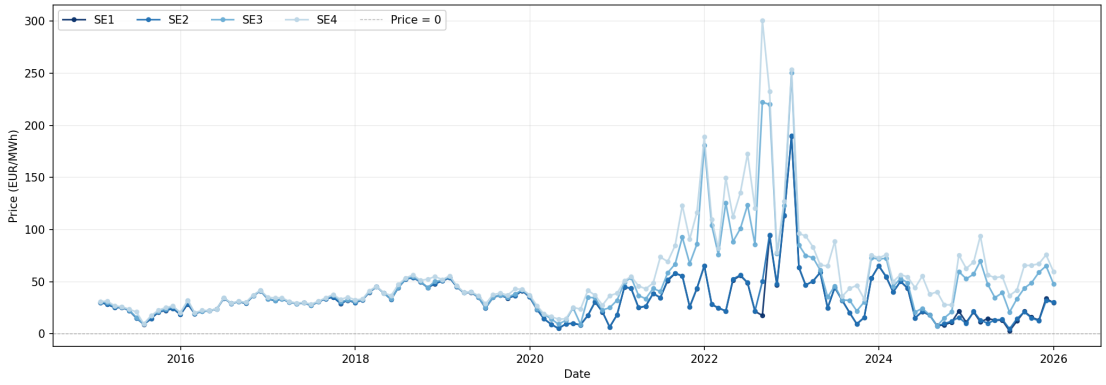


Figure 3.7: Price level (raw), monthly average

Source: Nord Pool, own calculations.

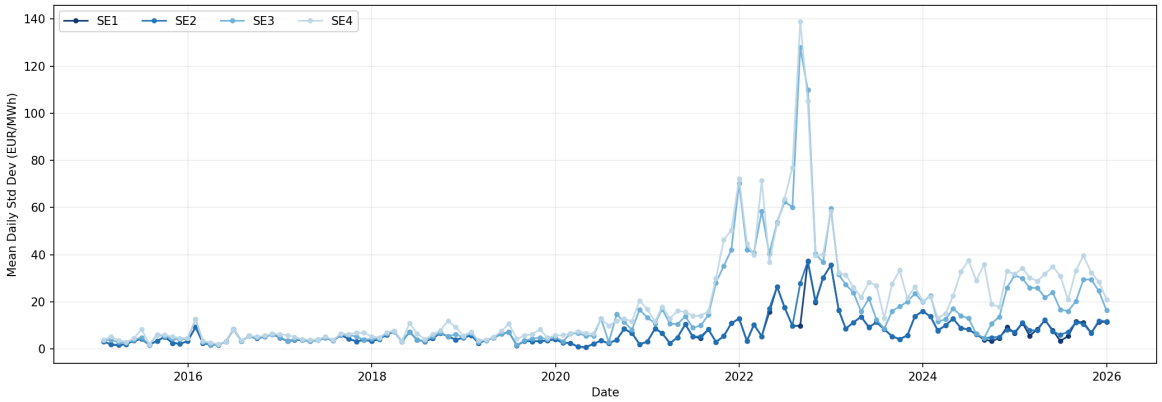


Figure 3.8: Price volatility (raw), monthly average

Source: Nord Pool, own calculations.

Price separation between zones was negligible before 2020. It rose sharply afterwards, with all three intra-Swedish corridors increasingly separating in price (Table 3.1). This increase in congestion partly reflects a structural change in how transmission capacity between bidding zones is calculated. On 30 October 2024, the Nordic day-ahead market transitioned from Available Transfer Capacity (ATC) to Flow-based Market Coupling (FBMC) (Nord Pool, 2026d). Under ATC, cross-zonal capacity was represented as transfer limits for each direction on each bidding zone border. Under FBMC, capacity is instead represented through flow-based parameters that account for how zonal trades load constrained grid elements across the wider network (Nordic RCC, 2024).

The change altered how existing grid constraints entered day-ahead market clearing, rather than changing the physical grid itself. From a methodological perspective, the system price is unaffected by the change as it is calculated unconstrained (Nord Pool, 2026a). External market reports suggest that this change contributed to wider Swedish price differences after 2024, especially between SE2 and the southern bidding zones (Energimarknadsinspektionen, 2025; Svenska Kraftnät, 2025b). By 2025, price differences between zones occurred in most hours. Importantly, the magnitude of separation differs strongly between corridors: the SE1–SE2 corridor saw frequent price differences, but the average spread remained close to zero. The SE2–SE3 corridor experienced a high frequency of price differences and a sharp widening in its magnitude, indicating that the post-2024 congestion is concentrated on this corridor. This transition represents a structural break in the institutional setting of Swedish zonal price formation and motivates the analysis of post-2024 wind-price sensitivities.

Table 3.1: Share of hourly price divergence between zones

	% hours with price difference			**Average price difference (%)**		
Year	**SE1−SE2**	**SE2−SE3**	**SE3−SE4**	**SE1−SE2**	**SE2−SE3**	**SE3−SE4**
2015	0.16%	7.55%	7.50%	0.06%	3.91%	4.08%
2016	0.00%	2.03%	5.27%	0.00%	0.98%	1.01%
2017	0.00%	3.76%	10.94%	0.00%	1.29%	3.02%
2018	0.00%	4.27%	15.42%	0.00%	0.70%	4.09%
2019	0.02%	7.40%	16.62%	0.00%	1.11%	3.76%
2020	0.06%	34.73%	29.06%	0.00%	47.28%	22.07%
2021	0.51%	47.63%	43.95%	0.15%	55.10%	22.00%
2022	4.43%	50.33%	21.26%	4.89%	108.58%	17.72%
2023	0.11%	22.97%	25.73%	0.01%	29.33%	25.49%
2024	19.68%	32.62%	42.05%	-1.63%	45.15%	38.97%
2025	96.24%	97.03%	96.74%	-1.07%	179.66%	30.70%

Note: The first set of columns reports the annual share of hours in which adjacent bidding zones had a non-zero price difference. The second set reports the average percentage price difference between adjacent zones. Negative values indicate that, on average, the first zone in the pair had a higher price than the second under the chosen ordering.

Chapter 4

Data and Methodology

4.1 Data

The sample covers Sweden's four bidding zones over the period 1 January 2015 to 31 December 2025. This section introduces the dependent variable, the main explanatory variable, and the control variables used in the empirical analysis.

Day-Ahead Spot Price The dependent variable is the hourly day-ahead spot price for each bidding zone, measured in EUR/MWh and sourced from Nord Pool. Descriptive statistics for all variables are reported in Table A.1.1 and Table A.1.2 in Section A.1. The spot price exhibits significant positive skewness and excess kurtosis across all zones. Skewness ranges from 3.96 in SE4 to 5.17 in SE1, while excess kurtosis ranges from 22.43 in SE4 to 46.53 in SE1. These values indicate a long right tail and infrequent but large upward price spikes. The price histograms in Figure A.1.1 confirm that the frequency of high prices increases between 2015 and 2025 across all zones. Negative prices remain limited over the full sample, but their frequency rises sharply from 2023 across all zones Figure A.2.6. Taken together, these patterns show that electricity prices are spike-prone and strongly non-Gaussian, which is a standard feature of power markets (Janczura et al., 2012; Weron, 2009).

We model the day-ahead spot price in logarithms. This follows the standard specification in the electricity price literature, where the log transformation is used to normalise the scale and fluctuation of the price series and to allow coefficients to be interpreted as elasticities (Ketterer, 2014). Because some hourly prices are negative, the series is shifted upward before taking logs so that the minimum observation equals 0.01. This is a practical adjustment that preserves the full sample when the logarithm would otherwise be undefined (Smith & Shively, 2018). The transformation has its largest

effect on low and negative prices, since the same constant is added to every observation before taking logs. When the original price is close to zero or negative, the shift makes up a large share of the transformed value. Hence, coefficients should be interpreted as elasticities of the shifted price rather than exact percentage effects on the original EUR/MWh price. We treat the shift as a practical preprocessing step to retain the full sample. The log price is deseasonalised before estimation to remove deterministic calendar variation from the series. Electricity prices exhibit systematic seasonality at the daily, weekly, and annual level, so the observed series contains both recurring calendar patterns and the underlying price variation that we want to model (Härdle & Trück, 2010). Following Ketterer (2014), we remove the deterministic calendar structure before estimating the price equation. We choose the final deseasonalisation specification by inspecting the autocorrelation function of the residual series after each step. If seasonal structure remains, it appears as spikes at the relevant seasonal lags. A residual ACF with no clear spikes at seasonal lags indicates that little systematic calendar structure remains (Enders, 2015).

The following deseasonalisation diagnostics use SE4 in 2025 as a representative example, but the same procedure is applied in all four zones. We begin with a simple deseasonalisation that removes separate dummies for hour-of-day, day-of-week, month-of-year, public holidays, and year effects. This dummy specification still leaves a spike of 0.52 at lag 24 and repeating peaks at multiples of 24 (Figure A.2.1). This pattern shows that the series still contains a clear daily calendar effect, but it also reflects the strong short-run persistence that is typical of electricity prices. We fit an AR(1) model to the partially deseasonalised series and inspect the ACF of its residuals. This step filters out the dominant first-order serial dependence and makes the remaining seasonal pattern easier to identify. Adding hour × day-of-week dummies reduces the 24-hour pattern but leaves a weekly spike at lag 168 (Figure A.2.2). Only when hour × month-of-year dummies are added does the residual ACF show no clear remaining seasonal spikes. We define the deseasonalised log price as the residual from a deterministic calendar regression:

$$\ln P_t = \sum_{h,d} \delta_{h,d} + \sum_{h,m} \lambda_{h,m} + \kappa \cdot 1_{\text{holiday},t} + \sum_{y} \mu_y + p_t \tag{4.1.0.1}$$

where P_t denotes the shifted day-ahead spot price after the adjustment described above, $\delta_{h,d}$ are hour-of-day × day-of-week interaction dummies, $\lambda_{h,m}$ are hour-of-day × month-of-year interaction dummies, $1_{\text{holiday},t}$ is a Swedish public holiday indicator, and μ_y are year dummies. The fitted component captures predictable calendar variation in the shifted log price, while the residual p_t captures the remaining within-hour

price variation after these effects have been removed. We use p_t as the deseasonalised dependent variable in all later estimations. In SE4 in 2025, the final specification explains 47.2% of the variation in log prices, compared with 30.2% when calendar effects enter only separately. The higher explanatory power shows that the interaction terms capture recurring within-week and within-year hourly patterns that separate hour, day, and month controls miss. With the seasonal component removed, we cap extreme observations rather than delete them. This preserves the full sample while limiting the influence of rare price spikes on estimation, in line with Gianfreda (2010). Any observation above the sample mean plus four standard deviations is set equal to that upper bound, and any observation below the sample mean minus four standard deviations is set equal to that lower bound. Ketterer (2014) applies the same logic using a three-standard-deviation rule. A visualisation of the outlier treatment can be found in Section A.3.

Wind Power Production Forecast The main variable of interest is the hourly wind power production forecast for each bidding zone, measured in MWh and sourced from Nord Pool. Because the day-ahead price is set before the delivery hour, the regressors should be aligned with the information available to market participants at the time of bidding. This means using day-ahead forecasts of wind production rather than realised quantities, since these are observed only after the price has been determined. This approach follows Würzburg et al. (2013), who stress that foreseen production and load are the basis for day-ahead trading decisions. Jónsson et al. (2010) also show that forecasted wind is the relevant explanatory variable when analysing day-ahead price formation. In the mean equation, the expected effect of wind is negative because wind enters the merit-order at near-zero marginal cost and displaces more expensive generation technologies. The expected effect in the variance equation is more ambiguous. Wind forecast is log-transformed and enters the regression without deseasonalisation, consistent with the treatment of wind generation in Ketterer (2014). Non-deseasonalisation is supported by the fact that the seasonal component is small and calendar dummies jointly explain only 12.0% of total variance in the log wind forecast in SE4 in 2025, with the remaining 88.0% attributable to weather-driven variation.

Consumption Forecast We include hourly consumption forecasts for each bidding zone as a proxy for electricity demand, measured in MWh and sourced from Nord Pool. This variable captures expected demand at the time the day-ahead price is set. Jónsson et al. (2010) show that wind has its strongest association with spot prices

when measured relative to forecasted load, while Ketterer (2014) shows that the same amount of wind can have different price effects under high and low demand. We include the consumption forecast to control for the level of demand in the market. As in the wind specification, we use the forecast rather than realised consumption because the day-ahead price is determined before delivery. Consumption is log-transformed and fully deseasonalised using hour-of-day × day-of-week and hour-of-day × month-of-year interaction dummies. Full deseasonalisation is justified by clear calendar patterns in the consumption forecast. As shown in Figure A.2.4, consumption is higher during the day than at night, lower on weekends than on weekdays, and higher in winter than in summer. Higher expected demand should increase the market-clearing price because more expensive generation is needed when forecasted consumption rises.

Net Exchange Flows We include hourly bilateral net exchange flows between each bidding zone and its neighbouring bidding zones, measured in MWh and sourced from Nord Pool. Following Würzburg et al. (2013), bilateral exchange flows are included as market controls because exports and imports contain information about price formation that may otherwise be absorbed by the estimated wind coefficient. The set of bilateral controls follows the Swedish bidding zone interconnections shown in Figure 3.2. Bilateral flows enter the regression in levels without log transformation or deseasonalisation. Log transformation is not included because net exchange is negative in many cases, since negative values indicate net exports and $\log(x)$ is undefined for non-positive values. Deseasonalisation is not applied to the exchange-flow controls, in line with the treatment of cross-border market-coupling variables in Ketterer (2014). The expected sign of net exchange coefficients varies by zone and neighbour, reflecting the direction of typical electricity flow. Although net exchange is jointly determined with prices in the market-coupling auction, we include bilateral exchange flows to account for cross-border trade. Their coefficients are not interpreted as independent effects on price. The purpose is instead to avoid attributing price variation linked to trade flows to wind production. Limitations of this approach are discussed in Section 6.3.

Hydro Reservoir Levels We include weekly hydro reservoir levels for each bidding zone, measured in GWh and sourced from Nord Pool. By including hydro reservoir levels, we control for the availability of hydro power generation. As shown in Figure 3.4, hydro power is the dominant electricity generation source in SE1 and SE2. Reservoir levels also play a central role in Nordic price formation, since Nord Pool prices are strongly shaped by hydro production capacity (Huisman et al., 2013). Actual hydro generation is not used because it is a dispatch outcome, as producers adjust hydro

production in response to price signals. Reservoir levels are instead a proxy for the stock of stored hydro energy available for generation. Hydro reservoir levels are log-transformed and partially deseasonalised using month-of-year dummies only. Full deseasonalisation is not applied because the series is observed at weekly frequency and then assigned to each hour within the corresponding week, meaning hour-of-day and day-of-week dummies explain 0.0% of variance by construction. Month dummies explain 97.1% of variance in log hydro reserves in SE4 and follow the Nordic hydro dispatch cycle visible in Figure A.2.5. Higher reservoir levels increase the supply of low-cost hydro generation, and the hydro reservoir level coefficient is expected to be negative.

Oil and Gas Prices Finally, we include the prices of US Light Crude Oil and Dutch TTF Natural Gas as controls, sourced from Bloomberg Terminal (Bloomberg Terminal, 2026). These are included to control for the cost of fossil fuel-based electricity generation. Actual fossil fuel generation is not used, since dispatch decisions respond to electricity prices and would raise endogeneity concerns. Fuel prices are instead a proxy for changes in fuel input costs faced by thermal generators in Sweden and in neighbouring interconnected markets, which can affect Swedish prices when thermal generation is marginal or when cross-border trade transmits price pressure to Sweden. Both series are log-transformed and enter with a 24-hour lag, so that the variables reflect information available to market participants before bids are submitted to the day-ahead auction. Deseasonalisation is not applied because the series are observed at a daily frequency and assigned to each hour of the corresponding trading day. As a result, hour-of-day and day-of-week dummies add no meaningful variation. Higher fossil fuel prices increase the cost of thermal electricity production and are expected to put upward pressure on spot prices (Woo et al., 2011). Hence, the coefficients on oil and gas are expected to be positive.

4.2 Methodology

4.2.1 Mean Equation

The mean equation is designed to account for persistence in hourly electricity prices while estimating the association between market fundamentals and the log day-ahead spot price. Figure A.2.1 shows the ACF of the deseasonalised log spot price for SE4 over 2025, which is representative of all four zones. The autocorrelation at lag 1 is 0.90 and decays slowly for the following lags, indicating that the current price is strongly

related to its recent past. To test this formally, we apply the Ljung-Box portmanteau test, which evaluates whether the autocorrelations up to a given lag are jointly equal to zero (Ljung & Box, 1978). Table 4.1 reports the test statistics for lags 1 through 20.

Table 4.1: Ljung-Box test for serial correlation in the deseasonalised log spot price

Lag	SE1	SE2	SE3	SE4
1	16,262.95***	16,216.19***	15,742.09***	15,124.84***
2	31,077.45***	30,857.81***	29,589.99***	27,914.72***
3	44,592.14***	44,164.20***	41,941.26***	38,926.43***
4	57,007.67***	56,409.63***	53,172.80***	48,614.78***
5	68,507.13***	67,785.50***	63,492.13***	57,272.94***
10	117,292.37***	115,529.34***	106,462.17***	91,553.87***
15	155,422.72***	151,782.13***	139,199.06***	116,564.14***
20	183,649.41***	177,771.94***	164,041.53***	135,253.51***

Notes: Ljung-Box Q-statistics for the deseasonalised log spot price series, estimated over the sample 1 January 2025 to 31 December 2025. The null hypothesis is no serial correlation. The series is tested prior to any model estimation. $^{***}p < 0.01$, $^{**}p < 0.05$, $^{*}p < 0.10$.

Table 4.1 rejects the null hypothesis of no serial correlation at the 1% level for every lag and every bidding zone. The rejection confirms that the log day-ahead spot price contains systematic persistence even after deseasonalisation. This persistence motivates an autoregressive mean equation, since omitting lagged price dynamics would leave serial structure in the residuals and make it harder to separate the wind-price relationship from general price persistence. To account for the serial correlation documented in Table 4.1, the mean equation is specified as an ARMAX model. For each bidding zone $z \in \{\text{SE1}, \text{SE2}, \text{SE3}, \text{SE4}\}$, the mean equation is:

$$\begin{aligned} p_{z,t} = \alpha_z &+ \sum_{i=1}^{p} \phi_i p_{z,t-i} + \beta_{\text{wind}} w_{z,t} + \beta_{\text{hydro}} r_{z,t} + \beta_{\text{cons}} c_{z,t} \\ &+ \sum_{n \in \mathcal{N}(z)} \beta_{\text{exch},n} X_{z,n,t} + \beta_{\text{oil}} o_{t-24} + \beta_{\text{gas}} g_{t-24} + \sum_{j=1}^{q} \theta_j \varepsilon_{z,t-j} + \varepsilon_{z,t} \end{aligned} \tag{4.2.1.1}$$

All variables in Equation 4.2.1.1 enter the model after the preprocessing described in the data section. The variable $p_{z,t}$ is the deseasonalised log day-ahead spot price in zone z at time t, defined as the residual from the deterministic calendar regression in Equation 4.1.0.1 and outliers capped. The variable $w_{z,t}$ denotes forecasted wind power production, $r_{z,t}$ denotes hydro reservoir levels, $c_{z,t}$ denotes forecasted consumption, and $X_{z,n,t}$ denotes bilateral net exchange between zone z and neighbouring zone or country n. The set $\mathcal{N}(z)$ denotes the neighbours of zone z. Positive values of $X_{z,n,t}$ indicate net imports into zone z from neighbour n. The variables o_{t-24} and g_{t-24} denote lagged oil

and gas prices. The autoregressive terms ϕ_i capture persistence in the deseasonalised log price, while the moving average terms θ_j capture the effect of past price shocks not explained by the autoregressive structure. The ARMA orders p and q are selected by comparing BIC values from a grid search over $p, q \in \{0, 1, 2, 3\}$, described in Chapter 5. The coefficient of interest is β_{wind}, which measures the association between log wind power production and the deseasonalised log day-ahead spot price. A 1% increase in wind power production is associated with an approximate $\beta_{\text{wind}}\%$ change in the deseasonalised log day-ahead spot price, holding all other covariates constant.

4.2.2 Variance Equation

The variance equation is designed to account for time-varying conditional price variance. To test whether such variance dynamics remain after estimating the mean equation, we apply Engle's ARCH test to residuals from Equation 4.2.1.1, estimated without a GARCH component (Engle, 1982). For this diagnostic step, we set $p = q = 1$. This low-order ARMA filter captures immediate autoregressive and moving average dependence while avoiding reliance on the final lag-order selection. Hence, the test examines whether ARCH effects remain after accounting for price persistence and market fundamentals. Table 4.2 reports the test statistics for lags 1 through 20.

Table 4.2: Engle's ARCH test for conditional heteroscedasticity in mean-only ARMAX(1,1) residuals

Lag	SE1	SE2	SE3	SE4
1	554.04***	252.89***	61.62***	79.47***
2	555.69***	409.18***	261.65***	195.58***
3	580.51***	478.05***	301.09***	248.96***
4	588.50***	478.80***	302.84***	251.84***
5	591.11***	482.77***	304.09***	270.06***
10	612.30***	489.73***	316.18***	296.64***
15	654.06***	497.85***	326.49***	321.39***
20	661.51***	506.82***	336.43***	391.84***

Notes: Engle's LM test statistics for ARCH effects in residuals from a mean-only ARMAX(1,1) specification estimated separately by bidding zone over the sample 1 January 2025 to 31 December 2025. The specification uses the conditional-mean variables defined in Equation 4.2.1.1 but excludes the GARCH-X variance equation. The null hypothesis is no ARCH effects up to the reported lag. $^{***}p < 0.01$, $^{**}p < 0.05$, $^{*}p < 0.10$.

The null hypothesis of no ARCH effects is rejected at the 1% level for every lag length and every bidding zone. This indicates that volatility clustering remains after accounting for price persistence and market fundamentals. Periods of large price movements tend

to be followed by further large movements, while calmer periods also tend to persist. Therefore, a model that assumes constant error variance is misspecified for this data. Engle's ARCH framework models this type of conditional heteroscedasticity by allowing the conditional variance to depend on past squared errors (Engle, 1982). Bollerslev's GARCH extension generalises this idea by also allowing past conditional variances to enter the variance equation, reducing the number of lag terms needed to capture persistent volatility dynamics (Bollerslev, 1986).

For each zone z, the variance equation is specified as a multiplicative GARCH-X(1,1) model:

$$h_{z,t} = \left(\omega_z + \alpha\varepsilon_{z,t-1}^2 + \delta h_{z,t-1}\right) \exp\left(\sum_k \gamma_k x_{z,k,t}\right) \tag{4.2.2.1}$$

where $h_{z,t}$ is the conditional variance of $\varepsilon_{z,t}$, ω_z is a zone-specific constant, $\varepsilon_{z,t-1}^2$ is the squared error from the previous period, and $h_{z,t-1}$ is the lagged conditional variance. The GARCH-X(1,1) specification builds on the GARCH framework introduced by Bollerslev (1986). In this specification, the $(1, 1)$ order means that the variance equation includes one lag of the squared error and one lag of the conditional variance. The set $\{x_{z,k,t}\}$ contains the same processed exogenous controls as the mean equation: $w_{z,t}$, $r_{z,t}$, $c_{z,t}$, the bilateral net exchange variables $X_{z,n,t}$, and the lagged fuel-price variables o_{t-24} and g_{t-24}. The parameters α and δ describe the GARCH part of the variance equation. α measures how strongly a large residual from the previous hour feeds into current volatility, while δ measures how strongly past volatility carries over. In a standard GARCH(1,1) model without exogenous variables, $\alpha + \delta < 1$ is the mean-reversion condition for the conditional variance (Bollerslev, 1986). In our GARCH-X specification, the conditional variance is allowed to vary with observed market variables and follows the approach in Ketterer (2014). Our implementation enters the exogenous variables through the multiplicative term $\exp(\sum_k \gamma_k x_{z,k,t})$. This means that the baseline GARCH component is scaled by the market controls rather than shifted additively. The main advantage is that $h_{z,t}$ remains positive by construction even when an exogenous coefficient is negative. The coefficient of interest in the variance equation is γ_{wind}. Since wind enters in logs, a positive γ_{wind} means that higher wind production is associated with higher conditional variance, while a negative γ_{wind} means that higher wind production is associated with lower conditional variance.

A further requirement for the ARMAX-GARCH-X framework is that the series entering the model are stationary. Table A.2.1 reports Augmented Dickey-Fuller tests for the series entering the 2025 estimation window. The tests reject the null of a unit root for the deseasonalised log day-ahead spot price, log wind production forecast,

deseasonalised log consumption forecast, deseasonalised log hydro reservoir levels, and all zone-specific net exchange variables across the four bidding zones. The only exceptions are the common oil and gas price series, for which the null is not rejected in this one-year window. We retain these variables as external fuel-cost controls because their role is secondary to the analysis. The robustness checks show that excluding them leaves the estimated wind-price sensitivity largely unchanged.

The mean and variance equations are estimated jointly by maximum likelihood. The conditional error is assumed to follow a Student's t distribution with degrees of freedom fixed at five. The choice of five is guided by the excess kurtosis documented in Section 4.1. It is not obtained by matching that raw distribution exactly since the model is estimated after the price transformation, and the GARCH-X equation captures part of the remaining tail behaviour through time-varying volatility. The fixed Student's t distribution instead provides a simple way to allow heavy-tailed errors. This is in line with electricity-price applications using Student's t errors (Koopman et al., 2007). Inference is based on Bollerslev-Wooldridge robust standard errors. Together, Equation 4.2.1.1 and Equation 4.2.2.1 define the ARMAX(p,q)-GARCH-X(1,1) specification used throughout this paper.

4.2.3 Distributional Heterogeneity and Quantile Regression

The baseline ARMAX-GARCH-X model estimates how the average conditional effect of wind on the log day-ahead spot price evolves. That framework remains the main specification of the thesis. We complement it with a quantile-regression model to study whether the wind effect differs across the conditional price distribution. This allows β_{wind} to vary between low-price, median-price, and high-price outcomes instead of imposing one average conditional effect. The method builds on the regression-quantile framework of Koenker and Bassett (1978) and follows electricity-price applications that use quantile regression with lagged prices and exogenous controls (Maciejowska, 2020). We estimate the model in rolling-windows with exogenous controls for each Swedish bidding zone.

For each zone $z \in \{\text{SE1}, \text{SE2}, \text{SE3}, \text{SE4}\}$ and each quantile $\tau \in \{0.10, 0.50, 0.90\}$, we use the following rolling QARX specification:

$$
\begin{aligned}
Q_\tau(p_{z,t} \mid \mathcal{F}_{z,t}) = \alpha_z(\tau) + \sum_{i=1}^{p} \phi_i(\tau) p_{z,t-i} + \beta_{\text{wind}}(\tau) w_{z,t} \\
+ \beta_{\text{hydro}}(\tau) r_{z,t} + \beta_{\text{cons}}(\tau) c_{z,t} + \sum_{n \in \mathcal{N}(z)} \beta_{\text{exch},n}(\tau) X_{z,n,t} \\
+ \beta_{\text{oil}}(\tau) o_{t-24} + \beta_{\text{gas}}(\tau) g_{t-24}. \qquad (4.2.3.1)
\end{aligned}
$$

All variables in Equation 4.2.3.1 enter the model after the preprocessing described in the data section. Here, $Q_\tau(p_{z,t} \mid \mathcal{F}_{z,t})$ denotes the conditional τ-quantile of the deseasonalised log day-ahead spot price in zone z at time t. The variable $p_{z,t}$ is the residual from the deterministic calendar regression defined in Equation 4.1.0.1. The information set $\mathcal{F}_{z,t}$ contains the lagged deseasonalised price terms and the processed exogenous controls. The variable $w_{z,t}$ denotes forecasted wind power production, $r_{z,t}$ denotes hydro reservoir levels, $c_{z,t}$ denotes forecasted consumption, and $X_{z,n,t}$ denotes bilateral net exchange between zone z and neighbouring zone or country n. The set $\mathcal{N}(z)$ denotes the neighbours of zone z. Positive values of $X_{z,n,t}$ indicate net imports into zone z from neighbour n. The variables o_{t-24} and g_{t-24} denote lagged oil and gas prices. The coefficient of primary interest is $\beta_{\text{wind}}(\tau)$, which measures the association between log wind power production and the conditional τ-quantile of the deseasonalised log day-ahead spot price. We estimate the quantile model at $\tau = 0.10$, $\tau = 0.50$, and $\tau = 0.90$. These quantiles represent the lower tail, median, and upper tail of the conditional price distribution. This choice allows us to compare $\beta_{\text{wind}}(\tau)$ across low-price, median-price, and high-price outcomes.

The quantile specification is a QARX extension of the baseline mean equation rather than a quantile version of the full ARMAX-GARCH-X model. It keeps the same dependent variable, wind measure, core exogenous controls, rolling-window design, and autoregressive lag order, but omits the moving average and GARCH components. The moving average component is omitted because lagged residual terms are less straightforward in quantile regression, where residuals depend on the estimated quantile. The GARCH component is omitted because quantile regression already studies different points of the conditional price distribution rather than modelling the conditional variance separately. We interpret the rolling quantile estimates as complementary evidence on distributional heterogeneity in $\beta_{\text{wind}}(\tau)$, not as direct substitutes for the baseline mean and variance coefficients. The autoregressive order is taken from the baseline specification to keep the dynamic structure aligned across models. The specification in Equation 4.2.3.1 is estimated in the same rolling one-year windows as the baseline model.

4.2.4 Zone-Level Estimation Strategy

The model is estimated separately for SE1, SE2, SE3, and SE4 due to the structural differences between Sweden's bidding zones. As outlined previously, SE1 and SE2 are net-exporters of energy, while SE3 and SE4 are net importers (Figure 3.3). Furthermore, SE1 and SE2 are hydro-dominated, while SE3 has a larger nuclear share and SE4 a larger wind share (Figure 3.4). A pooled specification with a common wind coefficient would restrict the wind-price relationship to be the same across SE1, SE2, SE3, and SE4, thus obscuring zone-level heterogeneity. Estimating the model at the zone level is consistent with earlier work that emphasises regional heterogeneity in electricity price formation and the importance of zone-specific market structure (Macedo et al., 2021; Woo et al., 2011). To keep estimates comparable, we estimate each zone using the same ARMA(p, q) lag structure once the common order has been selected. Differences in wind-price sensitivity can then be interpreted as differences in the wind-price relationship rather than as results of zone-specific changes in lag structure.

4.2.5 Rolling-Window Estimation

We re-estimate the model in rolling one-year windows from 2015 to 2025 to examine whether the wind-price relationship changes over time within each bidding zone. This rolling-window design follows earlier merit-order studies that allow the wind-price relationship to vary over time (Clò et al., 2015; Ketterer, 2014). To keep estimates comparable across windows, we hold the selected ARMA(p, q) lag structure and the GARCH-X$(1, 1)$ variance specification fixed in every window. Changes in the estimated coefficients can then be interpreted as changes in the conditional wind-price relationship rather than as results of a changing model specification. All preprocessing steps described in Section 4.1 are applied independently within each estimation window. For each one-year window, the level shift, log transformation, deseasonalisation, and outlier capping are carried out using only the observations in that window. The outlier threshold is computed from the mean and standard deviation of the deseasonalised log prices within that window, so the $\pm 4\sigma$ bounds reflect the price distribution in that specific period rather than the full 2015–2025 sample. This prevents the extreme price levels of the 2021–2022 energy crisis from distorting the outlier bounds of windows drawn from calmer periods, and vice versa.

Chapter 5

Results

5.1 Model Selection

We select the ARMA order by estimating Equation 4.2.1.1 and Equation 4.2.2.1 jointly over the sample 1 January 2025 to 31 December 2025. The grid search covers $p, q \in \{0, 1, 2, 3\}$. The resulting BIC values are reported in Table A.4.1–Table A.4.4. The full ARMA–GARCH-X model is estimated jointly in every case, but the tables report only the autoregressive and moving average orders used to document lag selection.

Model choice is based on BIC together with three additional requirements. First, all roots of the autoregressive polynomial must lie outside the unit circle. Second, all roots of the moving average polynomial must lie outside the unit circle. Third, autoregressive and moving average roots must be sufficiently separated, since near-cancellation implies that the autoregressive and moving average terms partly offset each other and weaken identification. Table A.4.1–Table A.4.4 show that ARMA$(3, 1)$ provides the strongest common specification across the four bidding zones. In SE3 and SE4, ARMA$(3, 1)$ attains the lowest BIC in the reported grid. In SE1 and SE2, nearby specifications achieve similarly low BIC values, but these gains are small and do not point to a clearly superior alternative that is robust across zones. Several competing specifications, such as ARMA$(2, 2)$, ARMA$(2, 3)$, and ARMA$(3, 3)$, also produce autoregressive and moving average terms that offset each other more closely, which weakens identification without significantly improving fit. Therefore, ARMA$(3, 1)$ provides the best balance of fit, parsimony, and stability across zones. Residual diagnostics do not alter this conclusion. The Ljung–Box test on standardised residuals rejects the null of no serial correlation at higher lags for most candidate specifications, indicating that low-order ARMA terms cannot fully absorb dependence in hourly electricity prices. This pattern is not specific to ARMA$(3, 1)$. The Ljung–Box test on squared standardised residuals, evaluated after

fitting the full ARMAX–GARCH-X model, shows a similar pattern across specifications and does not favour a different ARMA order. We impose ARMA$(3, 1)$ as the common specification across all zones and all rolling-windows.

5.2 Baseline Estimation

With the ARMA$(3, 1)$ lag structure selected, we report the baseline estimates from the jointly estimated ARMAX(3,1)-GARCH-X(1,1) model for the sample 1 January 2025 to 31 December 2025. Table 5.1 reports the coefficients from the mean and variance equations across all four bidding zones, while the bilateral net exchange coefficients are reported separately in Table A.5.1–Table A.5.4.

The wind coefficient $\hat{\beta}_{\text{wind}}$ is negative and significant at the 1% level in all four zones. The magnitude of the effect differs substantially across zones. SE3 exhibits the strongest wind-price sensitivity ($\hat{\beta}_{\text{wind}} = -0.121$), followed by SE2 at -0.090 and SE4 at -0.073. SE1 exhibits the weakest effect at -0.014, well below the estimates for the other three zones. Because the coefficient is an elasticity, the SE3 estimate implies that a 1% increase in forecasted wind production is associated with an approximate 0.121% decrease in the deseasonalised log day-ahead spot price, holding all other covariates constant. A notable feature of the baseline estimates is the size of the gap within the northern pair. Despite their similar net-export positions and broadly similar generation mixes, SE2's wind elasticity (-0.090) is far more negative than SE1's (-0.014). Whether this gap is specific to 2025 or reflects a persistent structural difference is examined in the rolling-window analysis in Section 5.3.

The consumption coefficient is positive in all four zones. It is substantially larger in SE3 and SE4, where $\hat{\beta}_{\text{cons}} = 1.233$ and 1.255, respectively, both significant at the 1% level. In SE1, the coefficient is 0.065, significant at the 10% level, while the SE2 estimate of 0.122 is statistically insignificant.

The hydro reservoir coefficient is positive and significant only in SE2 ($\hat{\beta}_{\text{hydro}} = 0.386$, $p < 0.01$) and statistically insignificant in the remaining three zones. The oil and gas price coefficients are statistically insignificant across all four zones. Both variables enter in logs with a 24-hour lag at daily frequency, so they are constant across all hours of a given trading day.

Bilateral net import coefficients in the mean equation are negative and significant across nearly all interconnections. The pattern is especially uniform in SE1, SE2, and SE3, where all bilateral import coefficients are negative and statistically significant. In SE4, net imports from DK2, Germany, and Poland are also associated with lower local

prices, while the coefficient on imports from SE3 is small and statistically insignificant. The autoregressive and moving average terms are all statistically significant across the four zones, and their primary function is to absorb serial dependence in prices.

Turning to the variance equation, the wind coefficient $\hat{\gamma}_{\text{wind}}$ is negative and significant at the 1% level in SE1 and SE2, at -0.394 and -0.675 respectively (Table 5.1). In SE3, the coefficient is small at -0.068 and statistically insignificant. In SE4, it is -0.082 and significant at the 5% level. The ARCH and GARCH terms are positive and significant in all four zones, with the implied persistence $\alpha + \delta$ remaining below 1 throughout. Consumption is associated with higher conditional variance in SE1 and SE2, but with lower conditional variance in SE3 and SE4. The remaining variance-equation coefficients are mixed in sign and significance across zones.

Table 5.1: ARMAX(3,1)-GARCH-X(1,1) baseline estimates, 2025

	SE1	**SE2**	**SE3**	**SE4**
Mean equation				
α_z	-0.435^{*}	0.559	1.768	0.454
	(0.228)	(0.536)	(1.126)	(1.179)
$w_{z,t}$	-0.0143^{***}	-0.0904^{***}	-0.1206^{***}	-0.0733^{***}
	(0.0023)	(0.0085)	(0.0117)	(0.0102)
$r_{z,t}$	0.046	0.386^{***}	-0.368	-0.240
	(0.062)	(0.119)	(0.307)	(0.212)
$c_{z,t}$	0.065^{*}	0.122	1.233^{***}	1.255^{***}
	(0.034)	(0.083)	(0.130)	(0.133)
o_{t-24}	0.071	-0.088	-0.135	0.187
	(0.057)	(0.149)	(0.317)	(0.362)
g_{t-24}	0.039	0.054	-0.081	-0.215
	(0.033)	(0.097)	(0.166)	(0.171)
ϕ_1	2.046^{***}	2.000^{***}	1.858^{***}	1.904^{***}
	(0.035)	(0.037)	(0.050)	(0.037)
ϕ_2	-1.312^{***}	-1.240^{***}	-1.031^{***}	-1.082^{***}
	(0.050)	(0.050)	(0.055)	(0.043)
ϕ_3	0.261^{***}	0.233^{***}	0.165^{***}	0.171^{***}
	(0.017)	(0.016)	(0.011)	(0.012)
θ_1	-0.770^{***}	-0.756^{***}	-0.755^{***}	-0.808^{***}
	(0.030)	(0.034)	(0.051)	(0.037)
Variance equation				
ω_z	-0.199	-4.901^{*}	-10.991^{***}	-10.112^{***}
	(2.743)	(2.581)	(2.338)	(2.488)
α	0.644^{***}	0.624^{***}	0.183^{***}	0.255^{***}
	(0.045)	(0.042)	(0.046)	(0.038)
δ	0.116^{***}	0.182^{***}	0.482^{***}	0.366^{***}
	(0.026)	(0.026)	(0.098)	(0.071)
$w_{z,t}$	-0.394^{***}	-0.675^{***}	-0.068	-0.082^{**}
	(0.038)	(0.049)	(0.045)	(0.037)
$r_{z,t}$	-0.050	-1.110	0.097	1.381^{**}
	(0.690)	(0.775)	(0.851)	(0.538)
$c_{z,t}$	2.759^{***}	2.062^{***}	-1.549^{**}	-1.444^{**}
	(0.985)	(0.799)	(0.646)	(0.583)
o_{t-24}	-0.867	1.488^{*}	1.219	1.152
	(0.919)	(0.899)	(0.800)	(0.836)
g_{t-24}	-0.690^{*}	-0.839^{*}	0.521	0.565
	(0.404)	(0.436)	(0.373)	(0.373)
Persistence ($\alpha + \delta$)	0.759	0.805	0.665	0.622
N	8,736	8,736	8,736	8,736
Log-likelihood	17,140	10,818	6,690	5,322
AIC	$-34{,}232$	$-21{,}585$	$-13{,}324$	$-10{,}592$
BIC	$-34{,}062$	$-21{,}401$	$-13{,}126$	$-10{,}408$

Notes: ARMAX(3,1)-GARCH-X(1,1) estimates with all exogenous controls entering both the mean and variance equations. The variance equation uses a multiplicative GARCH-X specification. Bilateral net exchange coefficients are reported separately in Table A.5.1–Table A.5.4. Robust standard errors in parentheses. $^{***}p < 0.01$, $^{**}p < 0.05$, $^{*}p < 0.10$.

5.3 Rolling-Window Results

5.3.1 Mean Equation

The rolling-window estimates place the 2025 baseline estimates in an eleven-year context by showing how $\hat{\beta}_{\text{wind}}$ evolves across successive one-year windows from 2015 to 2025. Figure 5.1 plots the sequence of annual rolling-window estimates, while Table A.7.1 reports the corresponding coefficients. The merit-order effect is present throughout almost the full sample, but its magnitude is not stable over time, and the cross-zone ordering shifts as market conditions change.

In the pre-2020 windows, SE1 and SE2 remain close to each other with coefficients near zero. SE3 and SE4 are consistently more negative and also relatively close to each other. The main exception is SE4 in 2015, where the coefficient is markedly more negative than in any other pre-2020 window. Apart from that early outlier, the pre-2020 pattern is stable, with a clear North-South ordering. The first clear widening in the gap between zones appears in the 2020 window. The zones separate into a distinct ordering, and SE3 becomes the most negative; its coefficient deepens far more sharply than SE4's and breaks from the earlier pattern of the two zones moving closely together. The strongest common deepening occurs in the crisis window of 2022. In 2022, the coefficient reaches -0.067 in SE1, -0.113 in SE2, -0.151 in SE3, and -0.103 in SE4. These are the most negative estimates in the sample for SE1, SE2, and SE4. The crisis also widens the spread between zones. SE3 remains the most wind-price sensitive zone, while SE2 becomes much more sensitive than SE1, and SE4 also deepens substantially. The coefficients recover in 2023, but only partially. All zones return toward their earlier range but do not reach pre-2020 levels. The recovery is especially incomplete in SE3, which remains substantially more negative than its pre-2020 level. After the partial recovery in 2023, the coefficients diverge sharply in 2025. The SE1–SE2 gap is clearly a late-sample outcome rather than a feature of the earlier windows. In 2023, the two zones still display similar coefficients, and by 2025, they have separated substantially despite their broadly comparable production structures and net-export positions. The timing of this divergence and a structural explanation are examined in Section 5.4.

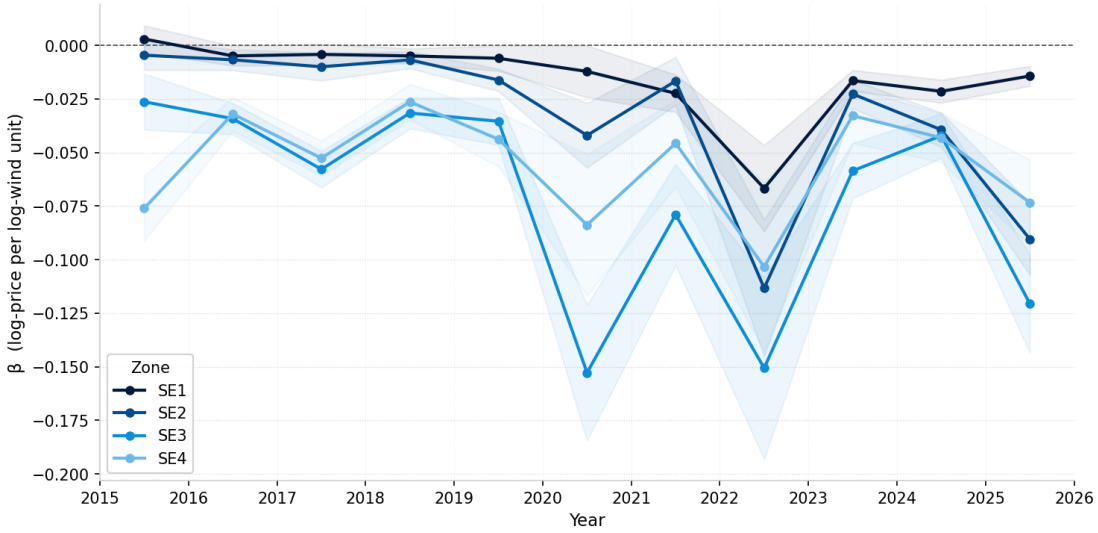


Figure 5.1: Rolling-window mean coefficient (1 year window, 1 year shift)

Source: Own calculations.

5.3.2 Variance Equation

The rolling-window estimates for the variance equation display a much less stable pattern than those in the mean equation. Figure 5.2 plots the annual sequence of rolling-window estimates for $\hat{\gamma}_{\text{wind}}$, while Table A.8.1 reports the corresponding coefficients. The variance coefficients do not display a stable pattern across zones or over time. The estimates switch between positive and negative values, confidence intervals are wider, and the cross-zone ordering is less persistent. Most coefficients in the windows prior to 2022 are small and statistically insignificant, with the exception of SE4 in 2017, where the coefficient is positive and significant at the 1% level.

The clearest cross-zone divergence appears in the 2022 window. The coefficient is negative and significant in SE1 at about -0.158, while in SE2 it is close to zero at -0.019 and statistically insignificant. By contrast, the coefficient is strongly positive in both SE3 and SE4, reaching about $+0.277$ and $+0.308$, both significant at the 1% level. This is the only period in the sample in which the sign differs systematically across the North-South divide.

The coefficients turn negative across all zones in 2023, although the estimates for SE3 and SE4 are small and statistically insignificant. In 2025, the coefficient falls to -0.395 in SE1 and -0.675 in SE2, both significant at the 1% level and the most negative values observed for any zone in any window. In SE3 and SE4, the coefficients remain much smaller at -0.068 and -0.082 and only SE4 is statistically significant. Therefore, the late-sample variance pattern differs from the pattern in the mean equation. In the

variance equation, SE1 and SE2 move together and separate from SE3 and SE4. In the mean equation, the main divergence towards the end of the sample occurs within the northern pair itself.

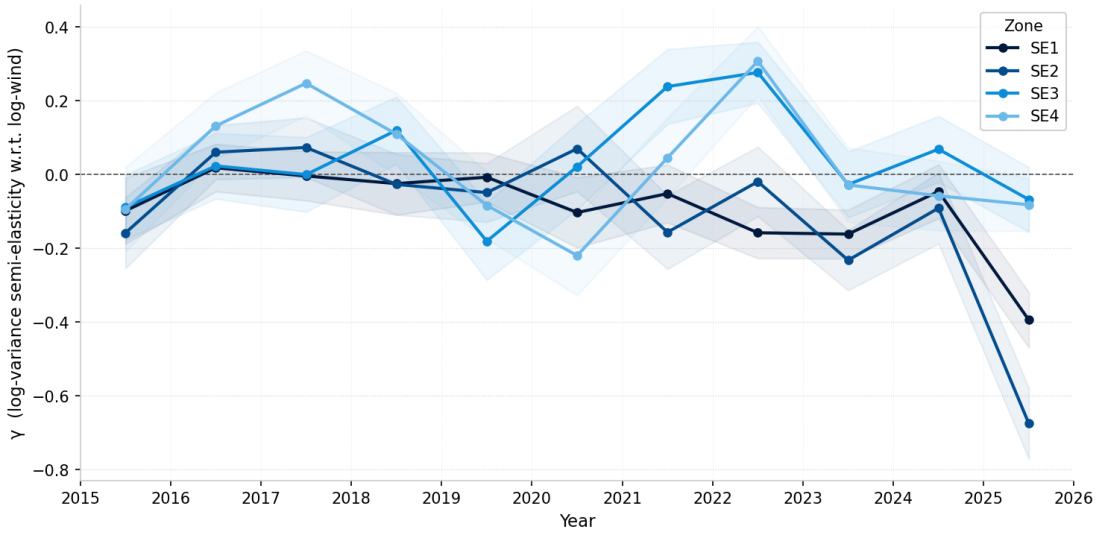


Figure 5.2: Rolling-window volatility coefficient (1 year window, 1 year shift)

Source: Own calculations.

5.4 SE1–SE2 Divergence and the FBMC Change

The late-sample divergence between SE1 and SE2 is a notable feature of the rolling-window mean equation and motivates further analysis in this section. In 2023, the two zones still display similar coefficients at approximately −0.016 in SE1 and −0.023 in SE2. By 2025, SE1 remains near −0.014 while SE2 deepens to −0.090. Figure 3.4 does not indicate a sharp change in the broad generation mix that would explain this break. The 2025 split is also not easily justified by a system-wide fuel-price shock as observed during the 2021–2022 European energy crisis. One possible explanation is that the transition from Available Transfer Capacity to Flow-Based Market Coupling (FBMC) on 30 October 2024 altered the wind-price relationship differently in SE1 and SE2.

To test whether the FBMC transition coincides with a stronger change in wind sensitivity in SE2 than in SE1, we estimate a pooled SE1–SE2 interaction regression over the 2024–2025 period. The specification includes an SE2 indicator, a post-FBMC indicator, and the wind variable. The coefficient of interest is the triple interaction, which captures whether the post-FBMC change in the wind coefficient differs between SE2 and SE1. The full specification and estimates are reported in Equation A.6.1.1 and Table A.6.1. The triple-interaction coefficient is negative at −0.0270 and significant at

the 1% level. The post-FBMC wind interaction for SE1 is also negative at −0.0359 and significant at the 1% level. The pre-existing SE2 differential in wind sensitivity is −0.0512 and significant at the 1% level. Hence, the implied post-FBMC change in the wind coefficient is −0.0359 in SE1 and −0.0630 in SE2. The wind effect becomes more negative after the FBMC transition in both northern zones, with a significantly larger deepening in SE2.

The interaction result links back to the market-background evidence in Chapter 3. That chapter showed that the FBMC transition changed how existing grid constraints enter day-ahead market clearing and that price separation widened after 2024, especially between SE2 and the southern bidding zones. Table 3.1 shows that SE2 and SE3 differ in price in 97.03% of hours in 2025, compared with 22.97% in 2023. The price-separation evidence does not by itself explain why the SE2 wind coefficient deepens relative to SE1. It instead motivates a narrower hypothesis about the source of that deepening. If the additional supply created by high SE2 wind production is less able to be exported south when SE2 and SE3 separate, then SE2 wind should place stronger downward pressure on SE2 prices in those hours. Under this mechanism, the wind-congestion interaction should be negative.

To test this mechanism, we estimate an additional 2025 SE2 ARMAX(3,1)-GARCH-X(1,1) model. The model keeps the 2025 SE2 baseline ARMAX(3,1)-GARCH-X(1,1) structure, but adds a congestion dummy and its interaction with the wind variable to the mean equation. The specification and selected estimates are reported in Equation A.6.2.1 and Table A.6.2. The estimates do not support the trapped-surplus mechanism. The wind coefficient is −0.0900 and significant at the 1% level. The wind–congestion interaction is positive at 0.0076 and significant at the 5% level. This implies a wind coefficient of −0.0824 in congested hours, compared with −0.0900 in uncongested hours. The congestion dummy is −0.0736 and significant at the 1% level, indicating lower SE2 prices in congested hours, holding the other controls fixed. Overall, the evidence from the two tests supports a post-FBMC differential shift in SE2, but not the narrower prediction that the stronger wind effect arises in locally congested SE2–SE3 hours.

5.5 Quantile Regression

We complement the rolling ARMAX-GARCH-X baseline with a rolling QARX model estimated over the same one-year windows. The quantile model uses three autoregressive lags, matching the autoregressive order selected for the baseline specification. Full estimates are reported in Subsection A.7.2. Because the quantile coefficients describe the price effect of wind at a specific point of the conditional price distribution rather

than its average effect, their magnitudes are not directly comparable to the baseline rolling-window coefficients. The quantile results are used to assess whether the sign, timing, and magnitude of the wind effect differ systematically across low, median, and high price states.

The 50th percentile in Figure A.7.2 and Table A.7.3 broadly follows the main pattern from the baseline mean model, but with less pronounced changes over time and smaller cross-zone differences. From 2020 to 2022, all four zones deepen, and SE3 stands out as the most price-sensitive zone. The partial normalisation in 2023 and the renewed late-sample divergence in 2025 are visible. SE1 remains close to zero and statistically insignificant in the crisis windows.

The 90th percentile in Figure A.7.3 and Table A.7.4 provides the first new distributional result. Before 2020, the four zones clustered more closely than in the baseline mean results, indicating that the early North-South gap was not driven mainly by high-price states. In 2022, SE3 became a clear outlier while SE1, SE2, and SE4 moved more closely together. The late-sample divergence between SE1 and SE2 is even sharper at the 90th percentile than in the baseline model, with SE2 as the most negative zone by 2025. The contrast with the 50th percentile is especially pronounced in SE1, where the coefficient remains near zero at the median but becomes more clearly negative at the 90th percentile.

The 10th percentile in Figure A.7.1 and Table A.7.2 provides the second new distributional result. From 2020 onward, the lower-tail coefficients in SE3 and SE4 deepen significantly, and from 2021 to 2022, they are more negative than both the 50th and the 90th percentile coefficients. SE1 shows the opposite pattern. Its lower-tail coefficient remains close to zero in the crisis windows, even though its 90th percentile coefficient is more clearly negative. SE2 lies between these patterns. Its lower-tail coefficient deepens strongly in 2022, but by 2025, its 90th percentile coefficient is far more negative than its 10th percentile coefficient.

Taken together, the quantile results reveal two forms of distributional heterogeneity. First, the wind effect is weakest at the centre of the conditional price distribution and strongest in the tails. Second, the dominant tail differs across zones and periods. The lower tail dominates in SE3 and SE4 from 2020 to 2022, while the upper tail dominates in SE1 and in SE2 by 2025.

5.6 Robustness Checks

5.6.1 Robustness to the Treatment of Negative Prices

The first robustness check tests whether the rolling-window patterns depend on the treatment of negative prices. In the preprocessing, the full price series is shifted upward before taking logarithms so that the minimum observation equals 0.01. This preserves the full sample, but alters every price observation. We estimate an alternative version in which negative prices are set to 0.01, while prices at or above zero are left unchanged. The log transformation, deseasonalisation, outlier treatment, and ARMAX(3,1)-GARCH-X(1,1) estimation are then applied as in the baseline specification. The corresponding rolling-window estimates are reported in Figure A.9.1 and Table A.9.1 for the mean equation, and in Figure A.9.2 and Table A.9.2 for the variance equation.

The mean-equation estimates support the main rolling-window interpretation. The crisis-period deepening remains visible in 2022, and the late-sample SE1–SE2 divergence remains visible in 2025. Under the alternative transformation, this divergence becomes even wider, with SE2 moving further below SE1 in the final window. The variance-equation estimates are unstable and do not support a separate interpretation. Flooring all negative prices at 0.01 creates an artificial pile-up at log(0.01) in the lower tail of the price distribution and changes the variance process being estimated.

5.6.2 Robustness Within the ARMAX-GARCH-X Specification

Table 5.2 reports the wind coefficient from the ARMAX(3,1)-GARCH-X(1,1) model across six progressively stripped specifications. The mean-equation results show that $\hat{\beta}_{\text{wind}}$ remains negative and statistically significant in all zones and all specifications. This confirms that the estimated price effect of wind is not driven by a single control variable. The magnitude of $\hat{\beta}_{\text{wind}}$ is stable until bilateral exchange controls are removed. In this specification, all bilateral exchange-flow variables for the relevant zone are removed simultaneously. In SE2, $\hat{\beta}_{\text{wind}}$ falls from -0.0904 in the full specification to -0.0191 when exchange-flow controls are removed. In SE1, it falls from -0.0143 to -0.0057. The coefficients in SE3 and SE4 move less, from -0.1206 to -0.1036 in SE3 and from -0.0733 to -0.0764 in SE4. Further removal of consumption and hydro controls produces only minor additional changes. Therefore, the mean-equation robustness check supports the sign of the wind effect but shows that its magnitude in SE1 and SE2 depends on the treatment of bilateral exchange flows. The variance-equation

results are more stable across the same stripping sequence. In the full specification, $\hat{\gamma}_{\text{wind}}$ is negative in all four zones. The effect is largest and highly significant in SE1 and SE2, at -0.394 and -0.675, respectively. These two northern coefficients remain negative, highly significant, and close in magnitude across all six specifications. SE3 also remains negative across all specifications, although its significance varies. SE4 is less stable, as the coefficient turns positive when exchange flows are removed and becomes insignificant in the later stripped specifications. Overall, the variance-equation results support the baseline finding that wind is associated with lower conditional price variance in SE1 and SE2, while the volatility effect is less robust in the southern zones.

Table 5.2: Wind coefficient by specification: ARMAX(3,1)-GARCH-X(1,1), 2025

Specification	SE1	SE2	SE3	SE4
Mean equation: $\hat{\beta}_{\text{wind}}$				
(1) Full model	-0.0143^{***}	-0.0904^{***}	-0.1206^{***}	-0.0733^{***}
	(0.0023)	(0.0085)	(0.0117)	(0.0102)
(2) Drop gas	-0.0142^{***}	-0.0906^{***}	-0.1210^{***}	-0.0741^{***}
	(0.0023)	(0.0085)	(0.0117)	(0.0102)
(3) Drop energy prices	-0.0141^{***}	-0.0906^{***}	-0.1215^{***}	-0.0741^{***}
	(0.0024)	(0.0085)	(0.0116)	(0.0102)
(4) Drop trade flows	-0.0057^{**}	-0.0191^{**}	-0.1036^{***}	-0.0764^{***}
	(0.0023)	(0.0081)	(0.0116)	(0.0111)
(5) Drop consumption	-0.0057^{**}	-0.0191^{**}	-0.0948^{***}	-0.0697^{***}
	(0.0023)	(0.0081)	(0.0118)	(0.0106)
(6) Drop hydro	-0.0057^{**}	-0.0189^{**}	-0.0949^{***}	-0.0694^{***}
	(0.0023)	(0.0080)	(0.0119)	(0.0106)
Variance equation: $\hat{\gamma}_{\text{wind}}$				
(1) Full model	-0.394^{***}	-0.675^{***}	-0.068	-0.082^{**}
	(0.038)	(0.049)	(0.045)	(0.037)
(2) Drop gas	-0.4141^{***}	-0.7005^{***}	-0.0533	-0.0679^{*}
	(0.0354)	(0.0468)	(0.0419)	(0.0349)
(3) Drop energy prices	-0.4244^{***}	-0.7006^{***}	-0.0383	-0.0541
	(0.0354)	(0.0464)	(0.0409)	(0.0351)
(4) Drop trade flows	-0.3701^{***}	-0.6503^{***}	-0.0709^{**}	0.0585
	(0.0376)	(0.0414)	(0.0352)	(0.0388)
(5) Drop consumption	-0.3864^{***}	-0.6709^{***}	-0.0705^{**}	-0.0206
	(0.0387)	(0.0415)	(0.0353)	(0.1261)
(6) Drop hydro	-0.3859^{***}	-0.6676^{***}	-0.0680^{*}	-0.0224
	(0.0387)	(0.0416)	(0.0353)	(0.1240)
N	8,736	8,736	8,736	8,736

Notes: $\hat{\beta}_{\text{wind}}$ is the elasticity of the log deseasonalised day-ahead spot price with respect to log wind forecast in the mean equation. $\hat{\gamma}_{\text{wind}}$ is the corresponding coefficient in the multiplicative GARCH-X variance equation. A negative value implies that higher wind production reduces conditional price variance. QML robust standard errors in parentheses. Specification (1) reproduces the full baseline model reported in Table 5.1. Specifications (2) to (6) strip controls progressively. $^{***}p < 0.01$, $^{**}p < 0.05$, $^{*}p < 0.10$.

5.6.3 Robustness to Excluding the GARCH-X Variance Equation

Table 5.3 provides a third robustness check by re-estimating the mean equation without the GARCH-X variance equation. This comparison is relevant because the baseline ARMAX-GARCH-X model is estimated jointly, so the conditional mean and conditional variance are linked through the likelihood. In a setting with conditional heteroscedasticity, estimating the mean equation without an explicit variance equation can leave the

mean estimates broadly similar, but it can affect efficiency and the estimated covariance matrix (Weiss, 1986). We do not expect the ARMAX and ARMAX-GARCH-X coefficients to be numerically identical. The relevant test is whether the sign, magnitude, and cross-zone ordering of $\hat{\beta}_{\text{wind}}$ remain similar once the GARCH-X structure is removed. This check is relevant as wind enters both the mean and variance equations in the baseline model. If the ARMAX estimates remain close to the baseline estimates, the mean-equation wind effect is unlikely to be driven by the volatility specification.

The full ARMAX specification produces estimates close to the baseline ARMAX-GARCH-X model. Since the GARCH-X equation is removed, this check only assesses the robustness of the mean-equation wind effect and not the variance-equation estimates. The wind coefficient equals -0.0190 in SE1, -0.0946 in SE2, -0.1184 in SE3, and -0.0778 in SE4, with all four coefficients significant at the 1% level. SE1 remains the least price-sensitive zone, while SE3 remains the most price-sensitive zone. This similarity shows that the negative mean-equation wind effect is not generated by the GARCH-X variance specification. The stripping sequence mirrors the pattern in Table 5.2. Dropping gas and then both energy price controls produce negligible changes in $\hat{\beta}_{\text{wind}}$. The largest shift again occurs when bilateral exchange flows are removed, especially in SE1 and SE2. In SE2, the coefficient falls from -0.0946 to -0.0286, while in SE1 it falls from -0.0190 to -0.0075. The coefficients in SE3 and SE4 remain more stable. Further removal of consumption and hydro controls produces only minor additional changes. The ARMAX robustness check reinforces the main conclusion from Table 5.2. The wind coefficient remains negative across specifications. Its magnitude is most sensitive to the treatment of bilateral exchange flows, not to the inclusion of the GARCH-X framework.

Table 5.3: Wind coefficient stability across specifications: ARMAX(3,1), 2025

Specification	SE1	SE2	SE3	SE4
Mean equation: $\hat{\beta}_{\text{wind}}$				
(1) Full model	-0.0190^{***}	-0.0946^{***}	-0.1184^{***}	-0.0778^{***}
	(0.0028)	(0.0099)	(0.0116)	(0.0108)
(2) Drop gas	-0.0189^{***}	-0.0945^{***}	-0.1190^{***}	-0.0788^{***}
	(0.0027)	(0.0098)	(0.0117)	(0.0108)
(3) Drop energy prices	-0.0189^{***}	-0.0945^{***}	-0.1188^{***}	-0.0789^{***}
	(0.0027)	(0.0098)	(0.0117)	(0.0108)
(4) Drop trade flows	-0.0075^{***}	-0.0286^{***}	-0.0968^{***}	-0.0759^{***}
	(0.0026)	(0.0089)	(0.0114)	(0.0111)
(5) Drop consumption	-0.0074^{***}	-0.0273^{***}	-0.0869^{***}	-0.0651^{***}
	(0.0026)	(0.0088)	(0.0116)	(0.0115)
(6) Drop hydro	-0.0075^{***}	-0.0272^{***}	-0.0877^{***}	-0.0651^{***}
	(0.0026)	(0.0088)	(0.0116)	(0.0115)
N	8,736	8,736	8,736	8,736

Notes: $\hat{\beta}_{\text{wind}}$ is the elasticity of the log deseasonalised day-ahead spot price with respect to log wind forecast in the mean equation of a plain ARMAX(3,1) model without GARCH. QML robust standard errors in parentheses. Specifications strip controls progressively. $^{***}p < 0.01$, $^{**}p < 0.05$, $^{*}p < 0.10$.

5.6.4 Trade-Partner Sensitivity in SE1 and SE2

Table A.10.1 examines the exchange-flow sensitivity in SE1 and SE2 in more detail. The previous robustness checks show the largest changes in $\hat{\beta}_{\text{wind}}$ when all bilateral exchange controls are removed simultaneously. This pattern is strongest in SE1 and SE2. Table A.10.1 removes one bilateral exchange variable at a time from the baseline ARMAX(3,1)-GARCH-X(1,1) specification, while keeping all other controls unchanged. This check identifies which specific bilateral exchange links account for the large change in $\hat{\beta}_{\text{wind}}$ when the full exchange-flow block is removed.

The mean-equation results show that the sensitivity is concentrated in specific bilateral links. In SE1, the largest changes occur when NO4 or SE2 is removed. In SE2, the largest changes occur when NO3 or SE3 is removed. The SE2 results show that a narrow interpretation in which the sensitivity is specific to the SE2–SE3 corridor alone is not enough, since removing NO3 produces a similar attenuation of $\hat{\beta}_{\text{wind}}$. The variance-equation estimates are more stable, with $\hat{\gamma}_{\text{wind}}$ remaining negative and significant across all partner removals in both SE1 and SE2. Taken together, the trade-partner check shows that bilateral exchange flows are central controls in the northern zone specifications. The large change in $\hat{\beta}_{\text{wind}}$ after removing the full exchange-flow block is not only a consequence of dropping many controls at once. It is concentrated in the

links that capture relevant transmission outcomes for SE1 and SE2. The table should still not be read as identifying a causal role for any single corridor, since exchange flows are jointly determined with zonal prices through market clearing.

Chapter 6

Discussion and Policy Implications

6.1 Economic Interpretation

This section provides the economic interpretation of the results reported in Chapter 5. The estimates show that wind power is associated with lower log day-ahead spot prices across Swedish bidding zones, confirming the merit-order effect. Wind power enters the merit-order at near-zero marginal cost and displaces more expensive generation technologies. This shifts the supply curve and reduces the equilibrium price. The magnitude of the merit-order effect varies across zones and over time. Thus, the following discussion focuses on why $\hat{\beta}_{\text{wind}}$ changes across market conditions. We proceed in the order of the rolling-window analysis with the pre-crisis ordering between northern and southern zones, the 2020 break, the energy crisis, the partial recovery, and the post-2024 divergence. Lastly, we discuss the volatility and distributional results.

Pre-crisis dynamics (2015–2019) The pre-2020 windows provide the reference point for interpreting later changes in $\hat{\beta}_{\text{wind}}$. During this period, $\hat{\beta}_{\text{wind}}$ is negative and stable across all zones. There is a persistent zonal-ordering where SE1 and SE2 remain close to zero and close to each other. SE3 and SE4 remain more negative and clustered together. This pattern is consistent with the market structure described in Chapter 3. SE1 and SE2 are hydro-dominated surplus zones. Thus, additional wind replaces other low-cost generation, which limits the price response. On the other hand, SE3 and SE4 face tighter local supply conditions and rely more on imports. This makes it more likely that additional wind replaces higher-cost marginal generation, which is consistent with the larger price response in the southern zones. The price-zone separation evidence is consistent with tighter price integration between SE1 and SE2 than between the northern surplus zones and the southern zones. Table 3.1 shows that the prices in

SE1 and SE2 separated rarely during the pre-crisis period. This means that the local wind shocks in the northern zones could be absorbed across a wider market and could explain why the SE1 and SE2 wind coefficients move close together. Price separation was more frequent between SE2–SE3 and SE3–SE4. This suggests that the southern zones were less integrated with the northern surplus zones already before the crisis and FBMC transition. Hence, local wind variation could have a stronger effect on local prices. The price-zone separation evidence does not prove this mechanism, but it supports the interpretation that market integration shaped the pre-crisis North-South ordering.

Ringhals and the steepening supply curve (2020) SE3's sharp deepening in 2020 breaks from the earlier SE3–SE4 pattern. Before 2020, the two southern zones moved closely together. In 2020, both coefficients became more negative, but the change was much larger in SE3 than in SE4. This coincides with the closure of the SE3 Ringhals 1 and 2 nuclear reactors in 2019 and 2020 (Vattenfall, 2026). Figure 3.4 supports this interpretation, showing that nuclear generation in SE3 fell from 66,130 GWh in 2019 to 49,198 GWh in 2020. Nuclear power is a baseload source with low marginal cost. When Ringhals' capacity was removed, more expensive technologies became more likely to set the marginal price in SE3. Additional wind replaces higher-cost generation more often than before. This is consistent with the larger negative $\hat{\beta}_{\text{wind}}$ estimated for SE3 in 2020. This suggests that SE3's marginal price became more responsive to additional wind already before the 2021–2022 crisis and that this was driven by a structural change in the local generation mix rather than external market shocks.

The energy crisis (2021–2022) The 2021–2022 windows show a sharp deepening of $\hat{\beta}_{\text{wind}}$ across all four zones. This coincides with the European energy crisis during which fuel costs rose sharply following the reduction in Russian energy exports (Holmberg & Tangerås, 2023). The mechanism of the deepening follows directly from the merit-order interpretation. When the price of fossil fuels rises, the marginal part of the interconnected European merit-order becomes more expensive in hours where gas or oil-based generation sets the clearing price. Additional wind then replaces or reduces exposure to marginal electricity supply that is more expensive than in normal periods. The price response to wind becomes stronger. However, the deepening of $\hat{\beta}_{\text{wind}}$ was not symmetric across zones. SE3 remains the most negative zone during 2021 and 2022, which is consistent with the post-Ringhals interpretation from 2020. SE2 also deepens more than SE1. Table 3.1 shows that the price differences between neighbouring zones

increased sharply during the crisis, especially between SE2 and SE3. SE3 and SE4 were more directly exposed to higher marginal-cost conditions because they are southern import-dependent zones with stronger links to continental European electricity markets, including Germany. SE1 remained more isolated as a northern surplus zone. SE2 sits between these parts of the system. This helps explain why its wind coefficient deepened more than SE1's. The price-separation evidence does not identify the exact cause of congestion. Nevertheless, it suggests that imperfect market integration helped shape the different responses in the crisis period between zones.

Partial recovery(2023) The partial recovery of coefficients in 2023 toward pre-2020 levels is consistent with the normalisation of European fossil fuel prices following the 2022 peak (International Energy Agency, 2023). As marginal electricity supply became less expensive, additional wind had less high-cost generation to replace. Its effect on spot prices weakened. Taken together, the 2021–2023 windows suggest that the wind coefficient is sensitive to the broader cost environment. When fossil-fuel generation becomes more expensive, wind has a stronger downward effect on spot prices. When those costs ease, the coefficient becomes less negative again. SE3 still remains the most negative zone in 2023, which is consistent with the earlier Ringhals interpretation.

FBMC and the SE1–SE2 split (post 2024) The sharp divergence in $\hat{\beta}_{\text{wind}}$ between SE1 and SE2 after 2023 is the main late-sample result. In 2023, SE1 and SE2 move closely together. By 2025, the two northern zones differ sharply. SE1 remains close to zero, while SE2 deepens substantially. The split is difficult to explain by broad generation structure alone. Figure 3.4 does not show a sharp change in the generation mix of either SE1 or SE2 between 2023 and 2025 that would justify such a large change in SE2 relative to SE1. Both zones remain northern surplus zones with generation dominated by low-cost hydropower. Neither was there a new system-wide fuel-price shock in 2025 that could explain the divergence. Instead, the timing points to the transition from ATC to FBMC on 30 October 2024.

The transition matters because it changed the way cross-zonal capacity was calculated and priced. The price-separation evidence in Table 3.1 suggests that SE2 became less integrated with SE3 after the transition. This matters for $\hat{\beta}_{\text{wind}}$ because local wind shocks are more likely to affect the local clearing price when the relevant pricing area becomes smaller. The interpretation is not that SE2 suddenly changed its generation structure, but that the market area over which SE2 wind was absorbed appears to have changed. This also helps to explain why the late-sample shift is stronger in SE2 than in SE1. SE2 is directly connected to the main internal boundary between northern

surplus and southern demand. When SE2 and SE3 are priced separately more often, SE2 wind is less likely to be absorbed by demand and marginal supply conditions in SE3 and SE4. The same wind variation can therefore have a larger effect on the SE2 clearing price. SE1 is further north and remains partly buffered by SE2. The SE1–SE2 corridor also separates more often after FBMC, but the average spread remains much smaller than on SE2–SE3. This suggests that the post-FBMC change weakened SE2's price linkage to the southern zones more than it weakened SE1's linkage to SE2.

The pooled SE1–SE2 FBMC interaction regression in Table A.6.1 supports this interpretation without proving it causally. In that specification, the coefficient of interest is the triple interaction between the SE2 indicator, the post-FBMC indicator, and the wind variable. The triple-interaction coefficient is -0.0270 and significant at the 1% level. This shows that the post-FBMC deepening of $\hat{\beta}_{\text{wind}}$ is larger in SE2 than in SE1. The SE2–SE3 local congestion interaction test in Table A.6.2 qualifies this interpretation. If the post-2024 SE2 deepening were driven by wind being trapped north of the SE2–SE3 boundary, the interaction between SE2 wind and the congestion indicator should be negative. The estimates do not support this mechanism. The estimated interaction instead has the opposite sign. The SE2 wind coefficient is -0.0900 outside congested hours, while the positive interaction of 0.0076 implies a slightly less negative coefficient of -0.0824 in hours classified as congested. This result contradicts the simple trapped-surplus mechanism, but it does not rule out a broader FBMC interpretation. FBMC changes price formation through the full network model and the allocation of cross-zonal capacity, so the relevant constraint does not need to be captured by a single binary SE2–SE3 congestion indicator. The evidence, therefore, points to FBMC as the leading explanation for the post-2024 SE1–SE2 split, but it does not identify which part of the flow-based calculation produced the change in SE2 wind sensitivity. A formal causal evaluation would require a study design beyond the scope of this paper, as outlined in Section 6.4.

6.1.1 Volatility Dynamics

The rolling estimates of $\hat{\gamma}_{\text{wind}}$ do not support a single wind-variance relationship over the full sample. Before 2022, the coefficient changes sign across zones and windows, and the cross-zone ordering is not stable. The discussion, therefore, focuses on the two periods where the variance estimates are both economically large and easier to interpret.

The 2022 crisis window is the first period in which $\hat{\gamma}_{\text{wind}}$ displays a distinct and economically interpretable cross-zone pattern. In this window, $\hat{\gamma}_{\text{wind}}$ is positive and

significant in SE3 and SE4, at 0.277 and 0.308. In contrast, the coefficient is negative and significant in SE1 at −0.158, while SE2 is close to zero and statistically insignificant. This pattern indicates that wind was associated with higher conditional variance only in the import-exposed southern zones. The result does not contradict the negative mean-equation wind effect. It shows that wind lowered the expected price while making price outcomes more dispersed around that expectation in SE3 and SE4. This combination is consistent with evidence from Germany and Portugal, where wind power is found to reduce electricity price levels while increasing conditional price volatility (Ketterer, 2014; Macedo et al., 2020). A plausible interpretation is that crisis conditions made the southern wind-price relationship more state-dependent. In some high-wind hours, additional wind could be absorbed locally or through the connected market, which allowed it to put downward pressure on prices. In other high-wind hours, congestion, import dependence, or high neighbouring prices prevented additional wind from lowering local prices to the same extent. This uneven price response is consistent with higher conditional variance in SE3 and SE4 during the crisis.

The 2025 window shows a sharp strengthening of the negative wind-variance relationship in SE1 and SE2. $\hat{\gamma}_{\text{wind}}$ is large and significant in SE1 and SE2, at −0.394 and −0.675. SE3 is small and statistically insignificant, while SE4 is negative but much smaller. This pattern differs from the mean equation. The mean equation shows a post-FBMC divergence between SE1 and SE2. The variance equation instead shows a common northern decline in conditional variance. The timing suggests a link to the post-FBMC increase in price separation, but the variance mechanism differs from the mean-equation mechanism. The increased price separation on the SE2–SE3 border plausibly reduced the exposure of SE1 and SE2 to southern scarcity and transmitted price shocks. In high-wind hours, SE1 and SE2 prices were less exposed to southern scarcity conditions and more closely tied to northern surplus conditions. This made price outcomes less dispersed around the expected price, which is consistent with the negative wind-variance coefficients in SE1 and SE2. This explains why the variance result appears as a common northern effect, even though the mean-equation effect is concentrated in SE2.

6.1.2 Distributional Heterogeneity

The quantile results add two dimensions to the mean-equation picture. First, the wind effect is strongest at the tails of the conditional price distribution and weakest at the median. This suggests that the merit-order effect is most pronounced outside normal price states. At the upper tail, wind reduces prices more strongly when expensive marginal generation would otherwise set the price. At the lower tail, additional wind

supply places further downward pressure on prices when the market is already close to the low-price segment of the merit-order. Second, the dominant tail differs by zone and period in a way that reflects each zone's structural market position. In SE3 and SE4 from 2020 to 2022, the lower tail is more sensitive than the upper tail. Wind reduces prices more strongly when prices are already low. This pattern does not follow the simplest merit-order intuition, where wind should have its largest effect when expensive marginal generation sets the price. A plausible interpretation is that high-price states in SE3 and SE4 during the crisis were shaped by electricity scarcity, congestion, and imported price pressure that local wind could not fully offset. By contrast, low-price states were more likely to occur when supply was abundant relative to demand. Additional wind was then associated with further downward pressure on prices. The pattern is different in SE1 and in late-sample SE2. In these cases, the upper tail dominates. This suggests that wind matters most when northern prices are high due to tight market conditions. In these hours, additional wind is associated with a stronger price reduction because it eases local scarcity. The late-sample SE1–SE2 divergence is concentrated in the upper tail of the conditional price distribution. In these high-price states, the SE2 wind coefficient becomes much more negative than the SE1 coefficient. This pattern is consistent with the broader FBMC interpretation because high-price states are the part of the distribution where local scarcity and cross-zonal capacity limits are most likely to affect price formation. The result does not identify the specific FBMC mechanism, but it shows that the SE1–SE2 divergence is largest where capacity limits should matter most.

6.2 Policy Implications

The Swedish Government's request for Svenska kraftnät to reassess Sweden's bidding zone structure makes the zonal heterogeneity documented in this thesis directly policy relevant (Regeringen och Regeringskansliet, 2025; Svenska Kraftnät, 2025a). A single Swedish bidding zone would eliminate price differences between SE1, SE2, SE3, and SE4 in the day-ahead market, but it would not remove the physical transmission constraints that create those differences under the current zonal structure. Congestion would instead have to be handled after market clearing through redispatch or other corrective measures. The current zonal structure takes the opposite approach by allowing prices to differ when local conditions differ. Price differences are not necessarily evidence of market failure but can be market signals that electricity is abundant in one part of the system and scarce in another. Our wind results strengthen the case for preserving location-specific price signals. The thesis shows that wind does not affect the day-ahead

spot price uniformly across Sweden. Instead, $\hat{\beta}_{\text{wind}}$ differs across zones and changes over time. The late-sample SE1–SE2 divergence suggests that the two northern surplus zones should not be treated as a single region. The timing of this divergence gives the result additional policy relevance as it appears after the Nordic transition from ATC to FBMC, which changed how cross-zonal transmission capacity is calculated in the day-ahead market. This does not identify FBMC as the sole cause of the divergence. It does show, however, that bidding zone design cannot be assessed without considering how transmission capacity is calculated and allocated between zones. These differences matter for bidding zone design because the price effect of wind reflects how local renewable supply interacts with demand, generation mix, and transmission constraints. Merging zones with different wind-price sensitivities would weaken the local price signals that guide where new generation should be built and where grid capacity should be improved. Our results do not prove that the current four-zone structure is optimal, but they argue against simple consolidation unless the underlying transmission constraints are reduced first.

Our results also matter for renewable investment incentives. The policy issue is not only whether Sweden should keep separate bidding zones, but also where new wind capacity is financially viable under the current grid. Since wind producers earn revenue in the local price area, a more negative $\hat{\beta}_{\text{wind}}$ means that additional wind is associated with lower prices in the same hours in which wind output is high. This corresponds to the market-value channel described by Hirth (2013), where high renewable output lowers the prices received by renewable producers. Our results add that this channel is not national in Sweden. It varies by zone and over time. The variance results add a risk dimension to the investment channel. Wind affects not only the expected spot price, but also the conditional price risk faced in high-wind states. The 2022 increase in conditional variance in SE3 and SE4 and the 2025 decline in SE1 and SE2 suggest that location affects both the expected market value of wind and the uncertainty around that value. This zonal variation matters because Swedish wind investment is already uneven. Wind capacity in operation and under construction differs substantially across bidding zones, and more than 1.8 GW of announced projects still depend on improved market conditions before reaching investment decision (Green Power Sweden, 2025). Policy should treat grid planning and renewable investment incentives together. Encouraging further wind build-out in a constrained surplus zone can lower local prices and weaken producer revenues unless transmission capacity expands with it. The implication is that policy should not evaluate wind expansion through national capacity targets alone. It should also assess whether local prices encourage wind investment where additional production can reduce energy scarcity without being trapped behind transmission constraints.

6.3 Limitations

The empirical design is built to compare the wind-price relationship across zones and over time. This comparability comes at the cost of some flexibility. The main restriction is that the same ARMA(3,1) mean specification and the same Student t tail parameter are imposed throughout the rolling-window analysis. The ARMA order is selected from the 2025 baseline specification and held fixed across SE1–SE4 and across all one-year windows from 2015 to 2025. The degrees of freedom in the Student t distribution are fixed at five in all windows to avoid letting changes in estimated tail thickness drive changes in the estimated wind coefficient. This makes movements in the wind coefficient easier to compare, since changes in the coefficient are not mixed with changes in lag order or tail specification. The cost is that the common specification may fit some rolling samples better than others. The fixed ARMA(3,1) structure and fixed Student t degrees of freedom may allocate variation differently than a specification reselected separately for that rolling sample. A full sensitivity analysis with lag orders and degrees of freedom reselected separately in each rolling sample would be needed to assess the impact of this restriction. The same restriction applies to stationarity diagnostics. We test stationarity for the baseline 2025 specification, but we do not repeat these tests for every one-year rolling-window. The rolling analysis assumes that the transformed variables remain sufficiently stationary within each window. If this assumption fails, part of the estimated coefficient variation may reflect changing time-series properties rather than changes in the wind-price relationship.

A second limitation concerns the transformation of the dependent variable. Since the logarithm is undefined for zero and negative prices, the day-ahead spot price is shifted upward before the log transformation is applied. The estimated wind coefficient measures the elasticity of the shifted log price rather than the exact elasticity of the original EUR/MWh price. This distinction matters most in low-price and negative-price hours, where the shift accounts for a larger share of the transformed value. The robustness check in Subsection 5.6.1 shows that the sign and cross-zone ordering of the wind coefficient are not sensitive to the choice of transformation, but the magnitude of the coefficient is affected.

A third limitation concerns the market variables used to isolate the wind effect. Bilateral net exchange flows are included to prevent the wind coefficient from absorbing cross-border market conditions, but flows and zonal prices are jointly determined in the day-ahead auction. They are useful controls, but not strictly exogenous regressors. The robustness checks show that transmission conditions matter for the estimated wind effect. Without an instrumental variable strategy, the model cannot determine

whether the change in the wind coefficient after removing exchange-flow controls reflects simultaneity bias or cross-border transmission of wind-price effects. The remaining controls are imperfect in different ways. Hydro reservoirs vary weekly, and oil and gas prices vary daily, so these controls provide limited within-day variation for an hourly model like ours. While they help account for broader supply-side conditions, they cannot fully capture the information set used in price formation. Therefore, the wind coefficient should be interpreted as the conditional relationship between wind production and the log day-ahead spot price after controlling for the observable market conditions included in the model.

A fourth limitation applies to the pooled SE1–SE2 interaction test in Table A.6.1. The specification is estimated by OLS on pooled hourly observations and does not model the dynamic price structure captured in the baseline ARMAX-GARCH-X framework. The specification is therefore useful as a simple interaction check, but its standard errors should be interpreted with caution. Serial dependence in hourly prices may make the reported standard errors too small and the significance levels too optimistic. The result should be used as supporting evidence, rather than as the main basis for interpreting the late-sample divergence.

A fifth limitation concerns the interpretation of changes in the wind coefficient over time. The rolling-window estimates show when the wind-price relationship changes, but they do not identify which market event caused the change. A movement in the wind coefficient between two windows can reflect changes in generation mix, fuel prices, transmission constraints, market design, or bidding behaviour. The links to the Ringhals closures, the European energy crisis, and FBMC are interpreted as economically motivated explanations of the observed coefficient movements. They are supported by timing and market context, but they should not be read as estimates of the causal effect of these events on the wind coefficient. The pooled FBMC and congestion tests narrow parts of this discussion, but they do not rule out all simultaneous changes in the Swedish and Nordic electricity systems.

A further limitation is that the model does not observe individual bids or strategic withholding. However, this is unlikely to be the main driver of results, since wind power is injected into the grid as it is generated, while storage remains costly and limited at scale. This is different from hydro production, for example, where delaying output can reflect the opportunity cost of stored water. Coordinated wind withholding aimed at raising the market-clearing price would instead fall closer to the type of withholding behaviour treated as potential market abuse under REMIT (Agency for the Cooperation of Energy Regulators [ACER], 2024). This is monitored through Nord Pool's market surveillance framework (Nord Pool, 2026b). Thus, we do not explicitly

model strategic bidding behaviour. The interpretation of the wind coefficient assumes that unobserved withholding is not driving the cross-zone and rolling-window variation in forecasted wind.

6.4 Directions for Further Research

The results point to several directions for further research. The first is a more formal evaluation of the FBMC transition. Our thesis uses the late-sample SE1–SE2 divergence to motivate a pooled interaction test around the October 2024 transition. The test shows that the post-FBMC change in the wind coefficient was significantly larger in SE2 than in SE1. However, it does not isolate FBMC as the cause of the divergence. Future research should combine the transition with more detailed data on cross-zonal transmission capacity. This would make it possible to separate a general post-2024 market shift that we notice from the specific effect of binding constraints on the SE2–SE3 corridor. This matters because it determines whether the SE1–SE2 divergence is a product of the bidding zone structure itself or the way transmission capacity is allocated under FBMC.

A second extension is to model wind-price spillovers across bidding zones more directly. Our thesis estimates the wind coefficient separately for SE1–SE4 and controls for bilateral exchanges. This shows how local wind production is associated with the local spot price, but it does not fully show how wind shocks in one zone move through to the other zones. Future research could model several connected bidding zones jointly rather than estimating each Swedish zone separately. The results from such an estimation would matter because wind build-out in SE2 has different implications if its price effect remains local than if it is transmitted south through the Nordic grid.

A third direction is to investigate the producer-side implications of the estimated merit-order effect. Our thesis shows that higher wind production is associated with lower local spot prices. However, it does not estimate how this affects wind producers' revenues. This distinction matters because investment returns depend on both the volume of electricity produced and the price received in the hours when production occurs. Future research could combine the estimated price effects with information on installed capacity and project location to compare the revenue implications of wind expansion across SE1–SE4. Such an extension would show whether stronger wind resources in a zone compensate for the lower prices created by high wind output, or whether the lower prices weaken the financial case for additional capacity.

A final extension is to include other forms of variable renewable production. This thesis

focuses on wind because wind is the central renewable source in the Swedish bidding zones during the sample period. Future research could extend the model by including solar production. This is most relevant for SE4, where solar has become a substantial part of the generation mix, as shown in Figure 3.4. Such an extension would show whether the price effects documented for wind also apply to renewable production with a different hourly generation profile.

Chapter 7

Conclusion

The objective of this paper was to investigate how wind power affects day-ahead electricity prices across Sweden's four bidding zones between 2015 and 2025. We estimated rolling ARMAX-GARCH-X models on each zone, complemented by quantile regressions. While the merit-order effect of wind on prices was confirmed across all zones and across the full sample, its size is not stable. The wind coefficient first deepens in 2020 and becomes more negative during the 2021–2022 energy crisis, before partially recovering in 2023. The coefficients then diverge sharply between SE1 and SE2 after the FBMC transition in October 2024. The robustness checks do not change this conclusion, although they show that the magnitude of the wind coefficient is sensitive to exchange-flow controls. The variance and quantile results show that wind also matters beyond the conditional mean. In the variance equation, the wind coefficient is predominantly negative in the northern zones, while the quantile estimates indicate that the price effect is often stronger in the tails than at the median.

The policy implication is that bidding zone reform should preserve the information contained in local price signals. A consolidation of Swedish bidding zones would smooth observed price differences, but it would not remove the physical constraints that create them. The post-FBMC divergence between SE1 and SE2 suggests that the SE2–SE3 corridor is central to understanding how northern wind production is priced, even though the congestion test does not identify a single corridor-level mechanism. Additional SE2 wind may have different market implications depending on whether the price effect remains local or is transmitted south through the Nordic grid. This means that grid investment and market design should be evaluated together, and that any policy assessment should account for the zone-level and time-varying dynamics documented here rather than relying on national averages alone. As long as transmission constraints remain, convergence in zonal prices and wind sensitivities should not be expected.

The broader context of rising fossil fuel prices and geopolitical disruption reinforces this conclusion. The rolling-window estimates show that the wind merit-order effect deepens in periods of increased cost of fossil fuel-based generation. A market structure that transmits wind surplus efficiently across zones reduces both average prices and exposure to external fuel-price shocks, especially in a system increasingly linked to Nordic and continental European price formation.

Chapter A

Appendix

A.1 Descriptive Statistics and Price Distributions

Table A.1.1 and Table A.1.2 report summary statistics for all variables across Sweden's four bidding zones over the full sample period, 1 January 2015 to 31 December 2025. Figure A.1.1 shows the distribution of hourly day-ahead spot prices for each zone in 2015, 2020, and 2025.

Table A.1.1: Descriptive statistics, 2015–2025 (Panel A: SE1 and SE2)

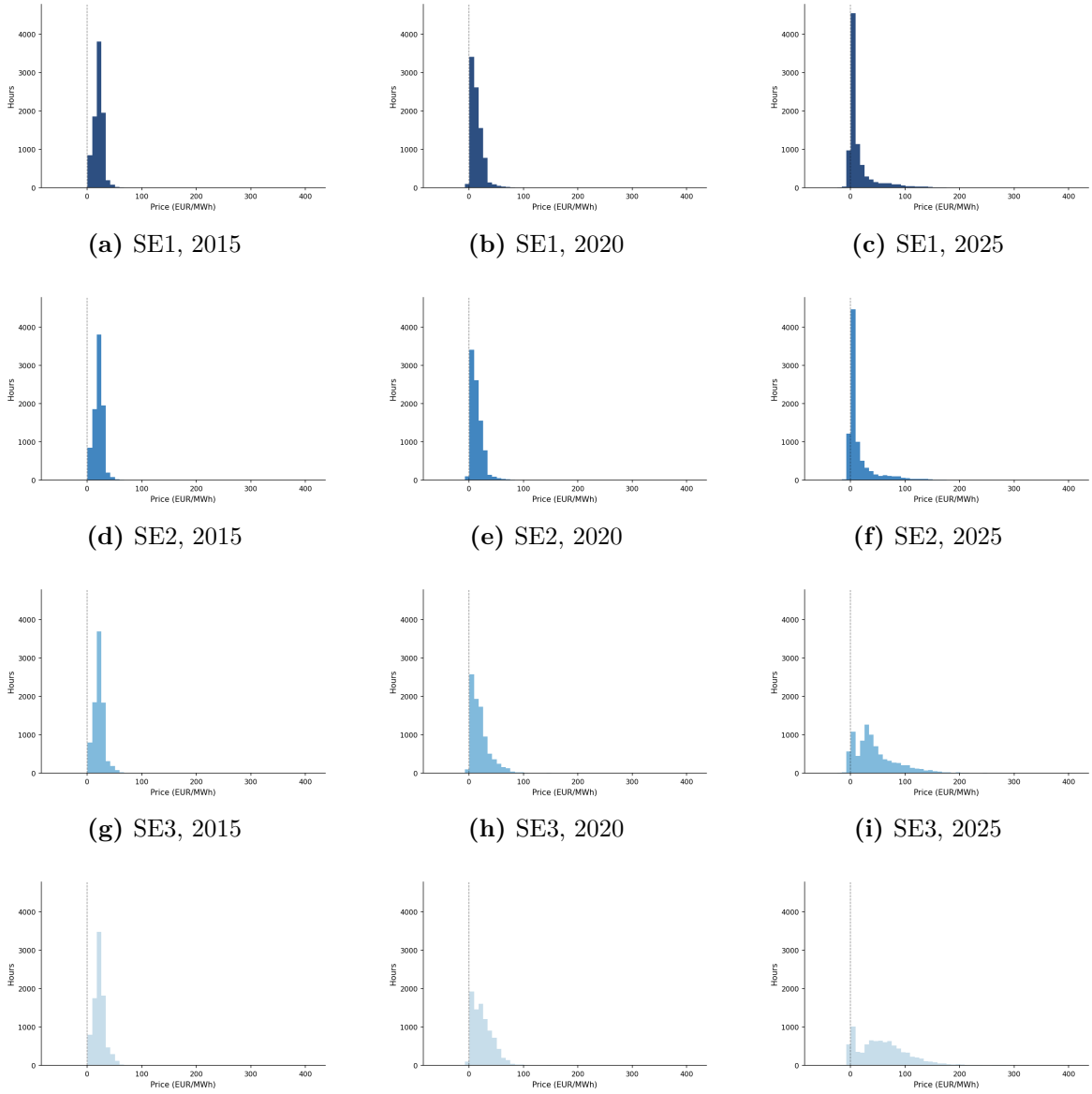
	SE1							SE2						
	Mean	SD	Skew	Kurt	Min	Max	*N*	Mean	SD	Skew	Kurt	Min	Max	*N*
Spot price (EUR/MWh)	32.79	33.20	5.17	46.53	−74.11	590.00	96,432	33.01	33.79	5.11	44.80	−60.04	590.00	96,432
Wind forecast (MW)	439	492	1.77	2.86	1	2,832	96,095	1,124	1,048	1.46	1.87	6	7,017	96,095
Consumption forecast (MW)	1,179	199	0.33	−0.58	650	1,798	96,336	1,859	372	0.44	−0.41	903	3,613	96,336
Net exchange (MW)	−1,546	892	0.16	−0.78	−4,526	776	96,432	−3,677	1,328	0.43	0.04	−8,752	556	96,432
Hydro reserves (GWh)	8,481	3,176	−0.30	−0.97	1,381	13,759	96,432	9,713	3,744	−0.62	−0.87	1,504	15,037	96,432
Oil price (USD/bbl)	62.19	17.30	0.43	0.46	12.88	124.77	2,854	*common across zones*						
Gas price (EUR/MWh)	35.86	38.16	3.04	10.94	3.62	311.00	2,671	*common across zones*						

Notes: Zone-specific variables are at hourly frequency; *N* reports the number of hourly observations. Oil and gas prices are at daily frequency and common across zones; their *N* reports the number of trading days. Statistics for oil and gas are reported once under SE1. Skewness and excess kurtosis are reported as moments of the empirical distribution. Net exchange is the aggregate net flow into the zone from all neighbours; positive values indicate net import. Zone-specific variables are sourced from Nord Pool; oil and gas prices from Bloomberg Terminal. Sample period: 1 January 2015 to 31 December 2025.

Table A.1.2: Descriptive statistics, 2015–2025 (Panel B: SE3 and SE4)

	SE3							**SE4**						
	Mean	SD	Skew	Kurt	Min	Max	*N*	Mean	SD	Skew	Kurt	Min	Max	*N*
Spot price (EUR/MWh)	46.85	56.79	4.53	29.69	−60.04	799.97	96,432	54.92	64.61	3.96	22.43	−60.04	799.97	96,432
Wind forecast (MW)	876	659	1.12	0.90	18	3,559	95,951	520	403	1.05	0.58	7	2,155	95,951
Consumption forecast (MW)	9,758	2,132	0.37	−0.52	5,130	18,215	96,336	2,667	639	0.43	−0.41	1,301	5,091	96,336
Net exchange (MW)	580	1,529	0.03	0.04	−4,661	6,853	96,432	1,732	634	0.14	−0.03	−496	3,972	96,432
Hydro reserves (GWh)	1,793	407	−0.34	−0.66	727	2,600	96,432	120	41	−0.19	−0.86	36	216	96,432
Oil price (USD/bbl)	*common across zones*							*common across zones*						
Gas price (EUR/MWh)	*common across zones*							*common across zones*						

Notes: Zone-specific variables are at hourly frequency; *N* reports the number of hourly observations. Oil and gas prices are at daily frequency and common across all four bidding zones; see Panel A for values. Skewness and excess kurtosis are reported as moments of the empirical distribution. Net exchange is the aggregate net flow into the zone from all neighbours; positive values indicate net import. Zone-specific variables are sourced from Nord Pool; oil and gas prices from Bloomberg Terminal. Sample period: 1 January 2015 to 31 December 2025.



(a) SE1, 2015 **(b)** SE1, 2020 **(c)** SE1, 2025

(d) SE2, 2015 **(e)** SE2, 2020 **(f)** SE2, 2025

(g) SE3, 2015 **(h)** SE3, 2020 **(i)** SE3, 2025

(j) SE4, 2015 **(k)** SE4, 2020 **(l)** SE4, 2025

Figure A.1.1: Price histograms per bidding zone and year

Source: Nord Pool, own calculations.

A.2 Variable Treatment and Preprocessing

The following figures document the seasonal structure of variables and the adequacy of the deseasonalisation specifications applied prior to estimation. All plots are based on SE4 over 2025 as a representative example; the same treatment and qualitative findings apply to all four bidding zones.

Day-Ahead Spot Price

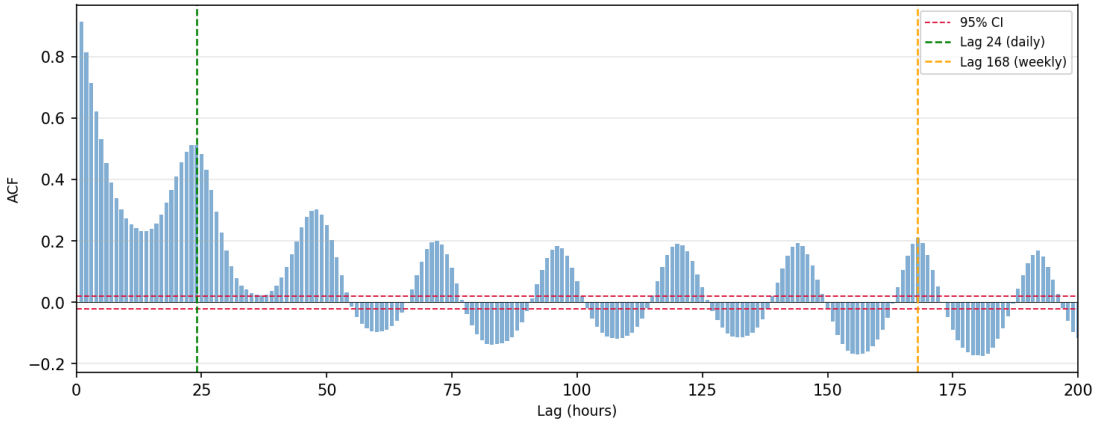


Figure A.2.1: ACF of deseasonalised log prices (SE4)

Note: Displays the autocorrelation function (ACF) of the deseasonalised log spot price under the baseline dummy specification for SE4 in 2025. The spike at lag 24 and the repeating pattern at multiples of 24 indicate remaining deterministic calendar effects not captured by hour-of-day, day-of-week, holiday, month, and year dummies.

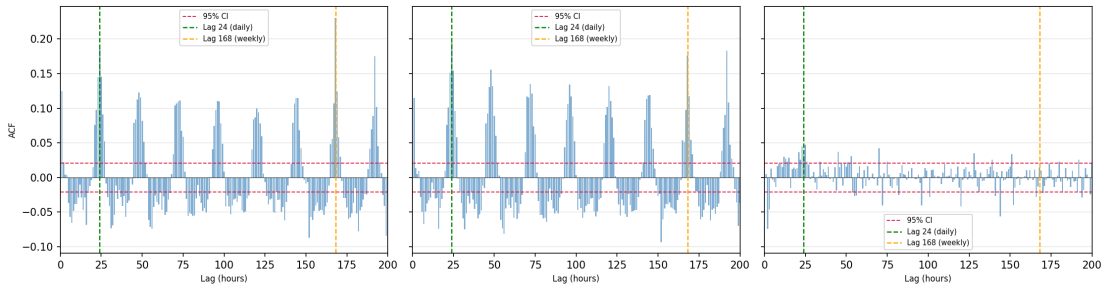


Figure A.2.2: ACF of AR(1) residuals under alternative deseasonalisation (SE4)

Note: Shows the autocorrelation function (ACF) of AR(1) residuals of the log spot price under three deseasonalisation specifications for SE4 in 2025. The full interaction specification (hour×day-of-week and hour×month dummies) removes remaining calendar effects, including the weekly cycle at lag 168. Dashed red lines indicate 95% confidence bands.

Wind Power Production Forecast

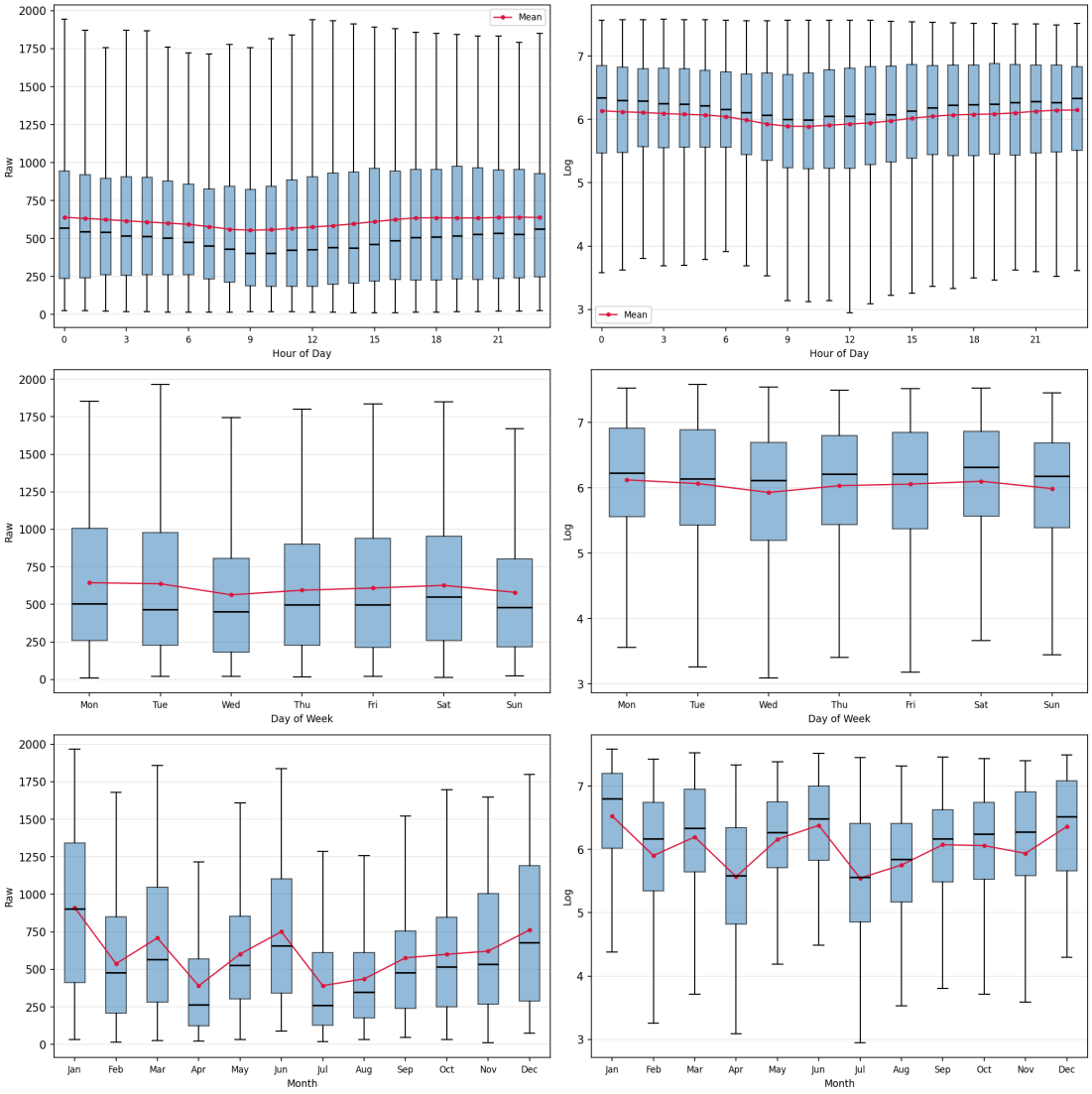


Figure A.2.3: Seasonal patterns in wind power production forecasts (SE4)

Note: Displays wind power production forecasts by hour-of-day, day-of-week, and month-of-year for SE4 in 2025. No systematic intra-day or intra-week patterns are observed. While average production is higher in winter months, substantial within-month variation suggests that weather-driven fluctuations dominate seasonal effects.

Consumption Forecast

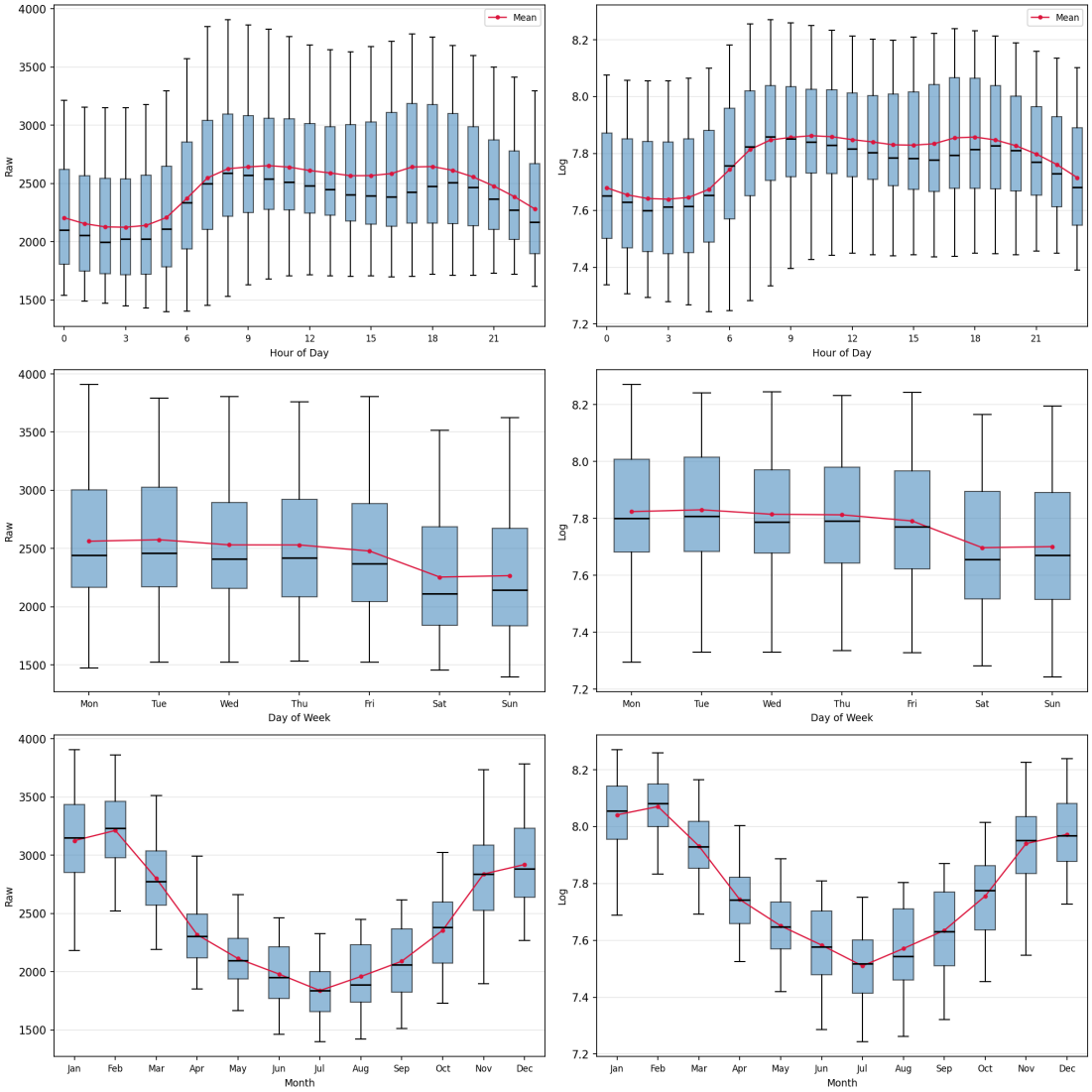


Figure A.2.4: Seasonal patterns in electricity consumption forecasts (SE4)

Note: Displays consumption forecasts by hour-of-day, day-of-week, and month-of-year for SE4 in 2025. Average consumption is substantially higher in winter months, reflecting heating demand, with January levels around 40% above those in July. Pronounced intra-day cycles and lower weekend demand indicate the need for full interaction-dummy deseasonalisation.

Hydro Reservoir Levels

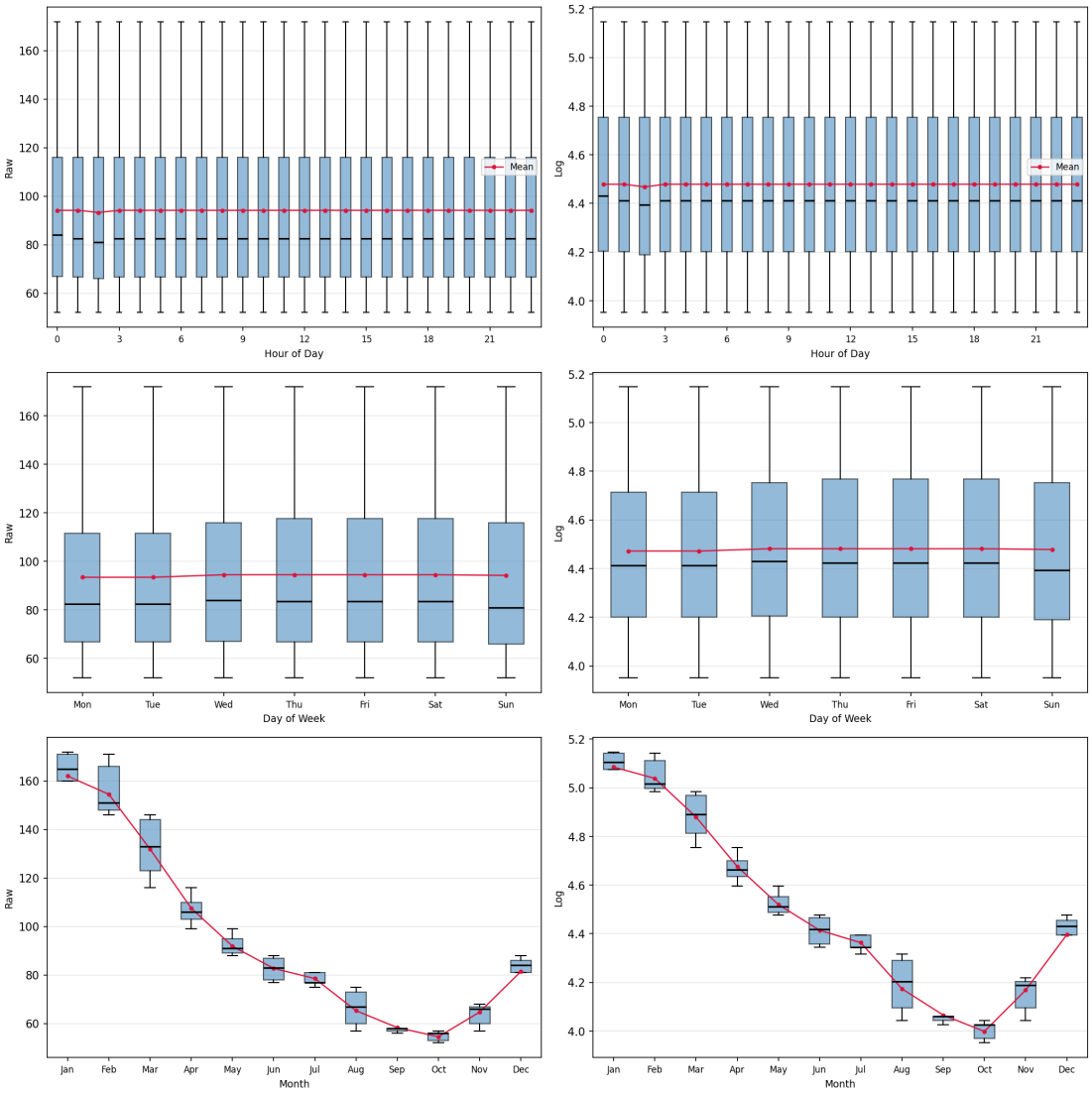


Figure A.2.5: Seasonal patterns in hydro reservoir levels (SE4)

Note: Displays hydro reservoir levels by month-of-year for SE4 in 2025. Reservoir levels peak in winter (January–February) and reach their lowest levels in summer (July–August), reflecting the Nordic hydro cycle. Month-of-year dummies explain 97.1% of the variance, while intra-day and intra-week effects are absent due to the weekly frequency of the data.

Negative prices

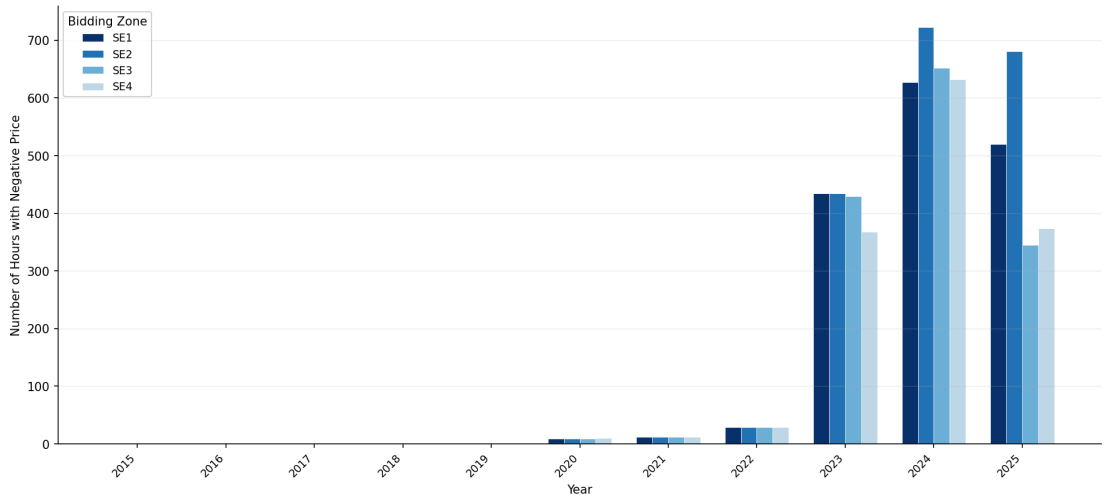


Figure A.2.6: Amount of negative prices per zone, 2015–2025

Source: Nord Pool, own calculations.

Stationarity Tests

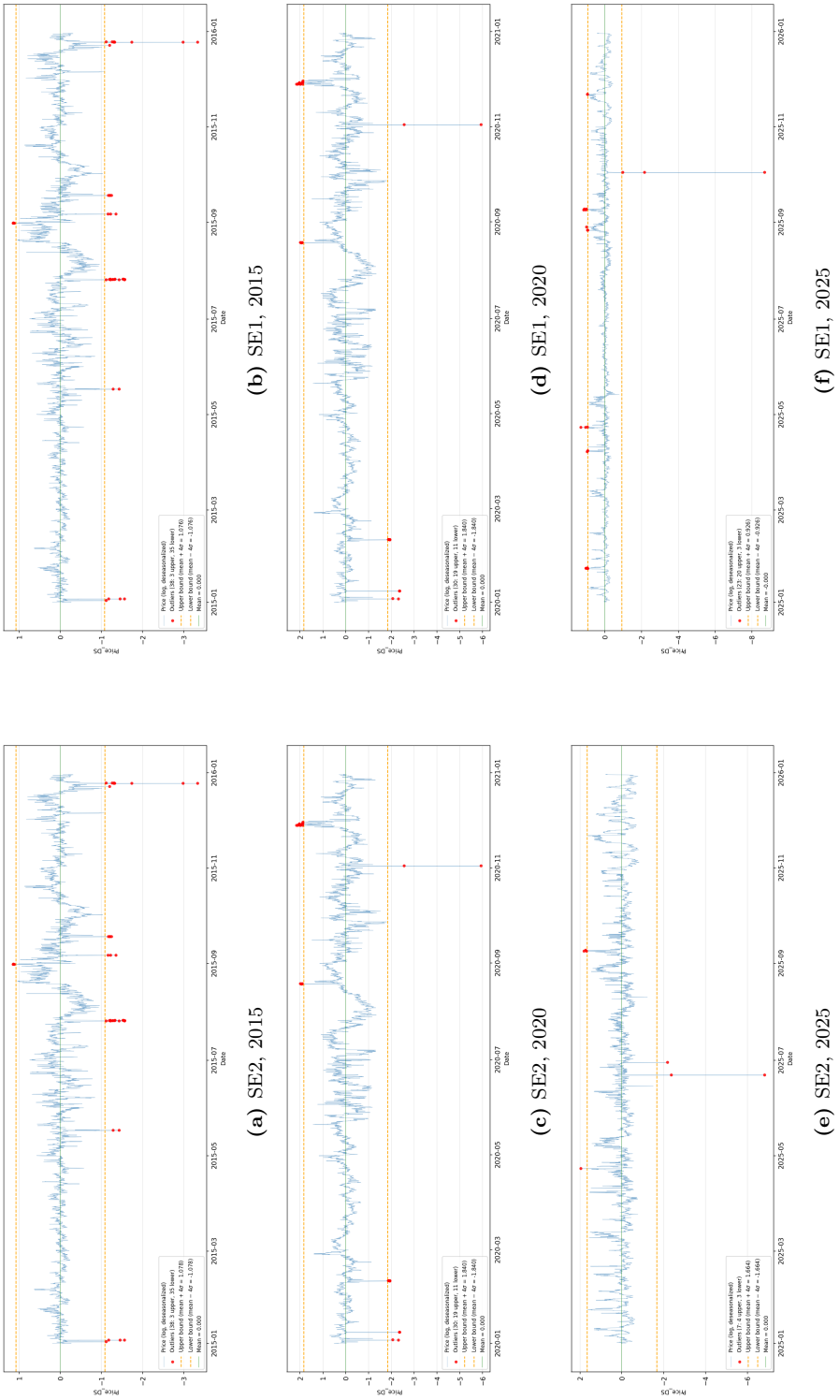
Table A.2.1 reports Augmented Dickey-Fuller test statistics for the transformed variables used in the 2025 baseline estimation window.

Table A.2.1: ADF tests for transformed model variables, 2025

Variable	SE1	SE2	SE3	SE4
Panel A: Zone-specific variables				
$p_{z,t}$	-10.36^{***}	-10.33^{***}	-10.63^{***}	-11.06^{***}
$w_{z,t}$	-8.45^{***}	-9.06^{***}	-10.19^{***}	-10.27^{***}
$r_{z,t}$	-5.61^{***}	-5.63^{***}	-4.95^{***}	-5.47^{***}
$c_{z,t}$	-7.10^{***}	-7.46^{***}	-6.74^{***}	-7.09^{***}
$X_{z,n,t}$	-7.52^{***}	-8.31^{***}	-7.64^{***}	-7.64^{***}
Panel B: Common controls				
o_{t-24}		-2.08 ($p = 0.252$)		
g_{t-24}		-1.50 ($p = 0.533$)		

Notes: Table reports Augmented Dickey-Fuller test statistics for the transformed variables used in the 2025 baseline estimation window. Row labels refer to the processed model variables defined in Equation 4.2.1.1. For $X_{z,n,t}$, the reported statistic is the weakest rejection among the bilateral exchange-flow variables included in the zone-specific specification. Oil and gas prices are common across zones. $^{***}p < 0.01$, $^{**}p < 0.05$, $^{*}p < 0.10$.

A.3 Outlier Bounds by Estimation Window



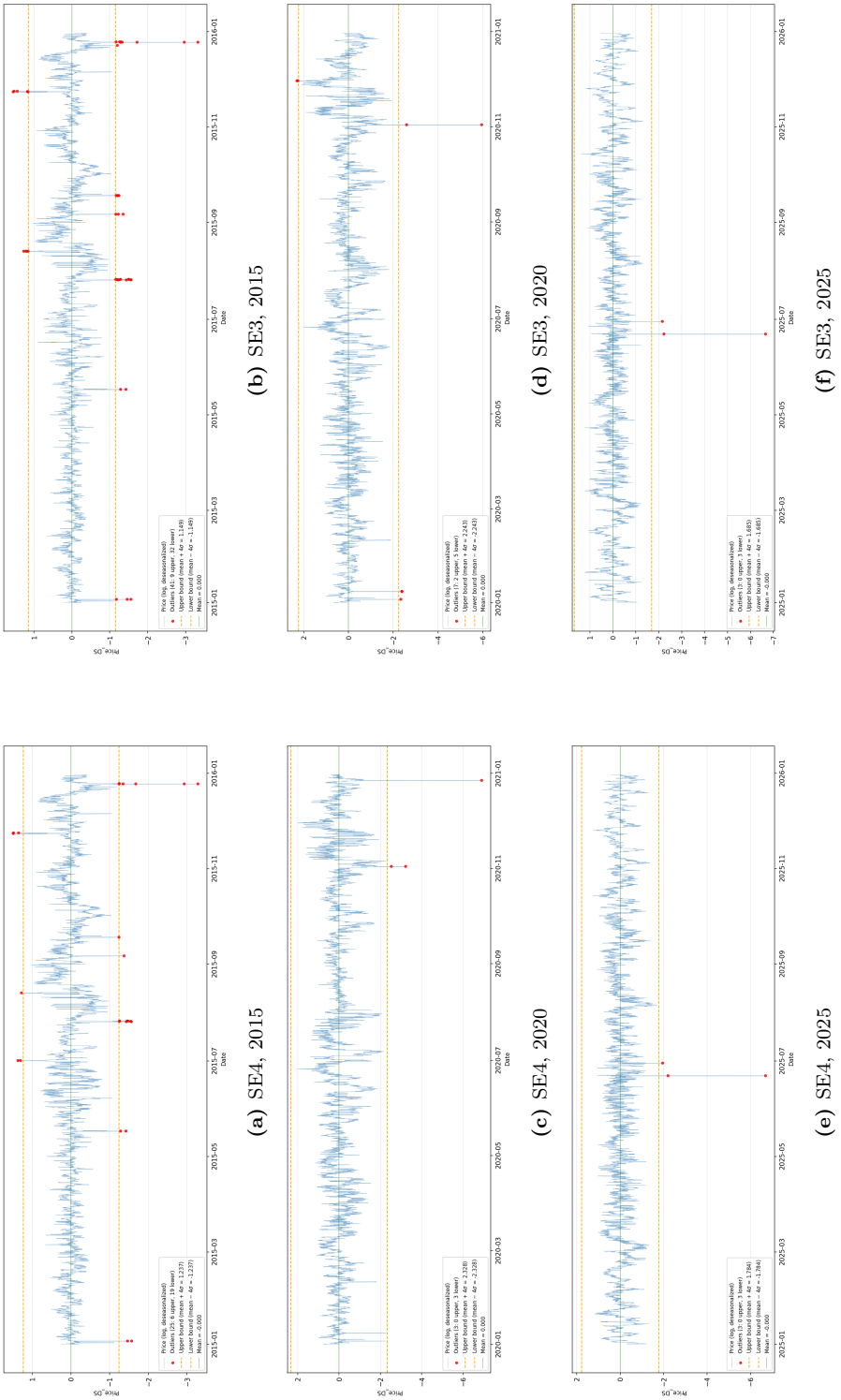
(a) SE2, 2015 (b) SE1, 2015

(c) SE2, 2020 (d) SE1, 2020

(e) SE2, 2025 (f) SE1, 2025

Figure A.3.1: Outlier capping bounds in SE1 and SE2

Note: Each panel shows the deseasonalised log price series within a one-year estimation window together with $\pm 4\sigma$ bounds computed from the window-specific mean and standard deviation. Observations exceeding these bounds are capped at the respective threshold. The figure compares representative estimation windows in SE1 and SE2.



(a) SE4, 2015 (b) SE3, 2015

(c) SE4, 2020 (d) SE3, 2020

(e) SE4, 2025 (f) SE3, 2025

Figure A.3.2: Outlier capping bounds in SE3 and SE4

Note: Each panel shows the deseasonalised log price series within a one-year estimation window together with $\pm 4\sigma$ bounds computed from the window-specific mean and standard deviation. Observations exceeding these bounds are capped at the respective threshold. The figure compares representative estimation windows in SE3 and SE4.

A.4 Grid Search Over ARMA Specifications

Table A.4.1: SE1: ARMA(p, q) grid-search results, 2025

	ARMA(p,q) specification														
	(0,1)	(0,2)	(0,3)	(1,0)	(1,1)	(1,2)	(1,3)	(2,0)	(2,1)	(2,2)	(2,3)†	(3,0)	(3,1)	(3,2)	(3,3)†
ϕ_1				0.972***	0.967***	0.963***	0.961***	1.262***	1.269***	1.188***	1.751***	1.260***	2.050***	0.776***	2.648***
				(0.003)	(0.004)	(0.004)	(0.004)	(0.015)	(0.029)	(0.060)	(0.033)	(0.015)	(0.034)	(0.073)	(0.019)
ϕ_2								−0.290***	−0.297***	−0.219***	−0.757***	−0.284***	−1.319***	0.310***	−2.559***
								(0.015)	(0.029)	(0.058)	(0.032)	(0.018)	(0.049)	(0.083)	(0.037)
ϕ_3												−0.004	0.264***	−0.129***	0.906***
												(0.009)	(0.017)	(0.027)	(0.019)
θ_1	0.698***	1.041***	1.221***		0.243***	0.290***	0.299***		−0.009	0.072	−0.503***		−0.772***	0.484***	−1.419***
	(0.006)	(0.011)	(0.014)		(0.010)	(0.013)	(0.014)		(0.027)	(0.057)	(0.035)		(0.029)	(0.072)	(0.022)
θ_2		0.505***	0.904***			0.077***	0.096***			0.028*	−0.164***			0.016	0.536***
		(0.007)	(0.013)			(0.009)	(0.012)			(0.014)	(0.015)			(0.022)	(0.023)
θ_3			0.374***				0.024***				−0.072***				0.186***
			(0.009)				(0.009)				(0.009)				(0.011)
AIC	−22,663	−26,170	−28,331	−33,677	−34,112	−34,189	−34,197	−34,196	−34,194	−34,195	−34,187	−34,194	−34,219	−34,196	−34,308
BIC	−22,514	−26,015	−28,168	−33,529	−33,956	−34,026	−34,027	−34,040	−34,031	−34,025	−34,011	−34,031	−34,049	−34,019	−34,124
Log-lik	11,352	13,107	14,188	16,860	17,078	17,117	17,122	17,120	17,120	17,121	17,119	17,120	17,133	17,123	17,180
N	8,736	8,736	8,736	8,736	8,736	8,736	8,736	8,736	8,736	8,736	8,736	8,736	8,736	8,736	8,736

Robust standard errors in parentheses. *** $p < 0.01$, ** $p < 0.05$, * $p < 0.10$.

All specifications include the exogenous controls from the mean and variance equations, which are omitted from the table.

`vce(robust)` corresponds to QML sandwich standard errors.

† Specification exhibits near-cancellation of AR and MA roots.

Table A.4.2: SE2: ARMA(p, q) grid-search results, 2025

	ARMA(p,q) specification														
	(0,1)	(0,2)	(0,3)	(1,0)	(1,1)	(1,2)	(1,3)	(2,0)	(2,1)	(2,2)	(2,3)	(3,0)	(3,1)	(3,2)	(3,3)
ϕ_1				0.969***	0.964***	0.959***	0.958***	1.232***	1.245***	1.012***	0.581***	1.229***	1.999***	2.016***	1.989***
				(0.003)	(0.003)	(0.004)	(0.004)	(0.015)	(0.029)	(0.065)	(0.060)	(0.015)	(0.038)	(0.078)	(0.076)
ϕ_2								−0.262***	−0.275***	−0.051	0.362***	−0.252***	−1.237***	−1.378***	−1.314***
								(0.015)	(0.028)	(0.063)	(0.057)	(0.019)	(0.052)	(0.103)	(0.123)
ϕ_3												−0.007	0.232***	0.352***	0.315***
												(0.010)	(0.016)	(0.032)	(0.056)
θ_1	0.715***	1.047***	1.212***		0.226***	0.267***	0.273***		−0.014	0.217***	0.650***		−0.756***	−0.784***	−0.759***
	(0.005)	(0.013)	(0.014)		(0.011)	(0.014)	(0.016)		(0.025)	(0.060)	(0.058)		(0.035)	(0.078)	(0.075)
θ_2		0.536***	0.905***			0.090***	0.098***			0.080***	0.200***			0.164***	0.137***
		(0.007)	(0.012)			(0.010)	(0.014)			(0.014)	(0.019)			(0.029)	(0.046)
θ_3			0.377***				0.011				0.046***				−0.014
			(0.007)				(0.009)				(0.009)				(0.017)
AIC	−10,584	−14,157	−16,206	−21,134	−21,494	−21,572	−21,572	−21,557	−21,556	−21,571	−21,574	−21,556	−21,572	−21,595	−21,594
BIC	−10,421	−13,988	−16,029	−20,971	−21,324	−21,395	−21,388	−21,388	−21,379	−21,387	−21,383	−21,379	−21,388	−21,404	−21,396
Log-lik	5,315	7,103	8,128	10,590	10,771	10,811	10,812	10,803	10,803	10,811	10,814	10,803	10,812	10,825	10,825
N	8,736	8,736	8,736	8,736	8,736	8,736	8,736	8,736	8,736	8,736	8,736	8,736	8,736	8,736	8,736

Robust standard errors in parentheses. *** $p < 0.01$, ** $p < 0.05$, * $p < 0.10$.

All specifications include the exogenous controls from the mean and variance equations, which are omitted from the table.

`vce(robust)` corresponds to QML sandwich standard errors.

Table A.4.3: SE3: ARMA(p, q) grid-search results, 2025

	ARMA(p,q) specification														
	(0,1)	(0,2)	(0,3)	(1,0)	(1,1)	(1,2)	(1,3)	(2,0)	(2,1)	(2,2)†	(2,3)	(3,0)	(3,1)	(3,2)	(3,3)
ϕ_1				0.963***	0.954***	0.956***	0.961***	1.104***	0.882***	0.410***	1.637***	1.112***	1.858***	1.857***	1.370***
				(0.003)	(0.004)	(0.004)	(0.004)	(0.012)	(0.045)	(0.094)	(0.062)	(0.013)	(0.050)	(0.061)	(0.304)
ϕ_2								−0.144***	0.071	0.519***	−0.646***	−0.203***	−1.031***	−1.027***	−0.158
								(0.012)	(0.044)	(0.089)	(0.060)	(0.016)	(0.055)	(0.100)	(0.554)
ϕ_3												0.053***	0.165***	0.163***	−0.222
												(0.010)	(0.011)	(0.050)	(0.254)
θ_1	0.719***	1.012***	1.119***		0.161***	0.154***	0.144***		0.230***	0.706***	−0.534***		−0.755***	−0.753***	−0.267
	(0.005)	(0.012)	(0.013)		(0.012)	(0.014)	(0.014)		(0.041)	(0.095)	(0.063)		(0.051)	(0.062)	(0.301)
θ_2		0.513***	0.840***			−0.016	−0.037***			0.091***	−0.139***			−0.002	−0.335
		(0.007)	(0.011)			(0.012)	(0.012)			(0.021)	(0.014)			(0.052)	(0.228)
θ_3			0.387***				−0.050***				−0.040***				−0.082*
			(0.008)				(0.011)				(0.011)				(0.042)
AIC	−4,796	−7,706	−9,410	−13,087	−13,268	−13,268	−13,290	−13,252	−13,268	−13,270	−13,314	−13,277	−13,313	−13,311	−13,313
BIC	−4,619	−7,522	−9,219	−12,911	−13,084	−13,077	−13,092	−13,068	−13,077	−13,071	−13,109	−13,086	−13,115	−13,106	−13,101
Log-lik	2,423	3,879	4,732	6,569	6,660	6,661	6,673	6,652	6,661	6,663	6,686	6,665	6,685	6,685	6,686
N	8,736	8,736	8,736	8,736	8,736	8,736	8,736	8,736	8,736	8,736	8,736	8,736	8,736	8,736	8,736

Robust standard errors in parentheses. *** $p < 0.01$, ** $p < 0.05$, * $p < 0.10$.

All specifications include the exogenous controls from the mean and variance equations, which are omitted from the table.

`vce(robust)` corresponds to QML sandwich standard errors.

† Specification exhibits near-cancellation of AR and MA roots.

Table A.4.4: SE4: ARMA(p, q) grid-search results, 2025

	ARMA(p,q) specification														
	(0,1)	(0,2)	(0,3)	(1,0)	(1,1)	(1,2)	(1,3)	(2,0)	(2,1)	(2,2)	(2,3)	(3,0)	(3,1)	(3,2)	(3,3)
ϕ_1				0.951***	0.939***	0.940***	0.946***	1.097***	0.890***	1.742***	0.575	1.104***	1.903***	1.910***	1.160***
				(0.004)	(0.005)	(0.005)	(0.005)	(0.013)	(0.051)	(0.034)	(0.398)	(0.013)	(0.037)	(0.069)	(0.195)
ϕ_2								−0.150***	0.047	−0.749***	0.346	−0.198***	−1.082***	−1.097***	0.274
								(0.012)	(0.048)	(0.032)	(0.371)	(0.016)	(0.043)	(0.122)	(0.358)
ϕ_3												0.044***	0.172***	0.179***	−0.443***
												(0.010)	(0.012)	(0.057)	(0.166)
θ_1	0.716***	1.001***	1.101***		0.166***	0.163***	0.154***		0.213***	−0.655***	0.527		−0.807***	−0.814***	−0.069
	(0.005)	(0.012)	(0.013)		(0.012)	(0.014)	(0.014)		(0.046)	(0.035)	(0.403)		(0.037)	(0.068)	(0.193)
θ_2		0.510***	0.823***			−0.007	−0.025*			−0.171***	0.044			0.008	−0.552***
		(0.008)	(0.010)			(0.012)	(0.014)			(0.011)	(0.079)			(0.060)	(0.153)
θ_3			0.381***				−0.034***				−0.022				−0.119***
			(0.008)				(0.010)				(0.020)				(0.028)
AIC	−2,663	−5,536	−7,171	−10,350	−10,531	−10,530	−10,539	−10,517	−10,530	−10,565	−10,536	−10,533	−10,576	−10,574	−10,577
BIC	−2,500	−5,366	−6,994	−10,188	−10,362	−10,353	−10,355	−10,347	−10,353	−10,381	−10,345	−10,356	−10,392	−10,383	−10,379
Log-lik	1,354	2,792	3,611	5,198	5,290	5,290	5,296	5,282	5,290	5,309	5,295	5,292	5,314	5,314	5,316
N	8,736	8,736	8,736	8,736	8,736	8,736	8,736	8,736	8,736	8,736	8,736	8,736	8,736	8,736	8,736

Robust standard errors in parentheses. *** $p < 0.01$, ** $p < 0.05$, * $p < 0.10$.

All specifications include the exogenous controls from the mean and variance equations, which are omitted from the table.

`vce(robust)` corresponds to QML sandwich standard errors.

A.5 Bilateral Net Import Coefficients

The following tables report the bilateral net import coefficients from the mean and variance equations of the ARMAX(3,1)-GARCH-X(1,1) baseline model. Results are reported separately for each bidding zone. The corresponding main model estimates are reported in Table 5.1.

Table A.5.1: Bilateral net import coefficients, SE1, 2025

	Coefficient	**Std. Error**
Mean equation		
Net import: FI	-0.000023^{***}	(0.000002)
Net import: NO4	-0.000029^{***}	(0.000002)
Net import: SE2	-0.000025^{***}	(0.000002)
Variance equation		
Net import: FI	-0.000689^{***}	(0.000055)
Net import: NO4	-0.000136	(0.000124)
Net import: SE2	-0.000560^{***}	(0.000060)

Notes: Bilateral net import coefficients for SE1 from the ARMAX(3,1)-GARCH-X(1,1) model estimated over 2025, reported in Table 5.1. $^{***}p < 0.01$, $^{**}p < 0.05$, $^{*}p < 0.10$.

Table A.5.2: Bilateral net import coefficients, SE2, 2025

	Coefficient	**Std. Error**
Mean equation		
Net import: NO3	-0.000058^{***}	(0.000003)
Net import: NO4	-0.000061^{***}	(0.000004)
Net import: SE1	-0.000055^{***}	(0.000003)
Net import: SE3	-0.000052^{***}	(0.000003)
Variance equation		
Net import: NO3	0.000234^{**}	(0.000092)
Net import: NO4	-0.000268^{**}	(0.000124)
Net import: SE1	-0.000277^{***}	(0.000075)
Net import: SE3	-0.000130^{***}	(0.000038)

Notes: Bilateral net import coefficients for SE2 from the ARMAX(3,1)-GARCH-X(1,1) model estimated over 2025, reported in Table 5.1. $^{***}p < 0.01$, $^{**}p < 0.05$, $^{*}p < 0.10$.

Table A.5.3: Bilateral net import coefficients, SE3, 2025

	Coefficient	**Std. Error**
Mean equation		
Net import: DK1	-0.000062^{***}	(0.000009)
Net import: FI	-0.000021^{***}	(0.000006)
Net import: NO1	-0.000046^{***}	(0.000005)
Net import: SE2	-0.000047^{***}	(0.000005)
Net import: SE4	-0.000042^{***}	(0.000004)
Variance equation		
Net import: DK1	−0.000116	(0.000099)
Net import: FI	−0.000083	(0.000059)
Net import: NO1	0.000073	(0.000081)
Net import: SE2	0.000006	(0.000049)
Net import: SE4	0.000347^{***}	(0.000052)

Notes: Bilateral net import coefficients for SE3 from the ARMAX(3,1)-GARCH-X(1,1) model estimated over 2025, reported in Table 5.1. $^{***}p < 0.01$, $^{**}p < 0.05$, $^{*}p < 0.10$.

Table A.5.4: Bilateral net import coefficients, SE4, 2025

	Coefficient	**Std. Error**
Mean equation		
Net import: DK2	-0.000041^{***}	(0.000008)
Net import: GER	-0.000048^{***}	(0.000011)
Net import: PL	-0.000039^{***}	(0.000012)
Net import: SE3	0.000005	(0.000004)
Variance equation		
Net import: DK2	0.000084	(0.000096)
Net import: GER	-0.000529^{***}	(0.000139)
Net import: PL	−0.000176	(0.000128)
Net import: SE3	-0.000437^{***}	(0.000045)

Notes: Bilateral net import coefficients for SE4 from the ARMAX(3,1)-GARCH-X(1,1) model estimated over 2025, reported in Table 5.1. $^{***}p < 0.01$, $^{**}p < 0.05$, $^{*}p < 0.10$.

A.6 Additional FBMC Interaction Tests

A.6.1 SE1–SE2 FBMC Interaction Test

$$\begin{aligned} p_{z,t} = {} & \alpha + \beta_1 D_z^{\mathrm{SE2}} + \beta_2 D_t^{\mathrm{FBMC}} + \beta_3 w_{z,t} \\ & + \beta_4 \left(D_z^{\mathrm{SE2}} \times D_t^{\mathrm{FBMC}} \right) + \beta_5 \left(D_z^{\mathrm{SE2}} \times w_{z,t} \right) \\ & + \beta_6 \left(D_t^{\mathrm{FBMC}} \times w_{z,t} \right) + \beta_7 \left(D_z^{\mathrm{SE2}} \times D_t^{\mathrm{FBMC}} \times w_{z,t} \right) + \varepsilon_{z,t}, \end{aligned} \tag{A.6.1.1}$$

where $p_{z,t}$ is the deseasonalised log day-ahead spot price in zone z at time t, D_z^{SE2} is a dummy equal to one for SE2 and zero for SE1, D_t^{FBMC} is a dummy equal to one after the FBMC transition on 30 October 2024, and $w_{z,t}$ denotes the wind variable used in the baseline mean equation. The coefficient of interest is β_7, which captures whether the post-FBMC change in the wind coefficient differs between SE2 and SE1.

Table A.6.1: Pooled SE1–SE2 FBMC interaction estimates, 2024–2025

	Dependent variable: $p_{z,t}$
Constant	0.3978^{***}
	(0.0108)
D_z^{SE2}	0.4303^{***}
	(0.0141)
D_t^{FBMC}	0.2048^{***}
	(0.0174)
$w_{z,t}$	-0.0619^{***}
	(0.0017)
$D_z^{\mathrm{SE2}} \times D_t^{\mathrm{FBMC}}$	0.2288^{***}
	(0.0225)
$D_z^{\mathrm{SE2}} \times w_{z,t}$	-0.0512^{***}
	(0.0020)
$D_t^{\mathrm{FBMC}} \times w_{z,t}$	-0.0359^{***}
	(0.0026)
$D_z^{\mathrm{SE2}} \times D_t^{\mathrm{FBMC}} \times w_{z,t}$	-0.0270^{***}
	(0.0031)
Observations	35,066
R^2	0.290

Notes: The table reports OLS estimates from the pooled SE1–SE2 specification in Equation A.6.1.1. The dependent variable is the deseasonalised log day-ahead spot price. SE1 before the FBMC transition is the reference category. D_t^{FBMC} is a dummy equal to one after the FBMC transition on 30 October 2024. The triple-interaction row corresponds to $\hat{\beta}_7$. Standard errors are reported in parentheses. $^{***}p < 0.01$, $^{**}p < 0.05$, $^{*}p < 0.10$.

A.6.2 SE2 Local Congestion Interaction Test

$$\begin{aligned} p_{\mathrm{SE2},t} = \alpha_{\mathrm{SE2}} &+ \sum_{i=1}^{3} \phi_i p_{\mathrm{SE2},t-i} + \beta_{\mathrm{wind}} w_{\mathrm{SE2},t} + \beta_{\mathrm{hydro}} r_{\mathrm{SE2},t} + \beta_{\mathrm{cons}} c_{\mathrm{SE2},t} \\ &+ \sum_{n \in \mathcal{N}(\mathrm{SE2})} \beta_{\mathrm{exch},n} X_{\mathrm{SE2},n,t} + \beta_{\mathrm{oil}} o_{t-24} + \beta_{\mathrm{gas}} g_{t-24} \\ &+ \beta_{\mathrm{cong}} D_t^{\mathrm{SE2–SE3}} + \rho \left(D_t^{\mathrm{SE2–SE3}} \times w_{\mathrm{SE2},t} \right) + \theta_1 \varepsilon_{\mathrm{SE2},t-1} + \varepsilon_{\mathrm{SE2},t}. \end{aligned} \tag{A.6.2.1}$$

All variables in Equation A.6.2.1 follow the preprocessing and notation used in the baseline mean equation in Equation 4.2.1.1. The variable $p_{\mathrm{SE2},t}$ is the deseasonalised log day-ahead spot price in SE2 at time t, $w_{\mathrm{SE2},t}$ denotes forecasted wind power production in SE2, $r_{\mathrm{SE2},t}$ denotes hydro reservoir levels, $c_{\mathrm{SE2},t}$ denotes forecasted consumption, and $X_{\mathrm{SE2},n,t}$ denotes bilateral net exchange between SE2 and neighbouring zone or

country n. The variables o_{t-24} and g_{t-24} denote lagged oil and gas prices. The dummy $D_t^{\text{SE2–SE3}}$ equals one when the SE2–SE3 corridor is locally congested. The coefficient of interest is ρ, which captures whether the wind coefficient differs between congested and uncongested SE2–SE3 hours. The model is estimated jointly with the same GARCH-X(1,1) variance equation and Student-t errors as the baseline specification.

Table A.6.2: SE2 local congestion interaction estimates, 2025

	Dependent variable: $p_{\mathbf{SE2},t}$
Constant	0.6590
	(0.4871)
$w_{\text{SE2},t}$	-0.0900^{***}
	(0.0086)
$r_{\text{SE2},t}$	0.3780^{***}
	(0.1073)
$c_{\text{SE2},t}$	0.1498^{*}
	(0.0782)
Net import: NO3	-0.000057^{***}
	(0.000003)
Net import: NO4	-0.000059^{***}
	(0.000004)
Net import: SE1	-0.000053^{***}
	(0.000003)
Net import: SE3	-0.000050^{***}
	(0.000003)
o_{t-24}	-0.1223
	(0.1414)
g_{t-24}	0.0636
	(0.0901)
$D_t^{\text{SE2–SE3}}$	-0.0736^{***}
	(0.0271)
$D_t^{\text{SE2–SE3}} \times w_{\text{SE2},t}$	0.0076^{**}
	(0.0035)
AIC	-21629.40
BIC	-21431.30

Notes: The table reports selected mean-equation coefficients from the SE2 local-congestion specification in Equation A.6.2.1. The model is estimated over 2025 as an ARMAX(3,1)-GARCH-X(1,1) model with Student-t errors with 5 degrees of freedom. The net import rows correspond to $X_{\text{SE2},n,t}$ and positive values denote net imports into SE2 from neighbouring zone or country n. The congestion terms are included in the mean equation. Baseline mean-equation controls are retained. ARMA terms are included in the estimation but omitted from the table for compactness. Robust standard errors are reported in parentheses. $^{***}p < 0.01$, $^{**}p < 0.05$, $^{*}p < 0.10$.

A.7 Rolling-Window Coefficient, Mean Equation

A.7.1 Mean Equation

Table A.7.1: Rolling-window estimates of $\hat{\beta}_{\text{wind}}$, mean equation

Year	SE1	SE2	SE3	SE4
2015	0.0030	−0.0046	−0.0263***	−0.0760***
2016	−0.0049**	−0.0067***	−0.0342***	−0.0320***
2017	−0.0042*	−0.0100***	−0.0578***	−0.0526***
2018	−0.0049***	−0.0068***	−0.0316***	−0.0264***
2019	−0.0060**	−0.0162***	−0.0354***	−0.0438***
2020	−0.0122**	−0.0420***	−0.1528***	−0.0838***
2021	−0.0224***	−0.0166***	−0.0790***	−0.0457***
2022	−0.0667***	−0.1133***	−0.1506***	−0.1034***
2023	−0.0164***	−0.0227***	−0.0586***	−0.0328***
2024	−0.0215***	−0.0394***	−0.0421***	−0.0432***
2025	−0.0143***	−0.0904***	−0.1206***	−0.0733***

Notes: Each entry reports $\hat{\beta}_{\text{wind}}$ from the mean equation of the ARMAX(3,1)-GARCH-X(1,1) model estimated over the calendar year indicated, using a one-year rolling-window with one-year steps. $^{***}p < 0.01$, $^{**}p < 0.05$, $^{*}p < 0.10$.

A.7.2 Rolling Quantile Regression Estimates

Table A.7.2: Rolling-window estimates of $\hat{\beta}_{\text{wind}}(\tau = 0.10)$

Year	SE1	SE2	SE3	SE4
2015	0.0083^{***}	0.0091^{***}	-0.0006	-0.0050^{*}
2016	-0.0021^{***}	-0.0040^{***}	-0.0074^{***}	-0.0117^{***}
2017	-0.0019^{**}	-0.0022^{*}	-0.0103^{***}	-0.0178^{***}
2018	-0.0033^{***}	-0.0009	-0.0089^{***}	-0.0087^{***}
2019	-0.0028^{**}	-0.0022^{*}	-0.0022	-0.0033
2020	0.0028	-0.0079^{***}	-0.0404^{***}	-0.0198^{***}
2021	-0.0042^{***}	-0.0020	-0.0277^{***}	-0.0293^{***}
2022	-0.0007	-0.0309^{***}	-0.0913^{***}	-0.0744^{***}
2023	-0.0028^{***}	-0.0053^{***}	-0.0171^{***}	-0.0095^{***}
2024	-0.0074^{***}	-0.0157^{***}	-0.0153^{***}	-0.0118^{***}
2025	-0.0025^{**}	-0.0073^{***}	-0.0249^{***}	-0.0151^{***}

Notes: Each entry reports $\hat{\beta}_{\text{wind}}(\tau = 0.10)$, the estimated elasticity of the conditional 10th quantile of the log day-ahead spot price with respect to log wind power production, from the rolling QARX(3) specification estimated separately for each one-year window. The dependent variable is the deseasonalised log day-ahead spot price. Estimation is by quantile regression with robust standard errors. $^{***}p < 0.01$, $^{**}p < 0.05$, $^{*}p < 0.10$.

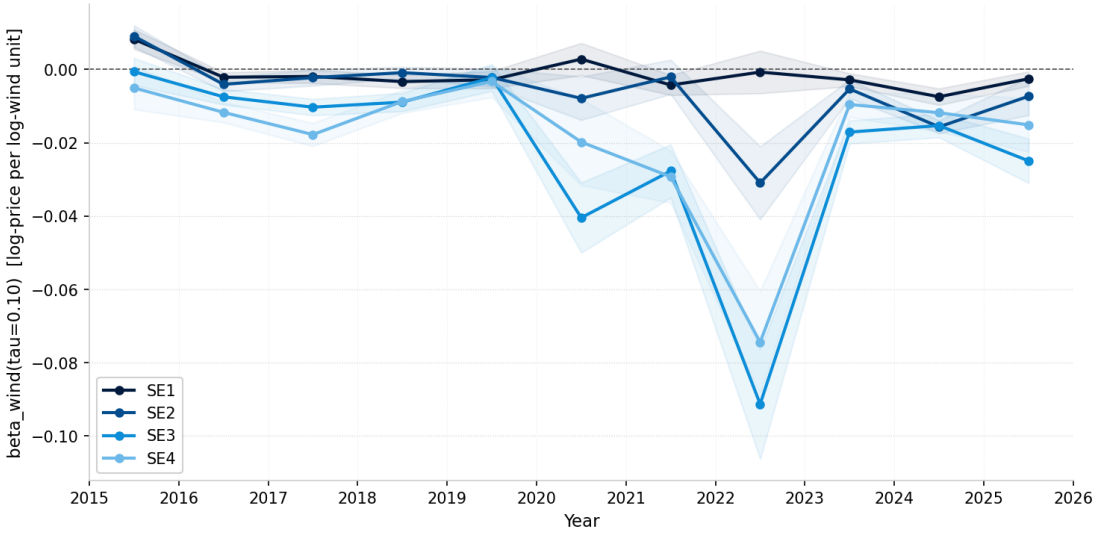


Figure A.7.1: Rolling-window estimates of $\hat{\beta}_{\text{wind}}(\tau = 0.10)$

Notes: Each point reports $\hat{\beta}_{\text{wind}}(\tau = 0.10)$ from the rolling QARX(3) specification estimated for the one-year window associated with the stated midpoint. The shaded band shows the 95% confidence interval based on robust standard errors. The horizontal dashed line marks zero.

Table A.7.3: Rolling-window estimates of $\hat{\beta}_{\text{wind}}(\tau = 0.50)$

Year	SE1	SE2	SE3	SE4
2015	0.0010^{**}	0.0013^{**}	-0.0003	-0.0034^{***}
2016	-0.0011^{***}	-0.0004	-0.0024^{***}	-0.0041^{***}
2017	-0.0011^{***}	-0.0006	-0.0046^{***}	-0.0054^{***}
2018	-0.0016^{***}	-0.0015^{***}	-0.0024^{***}	-0.0028^{***}
2019	-0.0023^{***}	-0.0030^{***}	-0.0052^{***}	-0.0074^{***}
2020	-0.0004	-0.0019^{*}	-0.0107^{***}	-0.0071^{***}
2021	-0.0005	-0.0027^{***}	-0.0086^{***}	-0.0061^{***}
2022	-0.0020	-0.0110^{***}	-0.0322^{***}	-0.0185^{***}
2023	-0.0019^{***}	-0.0028^{***}	-0.0060^{***}	-0.0052^{***}
2024	-0.0029^{***}	-0.0049^{***}	-0.0058^{***}	-0.0067^{***}
2025	-0.0024^{***}	-0.0090^{***}	-0.0138^{***}	-0.0127^{***}

Notes: Each entry reports $\hat{\beta}_{\text{wind}}(\tau = 0.50)$, the estimated elasticity of the conditional median of the log day-ahead spot price with respect to log wind power production, from the rolling QARX(3) specification estimated separately for each one-year window. The dependent variable is the deseasonalised log day-ahead spot price. Estimation is by quantile regression with robust standard errors. $^{***}p < 0.01$, $^{**}p < 0.05$, $^{*}p < 0.10$.

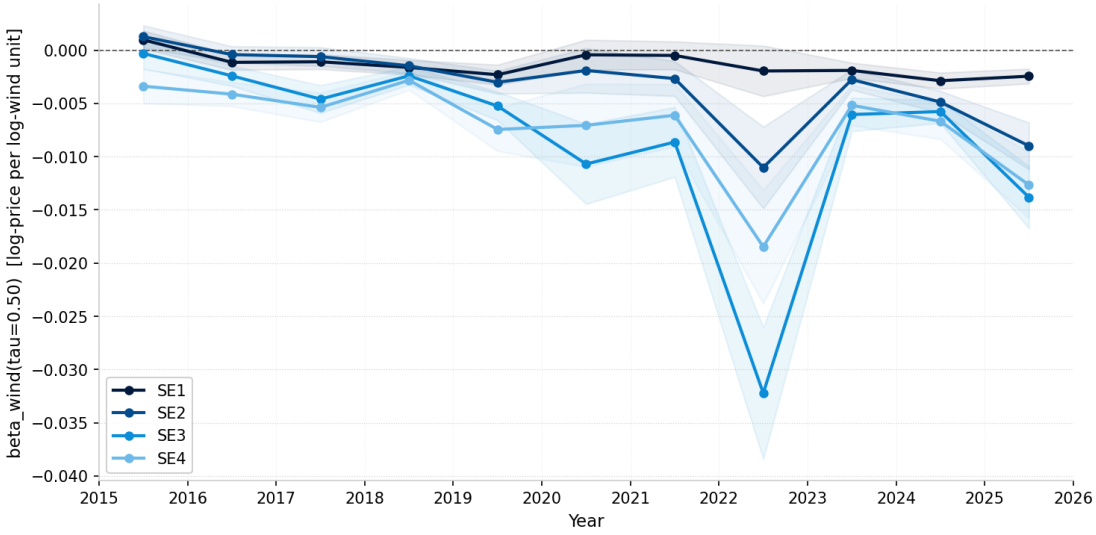


Figure A.7.2: Rolling-window estimates of $\hat{\beta}_{\text{wind}}(\tau = 0.50)$

Notes: Each point reports $\hat{\beta}_{\text{wind}}(\tau = 0.50)$ from the rolling QARX(3) specification estimated for the one-year window associated with the stated midpoint. The shaded band shows the 95% confidence interval based on robust standard errors. The horizontal dashed line marks zero.

Table A.7.4: Rolling-window estimates of $\hat{\beta}_{\text{wind}}(\tau = 0.90)$

Year	SE1	SE2	SE3	SE4
2015	-0.0039^{***}	-0.0035^{***}	-0.0063^{***}	-0.0084^{***}
2016	-0.0003	-0.0003	-0.0017^{**}	-0.0011
2017	-0.0016^{**}	-0.0017	-0.0032^{**}	-0.0039^{**}
2018	-0.0028^{***}	-0.0045^{***}	0.0005	-0.0002
2019	-0.0052^{***}	-0.0070^{***}	-0.0099^{***}	-0.0105^{***}
2020	-0.0111^{***}	-0.0111^{***}	-0.0367^{***}	-0.0318^{***}
2021	-0.0040^{***}	-0.0108^{***}	-0.0070^{**}	-0.0072^{*}
2022	-0.0194^{***}	-0.0235^{***}	-0.0526^{***}	-0.0243^{***}
2023	-0.0096^{***}	-0.0119^{***}	-0.0129^{***}	-0.0116^{***}
2024	-0.0074^{***}	-0.0129^{***}	-0.0083^{***}	-0.0139^{***}
2025	-0.0123^{***}	-0.0488^{***}	-0.0284^{***}	-0.0286^{***}

Notes: Each entry reports $\hat{\beta}_{\text{wind}}(\tau = 0.90)$, the estimated elasticity of the conditional 90th quantile of the log day-ahead spot price with respect to log wind power production, from the rolling QARX(3) specification estimated separately for each one-year window. The dependent variable is the deseasonalised log day-ahead spot price. Estimation is by quantile regression with robust standard errors. $^{***}p < 0.01$, $^{**}p < 0.05$, $^{*}p < 0.10$.

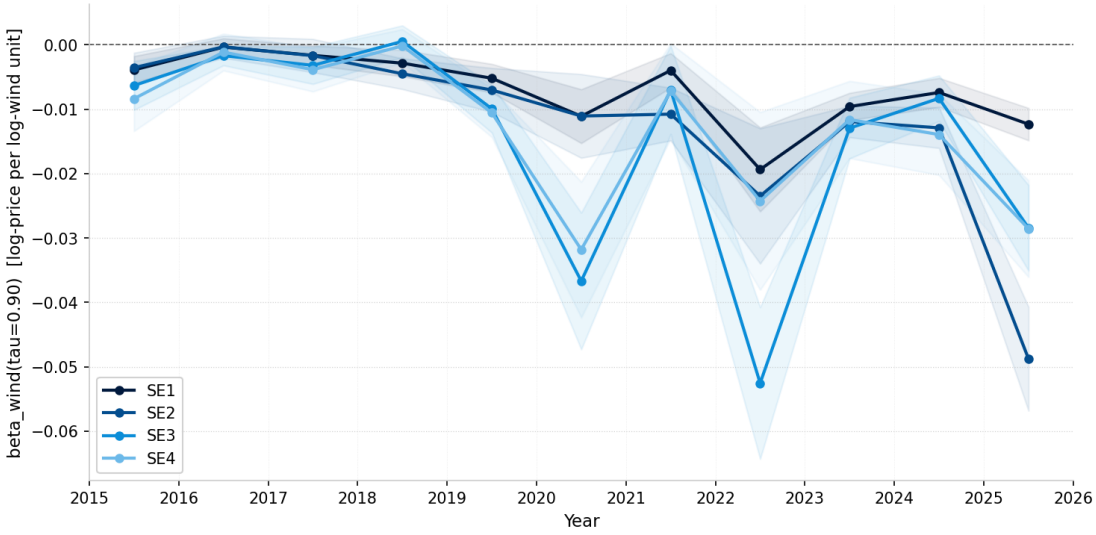


Figure A.7.3: Rolling-window estimates of $\hat{\beta}_{\text{wind}}(\tau = 0.90)$

Notes: Each point reports $\hat{\beta}_{\text{wind}}(\tau = 0.90)$ from the rolling QARX(3) specification estimated for the one-year window associated with the stated midpoint. The shaded band shows the 95% confidence interval based on robust standard errors. The horizontal dashed line marks zero.

A.8 Rolling-Window Coefficient, Variance Equation

Table A.8.1: Rolling-window estimates of $\hat{\gamma}_{\text{wind}}$, variance equation

Year	SE1	SE2	SE3	SE4
2015	-0.0983^{**}	-0.1582^{***}	-0.0888^{**}	-0.0943
2016	0.0185	0.0605	0.0235	0.1320^{***}
2017	-0.0038	0.0734^{*}	-0.0001	0.2477^{***}
2018	-0.0246	-0.0267	0.1201^{***}	0.1095^{*}
2019	-0.0071	-0.0489	-0.1808^{***}	-0.0833^{*}
2020	-0.1029^{**}	0.0702	0.0214	-0.2197^{***}
2021	-0.0517	-0.1564^{***}	0.2387^{***}	0.0455
2022	-0.1579^{***}	-0.0191	0.2769^{***}	0.3075^{***}
2023	-0.1615^{***}	-0.2323^{***}	-0.0270	-0.0282
2024	-0.0458	-0.0910^{*}	0.0689	-0.0576
2025	-0.3945^{***}	-0.6754^{***}	-0.0678	-0.0819^{**}

Notes: Each entry reports $\hat{\gamma}_{\text{wind}}$ from the variance equation of the ARMAX(3,1)-GARCH-X(1,1) model estimated over the calendar year indicated, using a one-year rolling-window with one-year steps. The multiplicative GARCH-X specification means $\hat{\gamma}_{\text{wind}}$ measures the effect of log wind production on log conditional variance. $^{***}p < 0.01$, $^{**}p < 0.05$, $^{*}p < 0.10$.

A.9 Robustness to the Treatment of Negative Prices

Table A.9.1: Rolling-window estimates of $\hat{\beta}_{\text{wind}}$ (negative-price floor)

Window midpoint	SE1	SE2	SE3	SE4
2015	0.0037	−0.0057	−0.0262***	−0.0751***
2016	−0.0057**	−0.0063***	−0.0344***	−0.0318***
2017	−0.0040	−0.0102***	−0.0568***	−0.0525***
2018	−0.0035*	−0.0053***	−0.0309***	−0.0272***
2019	−0.0060**	−0.0169***	−0.0330***	−0.0487***
2020	−0.0206***	−0.0544***	−0.1744***	−0.0913***
2021	−0.0209***	−0.0315***	−0.0903***	−0.0612***
2022	−0.0667***	−0.1154***	−0.1589***	−0.1059***
2023	−0.0470***	−0.0082	−0.1159***	−0.0557**
2024	−0.0220	−0.0740**	−0.0877**	−0.1057***
2025	−0.1115***	−0.4454***	−0.1366***	−0.1205***

Notes: Each entry reports $\hat{\beta}_{\text{wind}}$ from the mean equation of the ARMAX(3,1)-GARCH-X(1,1) model estimated for the one-year window associated with the stated midpoint. Negative prices are set to 0.01 before taking logarithms, while prices at or above zero are left unchanged. The dependent variable is the deseasonalised log day-ahead spot price under this alternative transformation. Robust standard errors are used for inference. $^{***}p < 0.01$, $^{**}p < 0.05$, $^{*}p < 0.10$.

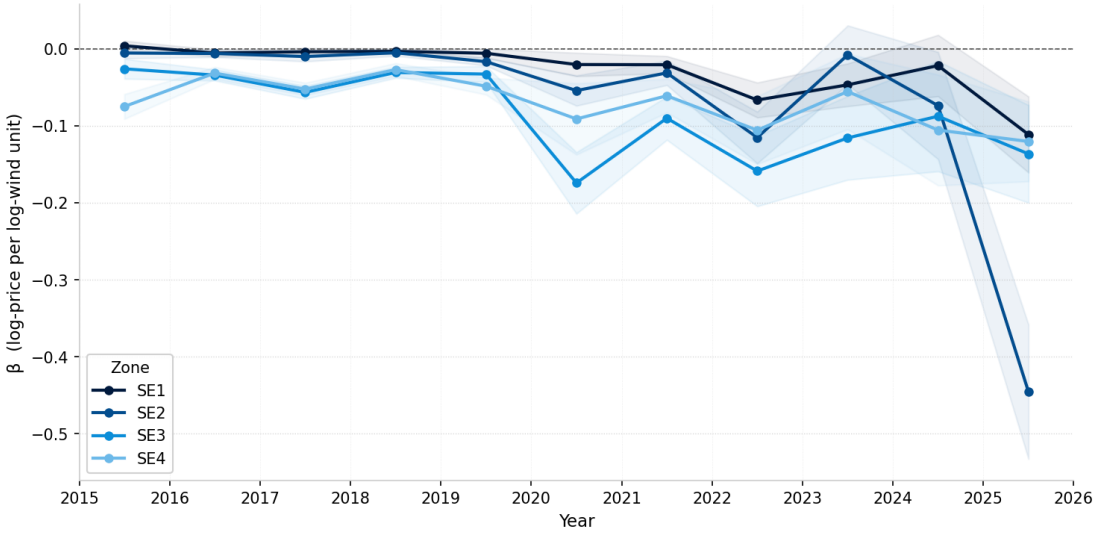


Figure A.9.1: Rolling-window estimates of $\hat{\beta}_{\text{wind}}$ (negative-price floor)

Notes: Each point reports $\hat{\beta}_{\text{wind}}$ from the mean equation of the ARMAX(3,1)-GARCH-X(1,1) model estimated for the one-year window associated with the stated midpoint. Negative prices are set to 0.01 before taking logarithms, while prices at or above zero are left unchanged. The shaded band shows the 95% confidence interval based on robust standard errors. The horizontal dashed line marks zero.

Table A.9.2: Rolling-window estimates of $\hat{\gamma}_{\text{wind}}$ (negative-price floor)

Window midpoint	SE1	SE2	SE3	SE4
2015	-0.1000^{**}	-0.1315^{***}	-0.1044^{**}	-0.1193^{**}
2016	0.0288	0.0737^{*}	0.0364	0.1320^{***}
2017	-0.0016	0.0764^{*}	-0.0101	0.2501^{***}
2018	-0.0380	-0.0348	0.1175^{**}	0.1094^{*}
2019	0.0012	-0.0433	-0.1739^{***}	-0.0793
2020	-0.0507	0.1470^{**}	0.0012	-0.1968^{***}
2021	-0.0814^{*}	-0.1932^{***}	0.1749^{***}	0.0136
2022	-0.1096^{***}	0.0112	0.2758^{***}	0.2536^{***}
2023	-0.0116	0.0512	-0.0507	-0.2323^{***}
2024	0.1804^{***}	0.3202^{***}	-0.0104	-0.1395^{***}
2025	-0.1235^{***}	0.1464^{***}	-0.0754^{*}	0.0693^{*}

Notes: Each entry reports $\hat{\gamma}_{\text{wind}}$ from the variance equation of the ARMAX(3,1)-GARCH-X(1,1) model estimated for the one-year window associated with the stated midpoint. Negative prices are set to 0.01 before taking logarithms, while prices at or above zero are left unchanged. The multiplicative GARCH-X specification means that $\hat{\gamma}_{\text{wind}}$ measures the effect of log wind production on log conditional variance. Robust standard errors are used for inference. $^{***}p < 0.01$, $^{**}p < 0.05$, $^{*}p < 0.10$.

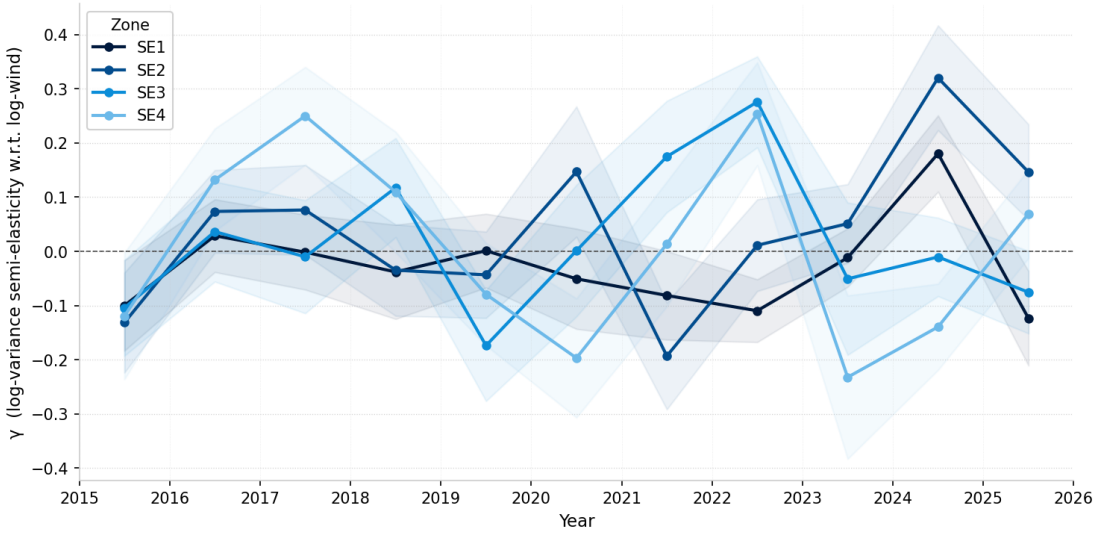


Figure A.9.2: Rolling-window estimates of $\hat{\gamma}_{\text{wind}}$ (negative-price floor)

Notes: Each point reports $\hat{\gamma}_{\text{wind}}$ from the variance equation of the ARMAX(3,1)-GARCH-X(1,1) model estimated for the one-year window associated with the stated midpoint. Negative prices are set to 0.01 before taking logarithms, while prices at or above zero are left unchanged. The shaded band shows the 95% confidence interval based on robust standard errors. The horizontal dashed line marks zero.

A.10 Trade-Partner Sensitivity in SE1 and SE2

This section reports the trade-partner sensitivity check for SE1 and SE2. Each specification removes one bilateral exchange-flow variable from the baseline ARMAX(3,1)-GARCH-X(1,1) model while keeping all other controls unchanged.

Table A.10.1: Trade-partner sensitivity of the wind coefficient in SE1 and SE2, ARMAX(3,1)-GARCH-X(1,1), 2025

Specification	*Mean eq.* $\hat{\beta}_{\text{wind}}$	*Var. eq.* $\hat{\gamma}_{\text{wind}}$
Panel A: SE1		
(1) Full model	-0.0144^{***}	-0.3947^{***}
	(0.0023)	(0.0385)
(2) Drop FI	-0.0101^{***}	-0.3380^{***}
	(0.0024)	(0.0443)
(3) Drop NO4	-0.0063^{***}	-0.3840^{***}
	(0.0022)	(0.0356)
(4) Drop SE2	-0.0072^{***}	-0.3317^{***}
	(0.0022)	(0.0409)
Panel B: SE2		
(1) Full model	-0.0906^{***}	-0.6752^{***}
	(0.0085)	(0.0490)
(2) Drop NO3	-0.0266^{***}	-0.7052^{***}
	(0.0081)	(0.0477)
(3) Drop NO4	-0.0506^{***}	-0.6285^{***}
	(0.0081)	(0.0481)
(4) Drop SE1	-0.0500^{***}	-0.6020^{***}
	(0.0083)	(0.0480)
(5) Drop SE3	-0.0289^{***}	-0.6199^{***}
	(0.0078)	(0.0460)
N	8,736	8,736

Notes: Each specification drops one bilateral net exchange variable from the full ARMAX(3,1)-GARCH-X(1,1) model, keeping all other controls unchanged. Panel A reports SE1, whose exchange partners are FI, NO4, and SE2. Panel B reports SE2, whose exchange partners are NO3, NO4, SE1, and SE3. $\hat{\beta}_{\text{wind}}$ is the mean-equation elasticity of the deseasonalised log day-ahead spot price with respect to log wind forecast. $\hat{\gamma}_{\text{wind}}$ is the corresponding coefficient in the multiplicative GARCH-X variance equation. QML robust standard errors in parentheses. $^{***}p < 0.01$, $^{**}p < 0.05$, $^{*}p < 0.10$.

Chapter B

Replication Code

All code used for data processing, model estimation, and the production of tables and figures is available in the following GitHub repository: https://github.com/valterstra/MScEconThesis.

Chapter C

Use of Artificial Intelligence

This thesis used generative AI tools, specifically Anthropic Claude, Anthropic Claude Code, OpenAI ChatGPT, and OpenAI Codex for language refinement and coding support. This includes refining sentences, correcting grammar, and sharpening the clarity of arguments. It also includes assisting with the implementation of Python scripts used for data processing, model estimation, and the production of tables and figures.

All empirical choices, including data collection, model specification, estimation strategy, and interpretation, were made independently by the authors. AI-assisted code was reviewed and modified by the authors before any output was used in the thesis. All reported findings and conclusions are based solely on the authors' assessment of the output.

Bibliography

Agency for the Cooperation of Energy Regulators. (2024, December). *Acer guidance on the application of remit* (6.1st Edition). Agency for the Cooperation of Energy Regulators. Retrieved May 30, 2026, from https://www.acer.europa.eu/sites/default/files/documents/Other%20Documents/6.1st_Edition_ACER_Guidance.pdf

Baskar, P. (2026). Iran and U.S. Blockades in the Strait of Hormuz: What to Know. *The New York Times*. Retrieved May 10, 2026, from https://www.nytimes.com/2026/04/24/world/middleeast/iran-us-strait-of-hormuz-blockade.html

Bloomberg Terminal. (2026). US Light Crude Oil and Dutch TTF Natural Gas.

Bollerslev, T. (1986). Generalized autoregressive conditional heteroskedasticity. *Journal of Econometrics*, *31*(3), 307–327. https://doi.org/10.1016/0304-4076(86)90063-1

Clò, S., Cataldi, A., & Zoppoli, P. (2015). The merit-order effect in the Italian power market: The impact of solar and wind generation on national wholesale electricity prices. *Energy Policy*, *77*, 79–88. https://doi.org/10.1016/j.enpol.2014.11.038

Cludius, J., Hermann, H., Matthes, F. C., & Graichen, V. (2014). The merit order effect of wind and photovoltaic electricity generation in Germany 2008–2016: Estimation and distributional implications. *Energy Economics*, *44*, 302–313. https://doi.org/10.1016/j.eneco.2014.04.020

Csereklyei, Z., Qu, S., & Ancev, T. (2019). The effect of wind and solar power generation on wholesale electricity prices in Australia. *Energy Policy*, *131*, 358–369. https://doi.org/10.1016/j.enpol.2019.04.007

Enders, W. (2015). *Applied econometric time series* (4th ed.). John Wiley & Sons, Inc.

Energimarknadsinspektionen. (2025). Sweden's electricity and natural gas market 2024: Ei r2025:19. Retrieved May 13, 2026, from https://ei.se/ei-in-english/publications/publications/reports-and-memos/2025/swedens-electricity-and-natural-gas-market-2024-ei-r202519

Engle, R. F. (1982). Autoregressive Conditional Heteroscedasticity with Estimates of the Variance of United Kingdom Inflation. *Econometrica*, *50*(4), 987. https://doi.org/10.2307/1912773

Forrest, S., & MacGill, I. (2013). Assessing the impact of wind generation on wholesale prices and generator dispatch in the australian national electricity market. *Energy Policy*, *59*, 120–132. https://doi.org/10.1016/j.enpol.2013.02.026

Gianfreda, A. (2010). Volatility and Volume Effects in European Electricity Spot Markets. *Economic Notes*, *39*(1-2), 47–63. https://doi.org/10.1111/j.1468-0300.2009.00220.x

Green Power Sweden. (2025). Statistics and forecast: Quarter three 2025. Retrieved May 10, 2026, from https://greenpowersweden.com/wp-content/uploads/2025/11/Statistik-och-prognos-Q3-2025_en.pdf

Hagfors, L. I., Paraschiv, F., Molnar, P., & Westgaard, S. (2016). Using quantile regression to analyze the effect of renewables on EEX price formation. *Renewable Energy and Environmental Sustainability*, *1*, 32. https://doi.org/10.1051/rees/2016036

Härdle, W. K., & Trück, S. (2010). *The dynamics of hourly electricity prices* (SFB 649 Discussion Paper No. 2010-013). Collaborative Research Center 649, Humboldt University Berlin. Retrieved May 10, 2026, from https://ideas.repec.org/p/zbw/sfb649/sfb649dp2010-013.html

Hirth, L. (2013). The market value of variable renewables: The effect of solar wind power variability on their relative price. *Energy Economics*, *38*, 218–236. https://doi.org/10.1016/j.eneco.2013.02.004

Holmberg, P., & Tangerås, T. P. (2023). The Swedish electricity market – today and in the future. *Sveriges Riksbank Economic Review*, (1), 5–35. Retrieved May 10, 2026, from https://www.riksbank.se/globalassets/media/rapporter/pov/artiklar/engelska/2023/230512/2023_1-the-swedish-electricity-market--today-and-in-the-future.pdf

Huisman, R., & Stet, C. (2022). The dependence of quantile power prices on supply from renewables. *Energy Economics*, *105*, 105685. https://doi.org/10.1016/j.eneco.2021.105685

Huisman, R., Stradnic, V., & Westgaard, S. (2013). Renewable Energy and Electricity Prices: Indirect Empirical Evidence from Hydro Power. *SSRN Electronic Journal*. https://doi.org/10.2139/ssrn.2340569

International Energy Agency. (2023, July). *Electricity market report update 2023*. International Energy Agency. Retrieved May 10, 2026, from https://iea.blob.core.windows.net/assets/2d1b41b0-2cf7-4b24-aa22-e8d0492e619c/ElectricityMarketReport_Update2023.pdf

Janczura, J., Trück, S., Weron, R., & Wolff, R. C. (2012). *Identifying spikes and seasonal components in electricity spot price data: A guide to robust modeling* (MPRA Paper No. 39277). Munich Personal RePEc Archive. Retrieved May 10, 2026, from https://mpra.ub.uni-muenchen.de/39277/

Jónsson, T., Pinson, P., & Madsen, H. (2010). On the market impact of wind energy forecasts. *Energy Economics*, *32*(2), 313–320. https://doi.org/10.1016/j.eneco.2009.10.018

Ketterer, J. C. (2014). The impact of wind power generation on the electricity price in Germany. *Energy Economics*, *44*, 270–280. https://doi.org/10.1016/j.eneco.2014.04.003

Koenker, R., & Bassett, G. (1978). Regression quantiles. *Econometrica*, *46*(1), 33–50. https://doi.org/10.2307/1913643

Koopman, S. J., Ooms, M., & Carnero, M. A. (2007). Periodic seasonal reg-ARFIMA-GARCH models for daily electricity spot prices. *Journal of the American Statistical Association*, *102*(477), 16–27. https://doi.org/10.1198/016214506000001022

Ljung, G. M., & Box, G. E. P. (1978). On a measure of lack of fit in time series models. *Biometrika*, *65*(2), 297–303. https://doi.org/10.1093/biomet/65.2.297

Macedo, D. P., Marques, A. C., & Damette, O. (2020). The impact of the integration of renewable energy sources in the electricity price formation: Is the Merit-Order Effect occurring in Portugal? *Utilities Policy*, *66*, 101080. https://doi.org/10.1016/j.jup.2020.101080

Macedo, D. P., Marques, A. C., & Damette, O. (2021). The Merit-Order Effect on the Swedish bidding zone with the highest electricity flow in the Elspot market. *Energy Economics*, *102*, 105465. https://doi.org/10.1016/j.eneco.2021.105465

Macedo, D. P., Marques, A. C., & Damette, O. (2022). The role of electricity flows and renewable electricity production in the behaviour of electricity prices in Spain. *Economic Analysis and Policy*, *76*, 885–900. https://doi.org/10.1016/j.eap.2022.10.001

Maciejowska, K. (2020). Assessing the impact of renewable energy sources on the electricity price level and variability: A quantile regression approach. *Energy Economics*, *85*, 104532. https://doi.org/10.1016/j.eneco.2019.104532

Maniatis, G. I., & Milonas, N. T. (2022). The impact of wind and solar power generation on the level and volatility of wholesale electricity prices in Greece. *Energy Policy*, *170*, 113243. https://doi.org/10.1016/j.enpol.2022.113243

Marsh, N., & Musafer, S. (2026). How Iran war laid bare the world's reliance on Gulf oil and gas. Retrieved May 10, 2026, from https://www.bbc.com/news/articles/c15x1y8d37vo

Mwampashi, M. M., Nikitopoulos, C. S., Konstandatos, O., & Rai, A. (2021). Wind generation and the dynamics of electricity prices in Australia. *Energy Economics*, *103*, 105547. https://doi.org/10.1016/j.eneco.2021.105547

Nord Pool. (2026a). *Impact of nordic flow-based on the nordic system price*. Retrieved May 10, 2026, from https://www.nordpoolgroup.com/en/trading/nordic-flow-based-day-ahead-market-coupling/impact-of-nordic-flow-based-on-the-nordic-system-price/

Nord Pool. (2026b). *Market surveillance*. Retrieved May 30, 2026, from https://www.nordpoolgroup.com/en/trading/Market-surveillance/

Nord Pool. (2026c). Nord Pool Data Portal. Retrieved January 10, 2026, from https://data.nordpoolgroup.com/auction/day-ahead/prices?deliveryDate=latest&currency=EUR&aggregation=MonthlyAggregate&deliveryAreas=AT,SE1

Nord Pool. (2026d). Nordic Flow-Based Market Coupling Project Go-Live set for 29th October 2024. Retrieved May 10, 2026, from https://www.nordpoolgroup.com/en/message-center-container/newsroom/exchange-message-list/2024/q3/nordic-flow-based-market-coupling-project-go-live-set-for-29th-october-2024/

Nordic RCC. (2024). Transitional solution for calculation and allocation of intraday cross-zonal capacities for continuous trading in the intraday timeframe. Retrieved May 13, 2026, from https://nordic-rcc.net/wp-content/uploads/2024/10/ATC_Extraction_Description_20241017.pdf

Paraschiv, F., Erni, D., & Pietsch, R. (2014). The impact of renewable energies on EEX day-ahead electricity prices. *Energy Policy*, *73*, 196–210. https://doi.org/10.1016/j.enpol.2014.05.004

Regeringen och Regeringskansliet. (2025). Svenska kraftnät får i uppdrag att göra en förnyad analys av Sveriges elområdesindelning. Retrieved May 10, 2026, from https://www.regeringen.se/pressmeddelanden/2025/05/svenska-kraftnat-far-i-uppdrag-att-gora-en-fornyad-analys-av-sveriges-elomradesindelning/

Saénz de Miera, G., del Río González, P., & Vizcaíno, I. (2008). Analysing the impact of renewable electricity support schemes on power prices: The case of wind electricity in spain. *Energy Policy*, *36*, 3345–3359. https://doi.org/10.1016/j.enpol.2008.04.022

Sandberg, R. (2024). *Wind and electricity prices in sweden - a statistical analysis* (tech. rep.). https://energiforsk.se/media/33100/2024-975-wind-and-electricity-prices-in-sweden-a-statistical-analysis.pdf

Smith, M. S., & Shively, T. S. (2018). Econometric modeling of regional electricity spot prices in the Australian market. *Energy Economics*, *74*, 886–903. https://doi.org/10.1016/j.eneco.2018.07.013

Sorknæs, P., Djørup, S. R., Lund, H., & Thellufsen, J. Z. (2019). Quantifying the influence of wind power and photovoltaic on future electricity market prices. *Energy Conversion and Management*, *180*, 312–324. https://doi.org/10.1016/j.enconman.2018.11.007

Statistics Sweden (SCB). (2025). *Bruttoproduktion, installerad effekt samt antal anläggningar fördelat på elområde. år 2015–2024*. Retrieved May 10, 2026, from https://www.statistikdatabasen.scb.se/pxweb/sv/ssd/START__EN__EN0105__EN0105A/AnlInstEffBrProd/

Svenska Kraftnät. (2025a). Analys av elområden. Retrieved May 10, 2026, from https://www.svk.se/utveckling-av-kraftsystemet/systemansvar--elmarknad/analysavelomraden

Svenska Kraftnät. (2025b). Quarterly summary: Svenska kraftnät's epad auctions to enhance hedging opportunities, second quarter 2025. Retrieved May 13, 2026, from https://www.svk.se/4a4f97/siteassets/english/stakeholder-portal/electricity-market/pilot-project-support/the-quarterly-report-epads-q2-2025.pdf

Svenska kraftnät. (2025). About us. Retrieved May 30, 2026, from https://www.svk.se/en/about-us/

Sveriges Riksdag. (2025). Förordning (2025:782) med instruktion för affärsverket svenska kraftnät. Retrieved May 30, 2026, from https://www.riksdagen.se/sv/dokument-och-lagar/dokument/svensk-forfattningssamling/forordning-2025782-med-instruktion-for_sfs-2025-782/

Swedish Institute. (2026). Sweden and sustainability. Retrieved May 10, 2026, from https://sweden.se/climate/sustainability/sweden-and-sustainability

The Guardian. (2026). US and Israel launch strikes on Iran: What we know so far | US-Israel war on Iran. Retrieved May 10, 2026, from https://www.theguardian.com/world/2026/feb/28/us-israel-launch-strikes-attack-iran-what-we-know-so-far-latest

Unger, E. A., Ulfarsson, G. F., Gardarsson, S. M., & Matthiasson, T. (2017). A long-term analysis studying the effect of changes in the Nordic electricity supply on Danish and Finnish electricity prices. *Economic Analysis and Policy*, *56*, 37–50. https://doi.org/10.1016/j.eap.2017.06.001

Unger, E. A., Ulfarsson, G. F., Gardarsson, S. M., & Matthiasson, T. (2018). The effect of wind energy production on cross-border electricity pricing: The case of western Denmark in the Nord Pool market. *Economic Analysis and Policy*, *58*, 121–130. https://doi.org/10.1016/j.eap.2018.01.006

Vattenfall. (2026). *Nuclear power*. Retrieved May 10, 2026, from https://group.vattenfall.com/our-operations/our-energy-sources/nuclear-power

Weiss, A. A. (1986). Asymptotic Theory for ARCH Models: Estimation and Testing. *Econometric Theory*, *2*(1), 107–131. https://doi.org/10.1017/S0266466600011397

Weron, R. (2009). Heavy-tails and regime-switching in electricity prices. *Mathematical Methods of Operations Research*, *69*(3), 457–473. https://doi.org/10.1007/s00186-008-0247-4

Weron, R. (2014). Electricity price forecasting: A review of the state-of-the-art with a look into the future. *International Journal of Forecasting*, *30*, 1030–1081. https://doi.org/10.1016/j.ijforecast.2014.08.008

Woo, C., Horowitz, I., Moore, J., & Pacheco, A. (2011). The impact of wind generation on the electricity spot-market price level and variance: The Texas experience. *Energy Policy*, *39*(7), 3939–3944. https://doi.org/10.1016/j.enpol.2011.03.084

Würzburg, K., Labandeira, X., & Linares, P. (2013). Renewable generation and electricity prices: Taking stock and new evidence for Germany and Austria. *Energy Economics*, *40*, S159–S171. https://doi.org/10.1016/j.eneco.2013.09.011

Zeier, I. (2026). How is the electricity price calculated? Retrieved May 10, 2026, from https://www.nordpoolgroup.com/en/the-power-market/how-is-the-electricity-price-calculated/